

**INVESTIGATION OF THERMAL EFFECTS ON TISSUES
DURING LASER APPLICATIONS**

**LAZER UYGULAMALARININ DOKULAR ÜZERİNDEKİ
TERMAL ETKİLERİNİN İNCELENMESİ**

UMUT KAYA

ASSIST. PROF. DR. ÖZGÜR EKİCİ

Supervisor

Submitted to Graduate School of Science and Engineering of Hacettepe University

as a Partial Fulfillment to the Requirements

for the Award of the Degree of Master of Science

in Mechanical Engineering

2019

This work titled “**Investigation Of Thermal Effects On Tissues During Laser Applications**” by **UMUT KAYA** has been approved as a thesis for the Degree of **Master Of Science in Mechanical Engineering** by the Examining Committee Members mentioned below.

Prof. Dr. Murat KÖKSAL

Head



Assist. Prof. Dr. Özgür EKİCİ

Supervisor



Assoc. Prof. Dr. Selis ÖNEL

Member



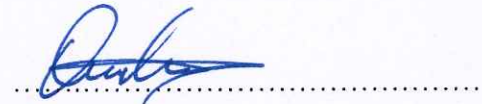
Assist. Prof. Dr. Bilsay SÜMER

Member



Assist. Prof. Dr. Onur BAŞ

Member



This thesis has been approved as a thesis for Degree of Master Of Science In Mechanical Engineering by Board of Directors of the Institute of Graduate School of Science and Engineering on / /.....

Prof. Dr. Menemşe GÜMÜŞDERELİOĞLU

Directors of the Institute of
Graduate School of Science and Engineering

ETHICS

In this thesis study, prepared in accordance with the spelling rules of Institute of Graduate School of Science and Engineering of Hacettepe University,

I declare that

- all the information and documents have been obtained in the base of the academic rules
- all audio-visual and written information and results have been presented according to the rules of scientific ethics
- in case of using others works, related studies have been cited in accordance with scientific standards
- all cited studies have been fully referenced
- I did not do any distortion in the data set
- and any part of this thesis has not been presented as another thesis study at this or any other university.

17 / 09 / 2019



UMUT KAYA

YAYINLANMA FİKRİ MÜLKİYET HAKKLARI BEYANI

Enstitü tarafından onaylanan lisansüstü tezimin/raporumun tamamını veya herhangi bir kısmını, basılı (kağıt) ve elektronik formatta arşivleme ve aşağıda verilen koşullarla kullanıma açma iznini Hacettepe üniversitesine verdiğimi bildiririm. Bu izinle Üniversiteye verilen kullanım hakları dışındaki tüm fikri mülkiyet haklarım bende kalacak, tezimin tamamının ya da bir bölümünün gelecekteki çalışmalarda (makale, kitap, lisans ve patent vb.) kullanım hakları bana ait olacaktır.

Tezin kendi orijinal çalışmam olduğunu, başkalarının haklarını ihlal etmediğimi ve tezimin tek yetkili sahibi olduğumu beyan ve taahhüt ederim. Tezimde yer alan telif hakkı bulunan ve sahiplerinden yazılı izin alınarak kullanması zorunlu metinlerin yazılı izin alarak kullandığımı ve istenildiğinde suretlerini Üniversiteye teslim etmeyi taahhüt ederim.

Yükseköğretim Kurulu tarafından yayınlanan “*Lisansüstü Tezlerin Elektronik Ortamda Toplanması, Düzenlenmesi ve Erişime Açılmasına İlişkin Yönerge*” kapsamında tezim aşağıda belirtilen koşullar haricince YÖK Ulusal Tez Merkezi / H. Ü. Kütüphaneleri Açık Erişim Sisteminde erişime açılır.

- Enstitü / Fakülte yönetim kurulu kararı ile tezimin erişime açılması mezuniyet tarihimden itibaren 2 yıl ertelenmiştir.
- Enstitü / Fakülte yönetim kurulu gerekçeli kararı ile tezimin erişime açılması mezuniyet tarihimden itibaren ay ertelenmiştir.
- Tezim ile ilgili gizlilik kararı verilmiştir.

17 / 09 /2019


UMUT KAYA

ABSTRACT

INVESTIGATION OF THERMAL EFFECTS ON TISSUES DURING LASER APPLICATIONS

Umut KAYA

Master of Sciences, Department of Mechanical Engineering

Thesis Supervisor: Assist. Prof. Dr. Özgür EKİCİ

September 2019, 104 Pages

With the development of technology, laser applications have become one of the important methods for the health sector. A better understanding of laser-tissue interaction can improve the effectiveness of treatment and diagnosis. Moreover, the usage of laser in the health sector can be expanded. However, laser application causes tissue to warm up. Undesirable conditions may be encountered during treatment or diagnosis if this warming does not fall within certain limits or if it cannot be maintained within the desired area / volume. With the help of mathematical models, this thermal effect which is experienced in laser tissue interactions can be calculated in advance. Thus, unwanted situations can be avoided.

In this study, a mathematical model was developed to understand the thermal effects of laser on tissues. This model is formed based on porous media theory. It is based on the fundamental energy equation and is derived as a macroscale model taking into account the mechanisms at the microscale. During the model derivation phase, tissue and blood were assumed to be under local thermal nonequilibrium conditions.

The developed model was solved using numerical methods. The solution was performed using MATLAB program. The obtained results were compared with Pennes and DPL model which are frequently used in literature. Differences between the results of the models were observed and the possible reasons of them were discussed. The effect of porosity and properties of laser irradiance on temperature was also investigated.

Keyword: Living Tissue, Bioheat transfer, laser irradiance, Porous media

ÖZET

LAZER UYGULAMALARININ DOKULAR ÜZERİNDEKİ TERMAL ETKİLERİNİN İNCELENMESİ

Umut KAYA

Yüksek Lisans, Makina Mühendisliği Bölümü

Tez Danışmanı: Dr. Öğr. Üyesi Özgür EKİCİ

Eylül 2019, 104 Sayfa

Teknolojinin gelişmesi ile birlikte lazer uygulamaları sağlık sektörü için önemli yöntemlerden birisi olmuştur. Lazer ile doku etkileşiminin daha iyi anlaşılması ile tedavi ve tanının etkinliği arttırılabilir. Dahası, sağlık sektöründe lazer kullanımı genişletilebilir. Ancak, lazer uygulaması dokunun ısınmasına neden olur. Bu ısınmanın belirli limitler içerisinde kalmaması durumunda veya istenen alan/hacim içinde tutulamamasına bağlı olarak tedavi ya da tanı sırasında istenmeyen durumlar ile karşılaşılabilir. Matematiksel modeller sayesinde lazer doku etkileşimlerinde ortaya çıkan bu termal etki önceden hesaplanabilir. Böylelikle istenmeyen durumların önüne geçilebilir.

Bu çalışmada lazerin doku üzerindeki termal etkisini anlamak amacıyla matematiksel bir model geliştirilmiştir. Bu model gözenekli ortam teorisi esas alınarak oluşturulmuştur. Temel enerji denklemine dayanmaktadır ve mikro ölçekte mekanizmaları dikkate alarak makro ölçekli bir model olarak türetilmiştir. Model türetme aşamasında doku ve kanın lokal olarak termal dengedışı koşullar altında olduğu varsayılmıştır.

Oluşturulmuş olan model numerik yöntem kullanılarak çözülmüştür. Çözüm işlemi MATLAB programı kullanılarak yapılmıştır. Elde edilen sonuçlar literatürde sıklıkla

kullanılan Pennes ve DPL modeli ile karşılaştırılmıştır. Modellerin sonuçları arasında farklılıklar gözlenmiş ve bu farklılıkların nedenleri tartışılmıştır. Aynı zamanda gözenekliliğin ve lazer ışınımının özelliklerinin sıcaklık üzerindeki etkisi de incelenmiştir.

Anahtar Kelimeler: Canlı doku, biyosı transferi, lazer ışınımı, gözenekli ortam

TABLE OF CONTENTS

ABSTRACT.....	I
ÖZET	III
LIST OF FIGURES	VII
LIST OF TABLES.....	IX
LIST OF ABBREVIATIONS.....	X
NOMENCLATURE	XI
CHAPTER 1	1
INTRODUCTION AND LITERATURE REVIEW	1
1.1 Introduction.....	1
1.2 Heat Transfer in Living Tissue	2
1.2.1 Classical (Fourier) Models.....	2
1.2.1.1 The Pennes Bio-heat Equation	2
1.2.1.2 Wulff Continuum Model.....	3
1.2.1.3 Klinger Continuum Model	3
1.2.1.4 Chen-Holmes (CH) Continuum Model.....	3
1.2.1.5 The Weinbaum and Jiji (WJ) Bio-heat Equation Model.....	5
1.2.2 Non-Fourier Continuum Models	5
1.2.2.1 Thermal wave model of bio-heat equation.....	6
1.2.2.2 Dual phase lag (DPL) Bio-heat Equation.....	6
1.2.2.3 Generalized Dual-Phase Lag Bio-heat Equations	7
1.2.3 Fractional Bio-heat Equation	7
1.2.4 Porous Media Models	8
1.2.4.1 Two Temperature Equation.....	8
1.2.4.2 Three Temperature Equation.....	8
1.2.5 Structural Vascular Network	9
1.3 Addition of Laser Irradiation as a Heat Source.....	13
1.4 Aim and Scope of the Thesis	13
CHAPTER 2	14
THEORY AND MODELING	14
2.1 Theory	14
2.1.1 Volume –Averaging Theory	15
2.2 Governing Equations.....	19

CHAPTER 3.....	27
SOLUTION METHODOLOGY	27
3.1 Numerical Solution Procedure.....	27
3.1.1 Discretization of Governing Equations	28
3.2 Convergence Study.....	30
3.2.1 Grid Convergence Study	32
3.2.2 Time Step Convergence Study	34
3.3 Code Validation.....	35
CHAPTER 4.....	39
RESULTS AND DISCUSSION	39
4.1 Comparison of Models	39
4.2 Effect of Porosity.....	41
4.3 Effect of Laser Irradiance and Exposure Time.....	44
CHAPTER 5.....	46
CONCLUSIONS AND FUTURE WORK	46
REFERENCES.....	48
APPENDIX A	57
Discretization of Model in This Study	57
APPENDIX B	63
Discretization of The Pennes Model	63
APPENDIX C	67
Discretization of DPL Model	67
APPENDIX D	73
MATLAB Code for Model in This Study	73
APPENDIX E.....	83
MATLAB Code for Pennes Model	83
APPENDIX F.....	92
MATLAB Code for DPL Model.....	92
APPENDIX G	102
MATLAB Code for Tzou’s Study	102
CURRICULUM VITAE	104

LIST OF FIGURES

Figure 1.1	Thermal damage after laser is applied [7]	1
Figure 1.2	Representation schematic of the volume of tissue [21,22]	4
Figure 1.3	Example of the fractal structure [69]	9
Figure 1.4	Classification of mathematical models based on Fourier approach	11
Figure 1.5	Classification of mathematical models based on Porous Media approach	12
Figure 2.1.	Representation of Biological Tissue [78]	15
Figure 2.2.	Example of Control Volume in Porous Media [79].....	16
Figure 2.3	Thermal dispersion effect on the other models in literature [66].	20
Figure 3.1.	Blood Vessel Alignment in Tissue[89].....	28
Figure 3.2.	Physical Model of 1D Analysis	29
Figure 3.3.	Grid System of 1D Analysis	29
Figure 3.4	The maximum temperature with respect of the number of grids in 808nm laser application (strongly scattering case).....	33
Figure 3.5	The maximum temperature with respect of the number of grids in 1940 nm laser application (highly absorbed case).....	33
Figure 3.6	The maximum temperature with respect of the time step in 808 nm laser application (strongly scattering case).	34
Figure 3.7	The maximum temperature with respect of the time step in 1940 nm laser application (highly absorbed case).	35
Figure 3.8.	The temperature distribution using Pennes equation.....	37
Figure 3.9.	The temperature distribution using DPL equation.....	37
Figure 3.10.	The temperature distribution using the mathematical model developed in this study.	38
Figure 4.1.	Evolution of temperature at the irradiated surface in 808 nm laser application (strongly scattering case).	40
Figure 4.2.	Evolution of temperature at the irradiated surface in 1940 nm laser application (highly absorbed case).	41
Figure 4.3.	In 808 nm laser application (strongly scattering case), the effect of porosity on the temperature at the irradiated surface.....	42
Figure 4.4.	In the 1940 nm laser application (highly absorbed case), the effect of porosity on the temperature at the irradiated surface.....	43

Figure 4.5. In 808 nm laser application (strongly scattering case), the effect of laser irradiance and exposure time on the temperature at the irradiated surface.44

Figure 4.6. In 1940 nm laser application (highly absorbed case), the effect of laser irradiance and exposure time on the temperature at the irradiated surface.45

LIST OF TABLES

Table 3.1	Thermophysical properties.	31
Table 3.2	Optical properties of tissue.	32
Table 4.1	Porosity and diameter of blood vessel.	42
Table 4.2.	The exposure time and intensity of laser irradiance	44

LIST OF ABBREVIATIONS

CH	Chen-Holmes
WJ	Weinbaum and Jiji
DPL	Dual phase lag
1D	One dimensional

NOMENCLATURE

α	Thermal diffusivity
k	Thermal Conductivity
k_{eff}	Effective Thermal conductivity
ρ	Density
c_p	Constant Pressure heat capacity
T	Temperature
t	Time
t_e	Exposure Time
β_t	Coefficient of thermal expansion
G	Coupling factor between intravascular and extravascular regime
τ	Viscous Stress Tensor
u	Velocity
u_m	Mean velocity
u_{lm}	Local mean velocity
p	Pressure
Q	External Heat Source
Q_s	Source Term
Q_p	Perfusion Term
Q_m	Metabolic Heat Generation
σ	Geometrical shape factor
V	Volume
Pe	Peclet Number
V_f	Volume of fluid
φ	Variable
ϑ	Intensity of Laser Irradiance
\emptyset	Extend of reaction
ΔH	Enthalpy of formation the metabolic reaction
ε	Porosity
n	Unit vector pointing outward from the fluid side to the membrane matrix side
n_v	Number of vein or artery

g	Perfusion bleed-off velocity per unit vessel surface area
A_{int}	Interfaces between the fluid and membrane matrix
a	Specific surface area
τ_q	Phase lag of the heat flux
τ_T	Phase lag of the temperature gradient
R	Radius of vessel
h	Interfacial heat transfer coefficient
R_d	Diffuse Reflectance
R_s	Specular Reflectance
μ_a	Absorption Coefficient
μ_s	Scattering Coefficient
μ_t	Attenuation Coefficient
δ	Effective optical penetration depth
g_a	Anisotropy factor
ϑ	Laser irradiance
Nu	Nusselt number

Subscripts

t	Tissue
s	Solid
b	Blood
a	Artery
v	Vein
i	Intravascular
e	Extravascular

Superscripts

(1)	Current time step
(0)	Previous time step
(-1)	One before previous time step

CHAPTER 1

INTRODUCTION AND LITERATURE REVIEW

1.1 Introduction

Owing to the current interdisciplinary scientific studies and research, many new technologies are emerging in the health sector. These new technologies provide a basis for improved diagnosis and treatment techniques. One of them is laser applications. Laser has recently been used extensively in the health sector for diagnostic and therapeutic purposes [1]. The main reason for that is; laser makes operations possible that cannot be performed by traditional methods [2]. Additionally, laser provides high precision for diagnosis and treatment [3]. Also for various applications, the use of laser is more practical compared to traditional methods [4]. Therefore, it is important to understand the interaction of laser radiation with tissue cells. Experimental and theoretical studies are performed to gain better understanding of the effects of laser on tissue with the objective of making laser applications safer and more efficient.

One of the effects caused by the laser radiation is the heat effect. Due to this effect, desired temperatures can be reached in the application zone [5]. However, the temperature rise may be an undesirable effect, depending on the purpose of the application. Because of the heat transfer mechanism, temperature increase is observed in the tissues around the primary application area. This increase in temperature can cause irreversible damage to the cells, as shown Figure 1.1 [6].

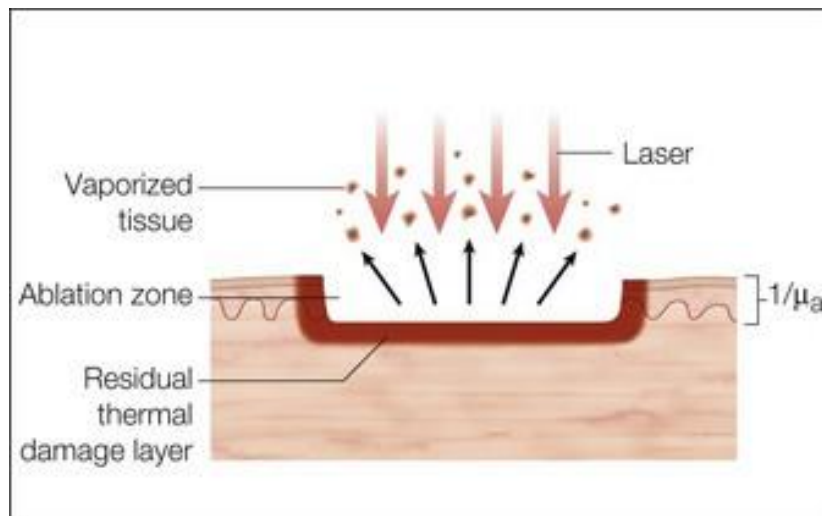


Figure 1.1 Thermal damage after laser is applied [7]

For this reason, it has been tried to calculate the temperature increase due to laser radiation by experimental and theoretical methods. Conducting experiments for each application are costly and require time. Therefore, the calculation of the temperature increase by mathematical models has become important. Thanks to these models, the temperature distribution within the tissue formed after the application can be estimated and the high temperatures that may occur during the application phase can be prevented.

1.2 Heat Transfer in Living Tissue

1.2.1 Classical (Fourier) Models

Heat conduction in the models presented in this section is explained by using Fourier's law of heat conduction. Perfusion term is included to consider the effects of blood flow. This term could behave as a heat source or sink depending on the conditions. These models consist of transient term, conduction term, perfusion term, metabolic heat source term and external heat source term as shown below.

$$\rho_t c_{p,t} \frac{\partial T_t}{\partial t} = \nabla \cdot (k_t \nabla T_t) + Q_p + Q_m + Q_s \quad (1.1)$$

1.2.1.1 The Pennes Bio-heat Equation

Pennes derived a bio-heat equation based on his experiment results in the late 1940s [8]. This equation is one of the oldest and most practical bio-heat equations. He tried to explain the heat transfer in living tissue by adding terms such as metabolic heat production and perfusion heat source to the standard energy equation. The amount of heat from the blood to the tissue can be calculated by the perfusion term, which refers to blood passing from the vascular system to tissue. In this equation, it is assumed that temperature of the blood leaving the tissue is equal to the tissue temperature in order to simplify the heat transfer calculation. As a result of the addition of the Fourier law of conduction to the energy equation, the equation called Pennes equation in the literature is derived.

$$\rho_t c_{p,t} \frac{\partial T_t}{\partial t} = \nabla \cdot (k_t \nabla T_t) + w_b \rho_b c_{p,b} (T_b - T_t) + Q_m + Q_s \quad (1.2)$$

where ρ_t is density of tissue, $c_{p,t}$ is specific heat capacity of tissue at constant pressure, T_t is temperature of tissue, k_t is thermal conductivity of tissue, w_b is blood perfusion, ρ_b

is density of blood, $c_{p,b}$ is specific heat capacity of tissue at constant pressure, T_b is temperature of blood. Because it is one of the fundamental models, many researchers have used this equation [9–14]. Although solution of this model is simple, there are some shortcomings. In order to eliminate these shortcomings, studies were conducted and the obtained results were compared with the Pennes equation.

1.2.1.2 Wulff Continuum Model

Wulff changed the assumptions made in order to overcome the shortcomings associated with the Pennes equation [15]. Pennes assumed that the heat transfer between blood and tissue is proportional to the difference in blood temperatures entering and leaving the tissue. Wulff, on the other hand, opposes this assumption and claims that this heat transfer is proportional to the temperature difference between flowing blood and tissue. As a result, the directional convective term is defined and this term is used instead of scalar perfusion term.

$$\rho_t c_{p,t} \frac{\partial T_t}{\partial t} = \nabla \cdot (k_t \nabla T_t) - \rho_b c_{p,b} u_{lm,b} \cdot \nabla T_t + \rho_b u_{lm,b} \Delta H \nabla \phi + Q_s \quad (1.3)$$

where $u_{lm,b}$ is local mean blood velocity, ΔH is specific enthalpy of metabolic reaction, ϕ is extent of reaction. The model was examined by the researchers and the effect of the terms added by Wulff on the results was examined [16,17].

1.2.1.3 Klinger Continuum Model

The convective term was added into the Pennes equation by Klinger; so that the lack of blood flow effect in the Pennes equation was tried to be eliminated [18].

$$\rho_t c_{p,t} \frac{\partial T_t}{\partial t} + \rho_b c_{p,b} u_b \cdot \nabla T_b = \nabla \cdot (k_t \nabla T_t) + Q_m + Q_s \quad (1.4)$$

Various studies have been done in the literature based on Klinger's research [19,20].

1.2.1.4 Chen-Holmes (CH) Continuum Model

Chen and Holmes [21] adopted the view that the tissue consists of two different regions. For this reason, it is divided into two areas called the solid-tissue region and the blood region, as shown in Figure 1.2.

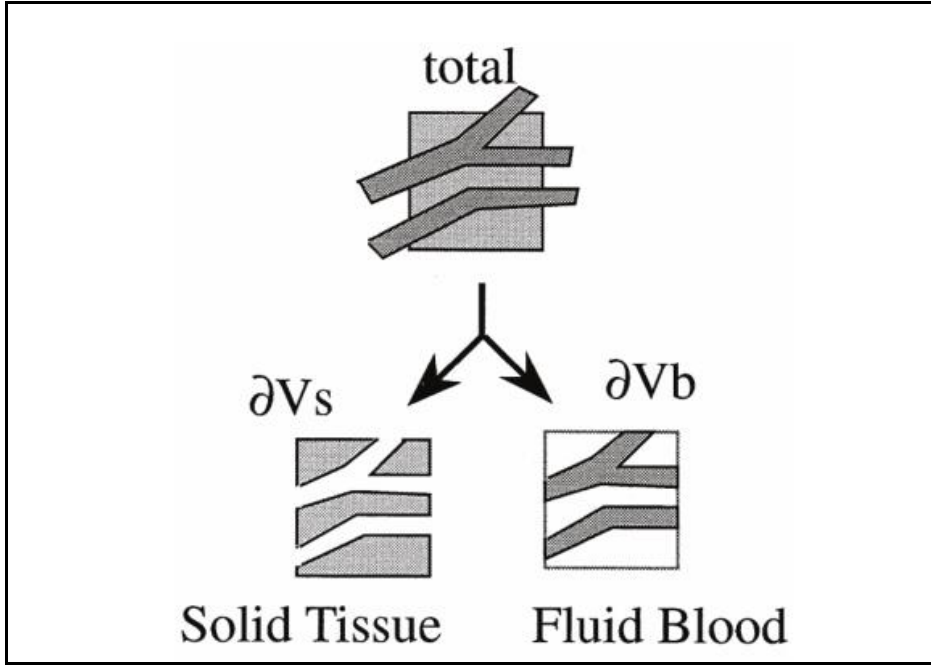


Figure 1.2 Representation schematic of the volume of tissue [21,22]

By using Volume-Average technique, energy equations are created separately for these two regions. The energy equation for the blood region, unlike the solid-tissue region, contains a term for the bulk fluid flow. The two equations then are combined using a porosity factor, which indicates the relationship between the two sub-volumes. Thus, a continuum model was created for the tissue. Based on the assumption that the porosity factor is less than one, the effective thermal conductivity coefficient is assumed to be equal to the thermal conductivity of the tissue. The heat transfer due to blood flow is divided into three different parts. Firstly, the blood perfusion part is limited that blood enters into the tissue from only micro vessels. The temperature of the blood entering the tissue was also assumed to be not equal to the temperature of the tissue. Secondly, the effect caused by the transport of blood is considered. Thirdly, the change of the thermal conduction coefficient due to the flow of blood is implied. The final form of the equation is formed by the addition of the perfusion term by combining these three factors into the equation formed.

$$\rho_t c_{p,t} \frac{\partial T_t}{\partial t} = \nabla \cdot (k_{eff} \nabla T_t) + w_b^* \rho_b c_{p,b} (T_b^* - T_t) - \rho_b c_{p,b} u_b \cdot \nabla T_t + \nabla \cdot (k_p \nabla T_t) + Q_m + Q_s \quad (1.5)$$

The results of this model have been used in various studies and their results have been examined [22–25].

1.2.1.5 The Weinbaum and Jiji (WJ) Bio-heat Equation Model

Weinbaum, Jiji and Lemons modified thermal conduction as effective thermal conduction using blood flow velocity and vessel geometry [26,27]. Arteries and veins were considered parallel to each other in the formation of vessel geometry. Flow directions are assumed to be opposite to each other and the countercurrent heat transfer effect between them is included in this way. The energy equation was written separately for the artery and vein. These equations are combined and then they added to the general energy equation to find out the interaction between tissue and blood. Consequently, contrary to the Pennes equation, the term perfusion is dependent on the arterial and vein temperature difference.

$$\rho_b c_{p,b} (n_v \pi R^2 u_{b,m}) \frac{d}{ds} [T_a - T_v] - \rho_b c_{p,b} (n_v 2\pi R g) (T_a - T_v) = \nabla \cdot (k_t \nabla T_t) + Q_m + Q_s \quad (1.6)$$

where n_v is the number of veins or arteries, R is the radius of vessel, $u_{b,m}$ is the mean velocity of blood, g is the perfusion velocity per unit vessel surface area. Since this model was difficult to implement, Weinbaum and Jiji simplified it [28]. This equation contained two unknowns, such as arterial and vein temperature. In order to calculate the tissue temperature, it was assumed that the average of these two temperatures was equal to the tissue temperature. In addition to that, heat transfer between artery and vein was expressed in terms of geometrical shape factor.

$$\frac{n_v \pi^2 R k_b}{4k_t} Pe \left(\frac{2gPe}{\sigma u_{b,m}} \frac{dT_t}{ds} - \frac{d}{ds} \left[\frac{RPe}{\sigma} \frac{dT_t}{ds} \right] \right) = \nabla \cdot (k_t \nabla T_t) + Q_m + Q_s \quad (1.7)$$

where Pe is the Peclet number, σ is the shape factor. Many researchers examined the simplified equation in the literature and obtained results were compared with results of other models [29–31].

1.2.2 Non-Fourier Continuum Models

Roemer et al. [32] and Mitra et al. [33] observed that temperature shows wave-like behavior and oscillations in experiments. These could not be explained by Fourier law of heat conduction. For this reason, in order to overcome this shortcoming, phase lags were added to the Fourier equation by researchers. These models show continuum characteristic.

1.2.2.1 Thermal wave model of bio-heat equation

Fourier law of heat conduction assumes infinite speed of heat wave propagation. However, the experimental results show that this propagation has a finite speed due to photon collision process [34]. This effect can be captured with the use of relaxation time. Based on this idea, Cattaneo [35] and Vernotte [36] added phase lag for the heat flux in the Fourier equation. By this concept, the general state of the thermal wave model of bio-heat equation has been obtained.

$$\frac{\partial^2 T_t}{\partial t^2} + \left(1 + \frac{w_b \rho_b c_{p,b}}{\rho_t c_{p,t}} \tau_q\right) \frac{\partial T_t}{\partial t} = \nabla \cdot (\alpha_t \nabla T_t) + \frac{w_b \rho_b c_{p,b}}{\rho_t c_{p,t}} (T_b - T_t) + \frac{Q_m}{\rho_t c_{p,t}} + \frac{Q_s}{\rho_t c_{p,t}} \quad (1.8)$$

where τ_q is the phase lag for heat flux. This model has been the subject of various researches due to advantages of capturing finite speed heat wave propagation. Using different boundary conditions, the results were compared with other models, especially with the one developed by Pennes [33,37–39].

1.2.2.2 Dual phase lag (DPL) Bio-heat Equation

In addition to relaxation behavior, Fourier law ignores the thermalization behavior. This behavior occurs due to finite speed energy transfer between photons and electrons in photon electron interaction, in other words a finite time is required to reach thermal equilibrium condition between photons and electrons. It causes a delay in temperature gradient [34]. Although the thermal wave model can solve the problem of infinite speed of heat wave propagation, it ignores the microstructural effect. Therefore, a phase lag for temperature has been added by Tzou to incorporate this microstructural effect.

$$\begin{aligned} \frac{\partial^2 T_t}{\partial t^2} + \left(1 + \frac{w_b \rho_b c_{p,b}}{\rho_t c_{p,t}} \tau_q\right) \frac{\partial T_t}{\partial t} &= \nabla \cdot (\alpha_t \nabla T_t) + \tau_T \frac{\partial}{\partial t} (\nabla \cdot (\alpha_t \nabla T_t)) \\ &+ \frac{w_b \rho_b c_{p,b}}{\rho_t c_{p,t}} (T_b - T_t) + \frac{Q_m}{\rho_t c_{p,t}} + \frac{Q_s}{\rho_t c_{p,t}} \end{aligned} \quad (1.9)$$

where τ_T is the phase lag for temperature. Many researchers preferred to use this model due to its ability to showing microstructural behavior. The results are compared with models such as Pennes equation and thermal wave model of bio-heat equation [40–44].

1.2.2.3 Generalized Dual-Phase Lag Bio-heat Equations

In the DPL equation, the effect of blood was added as a perfusion heat source and the blood region was neglected. Zhang argued that the blood region should be taken into consideration and the blood and tissue regions should be handled separately [45]. Therefore, Zhang formed two different equations, one of which is for blood, and the other one is for tissue. Then a single equation was obtained by combining these equations. Using the assumption suggested by Khaled and Vafai [46], blood velocity was eliminated from the equation. Finally, this equation was transformed into the form of DPL equation. As a consequent of these, phase lags of DPL equations can be expressed in terms of blood and tissue parameters.

$$\begin{aligned} \tau_q \frac{\partial^2 T_t}{\partial t^2} + \frac{\partial T_t}{\partial t} = \nabla \cdot (\alpha_{eff} \nabla T_t) + \tau_T \frac{\partial}{\partial t} (\nabla \cdot (\alpha_{eff} \nabla T_t)) + \frac{G}{(\rho c_p)_{eff}} (T_b - T_t) \\ + \frac{(1 - \varepsilon) Q_m + Q_r}{(\rho c_p)_{eff}} + \frac{\varepsilon \rho_b c_b}{G(\rho c_p)_{eff}} \left[(1 - \varepsilon) \frac{\partial Q_m}{\partial t} + \frac{\partial Q_s}{\partial t} \right] \end{aligned} \quad (1.10)$$

$$\text{where} \quad \tau_q = \frac{\varepsilon(1-\varepsilon)\rho_b c_b \rho_s c_s}{G(\rho c)_{eff}} \quad \tau_T = \frac{\varepsilon(1-\varepsilon)\rho_b c_b k_s}{G k_{eff}}$$

The results obtained under different conditions were compared with the results of DPL model and other models in the literature [47–50].

1.2.3 Fractional Bio-heat Equation

Pennes equation has several assumptions that decrease its accuracy. In order to increase the accuracy of results, fractional differential equation is embedded into Pennes equation [51,52]. So, the effects of anomalous heat transport phenomena are tried to be captured. This process can be done by time fractional and/or space fractional equation [53]. General form of the fractional bio-heat equation for 1D is as following;

$$\rho_t c_{p,t} \frac{\partial^\alpha T_t}{\partial t^\alpha} = k_t \frac{\partial^\beta T_t}{\partial x^\beta} (T_t) + w_b \rho_b c_{p,b} (T_b - T_t) + Q_m + Q_s \quad (1.11)$$

$$\text{where} \quad \alpha \in (0,1] \quad \text{and} \quad \beta \in (1,2]$$

In addition to fractional form of Pennes equation, fractional form of thermal wave model of bio-heat equation and fractional form of dual phase lag bio-heat equation are studied in the literature [54–56].

1.2.4 Porous Media Models

In Porous media models, it is assumed that the tissue consists of two regions which are solid matrix and blood flowing through the spaces between this matrix. Then they were evaluated separately. It was created based on the microstructure in the formation of equations and then extended to apply to macro structures. This was done by using volume-averaging theory [57]. The assumptions of local thermal equilibrium [58] or local thermal non-equilibrium [59] were used to combine these generated equations.

1.2.4.1 Two Temperature Equation

In this method, the tissue is divided into two different regions. The energy equations are written separately for the regions expressed as blood and solid [60,61]. A volumetric relationship was established between each other using the porosity factor.

$$\varepsilon\rho_b c_b \left[\frac{\partial T_b}{\partial t} + u_b \cdot \nabla T_b \right] = \nabla \cdot (k_{eff,b} \nabla T_b) + a_b h_b (T_s - T_b) + \varepsilon Q_s \quad (1.12)$$

$$(1 - \varepsilon)\rho_s c_s \frac{\partial T_s}{\partial t} = \nabla \cdot (k_{eff,s} \nabla T_s) - a_b h_b (T_b - T_s) + (1 - \varepsilon)Q_m + (1 - \varepsilon)Q_s \quad (1.13)$$

where ε is the porosity of tissue, a_b is the specific surface area, h_b is the interfacial heat transfer coefficient. The results of the studies using this model are compared with the other models in the literature [62–64].

1.2.4.2 Three Temperature Equation

In these models, the blood region is divided into 2 parts as arterial and venous region in order to incorporate the countercurrent heat transfer effect. The equations for these three regions are written separately [65]. When writing these equations, two different porosity factors are used, one for the artery and the other for the venous regions.

$$\varepsilon_a \rho_a c_{p,a} \left[\frac{\partial T_a}{\partial t} + u_a \cdot \nabla T_a \right] = \nabla \cdot (k_{eff,a} \nabla T_a) + a_a h_a (T_s - T_a) + \varepsilon_a Q_s \quad (1.14)$$

$$\varepsilon_v \rho_v c_{p,v} \left[\frac{\partial T_v}{\partial t} + u_v \cdot \nabla T_v \right] = \nabla \cdot (k_{eff,v} \nabla T_v) + a_v h_v (T_s - T_v) + \varepsilon_v Q_s \quad (1.15)$$

$$(1 - \varepsilon_a - \varepsilon_v) \rho_s c_{p,s} \frac{\partial T_s}{\partial t} = \nabla \cdot (k_{eff,s} \nabla T_s) - a_a h_a (T_s - T_{b,a}) - a_v h_v (T_s - T_v) + (1 - \varepsilon_a - \varepsilon_v) Q_m + (1 - \varepsilon_a - \varepsilon_v) Q_s \quad (1.16)$$

The effect of countercurrent heat transfer is investigated with this approach and results are compared with similar models in literature [66,67].

1.2.5 Structural Vascular Network

In structural vascular network models, a vascular network is created to add the effect of blood for heat transfer phenomena. Two approaches are commonly used to construct the vascular network. In the first approach, the fractal vascular network is formed by using laws such as Murray law. Then the temperature distribution is obtained for this region. Since the fractal structure is an approximate structure to the actual vessel network, the temperature distribution can be estimated in this way [68]. One of the examples of the fractal structure is shown in Figure 1.3.

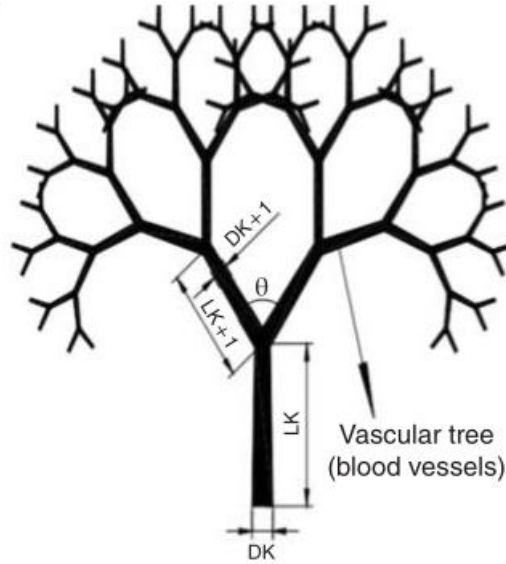


Figure 1.3 Example of the fractal structure [69]

In the second approach, a general structure was designed using anatomical information. General temperature distribution was obtained with this structure [70]. However, due to the complexity of the vessel structure, these models have been difficult to form and solve.

Although there are different methods of calculating the temperature values in living tissue cells, these can be categorized in two different groups. In the first type of classification, the use of Fourier approach or non-Fourier approach in the calculation of the heat conduction is taken into consideration (Figure 1.1). The second type of classification is based on the usage of porous media approach in the models (Figure 1.2). According to these two different characteristics, the classification of the models in the literature is expressed as follows.

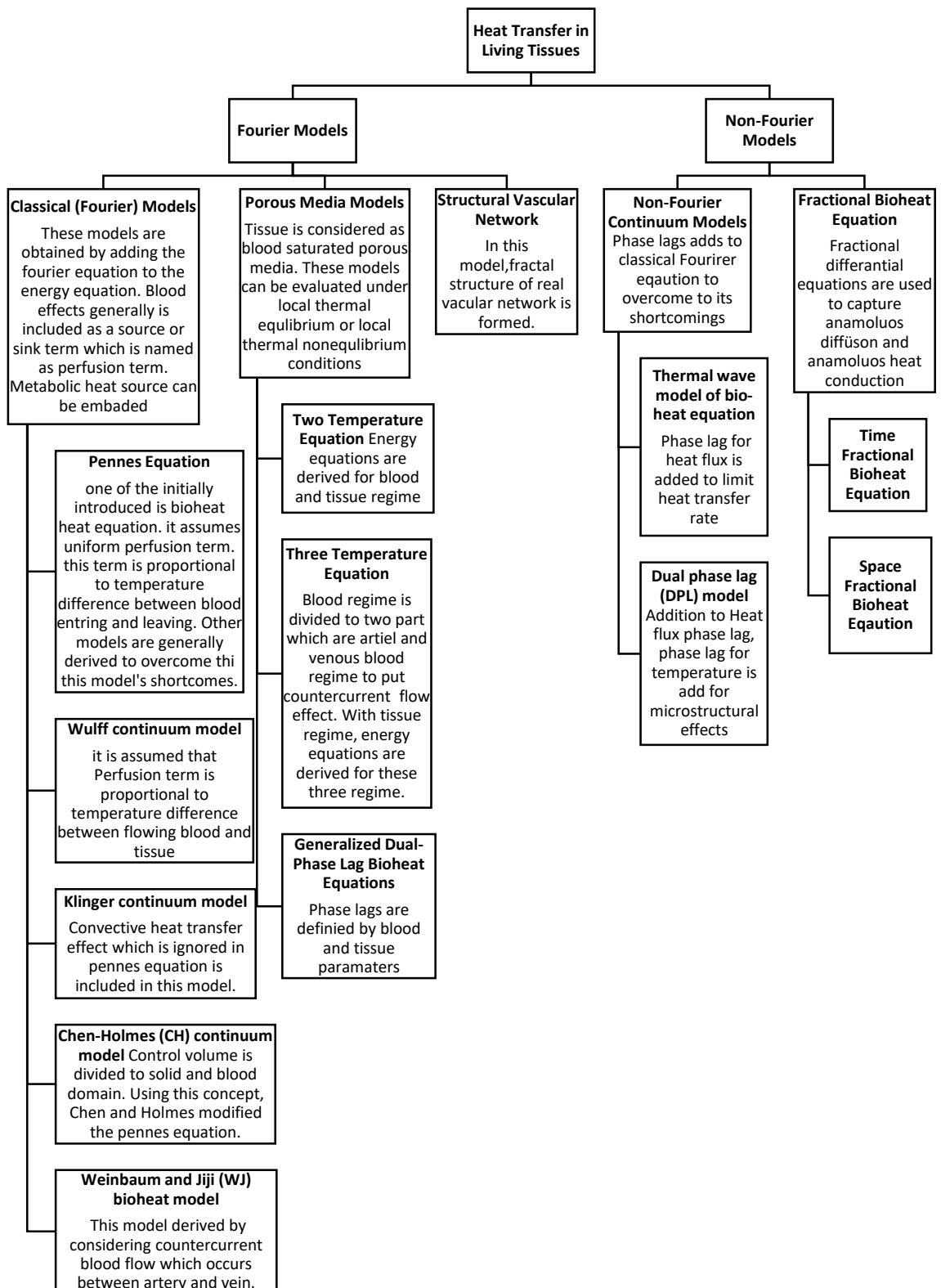


Figure 1.4 Classification of mathematical models based on Fourier approach

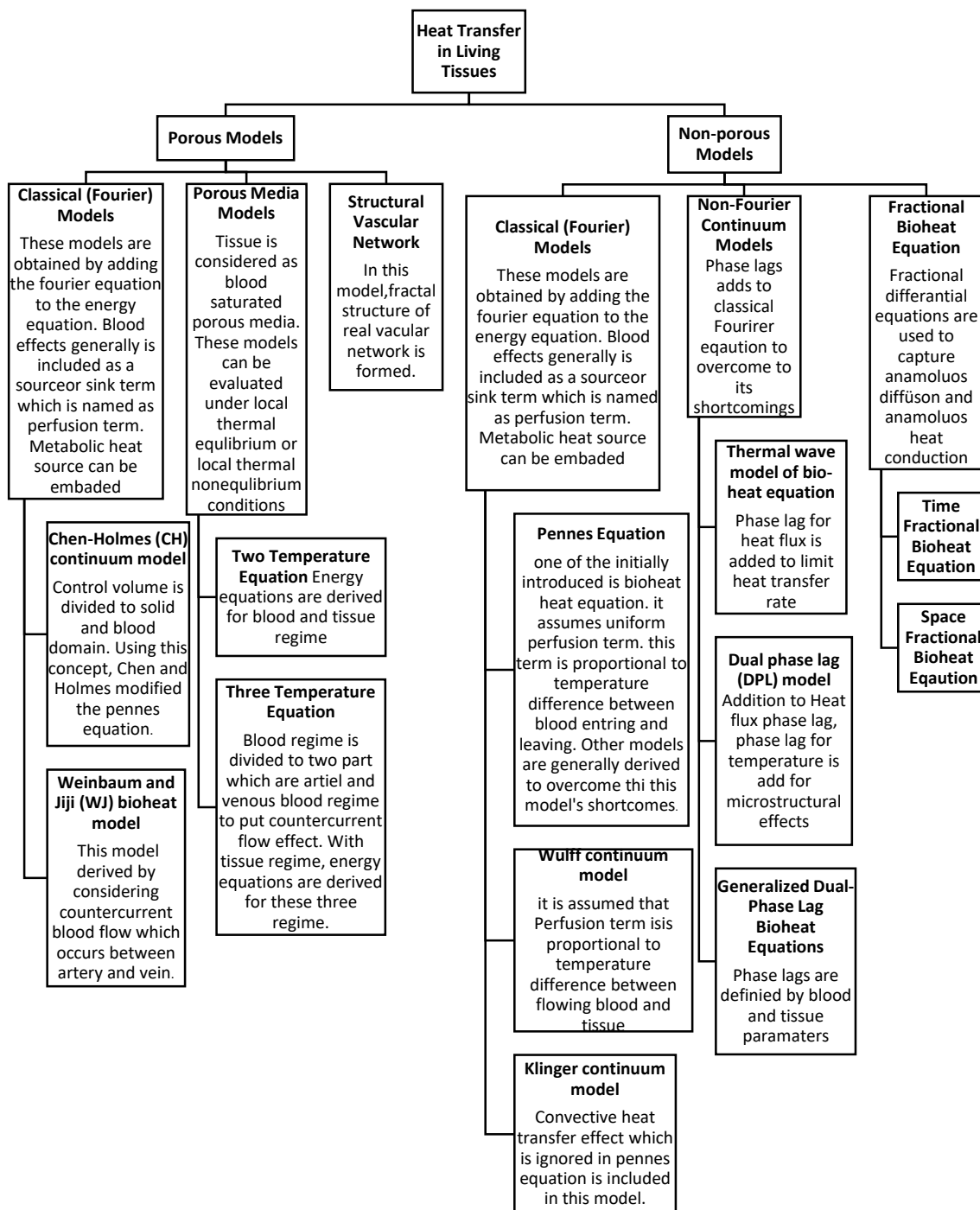


Figure 1.5 Classification of mathematical models based on Porous Media approach

1.3 Addition of Laser Irradiation as a Heat Source

In general, two methods have been followed to include the radiation effect. One of these is that the heat generated by the laser is defined as the boundary condition. The other one is the addition of this effect into the equation as a volumetric heat source. In the first case, it is assumed that the tissue has a high absorbency. As a result of this assumption, the laser beam is considered to be absorbed at a very small depth. This situation leads to occurrence of a heat flux on the surface. Beer-Lambert law can be used to calculate this heat flux [71,72].

In the other method, different approaches can be used. One of these approaches, the equation which directly explains this radiation effect is added to the model as a volumetric heat source [73]. The other approach assumes that the tissue has strongly scattering characteristic. In this case, radiation effect can be calculated by using diffusion theory and added as a volumetric heat source. For calculation of the unknown coefficients in diffusion theory, Monte Carlo simulation is preferred [74][75].

1.4 Aim and Scope of the Thesis

Several studies have been conducted to understand the heat transfer within the tissue. It is important to gain a better understanding of heat transfer in laser tissue interaction to prevent possible errors and to benefit from it more in laser treatment. Therefore, in this study, a mathematical model will be derived from the basic energy equation. In the derivation of this model, it is going to be done by using porous media assumption which is the subject of many researches. In the derivation phase, it is aimed to obtain results that are more realistic by minimizing the assumptions made. At the same time, the terms that will make the calculation difficult will be reduced by using assumptions. In this way, it is aimed to create an easy to use and general mathematical model. The results of this model will be compared with the other models in the literature.

CHAPTER 2

THEORY AND MODELING

2.1 Theory

In order to gain understanding of laser and tissue interaction, basic energy transfer mechanism should be examined. The energy conservation equation with temperature formulation is given below [76].

$$\rho c_p \frac{DT}{Dt} = \nabla \cdot (k \nabla T) + T \beta \frac{Dp}{Dt} + \nabla v : \tau + Q_s \quad (2.1)$$

Compression and expansion work and viscous dissipation terms are small enough in most convective heat transfer processes, so that they can be neglected. If they are neglected, the general form of equation can be reduced to

$$\rho c_p \left(\frac{\partial T}{\partial t} + \nabla \cdot (u \cdot T) \right) = \nabla \cdot (k \nabla T) + Q_s \quad (2.2)$$

The living tissue has a complex structure. Heat transfer mechanism in this structure is affected by factors such as heat conduction in the tissue, heat convection due to blood flow and blood perfusion. It is therefore difficult to understand and explain the details by direct application of this equation where the tissue is considered to be a single homogeneous structure. The tissue can be considered as porous media when the general structure of it is considered [77]. This structure can be expressed in two regions: intravascular region and extravascular region (Figure 2.1). Intravascular region is composed of voids and blood. The extravascular region consists of biological cells and other solid parts. Therefore, the tissue structure can be approximated as fluid saturated porous media.

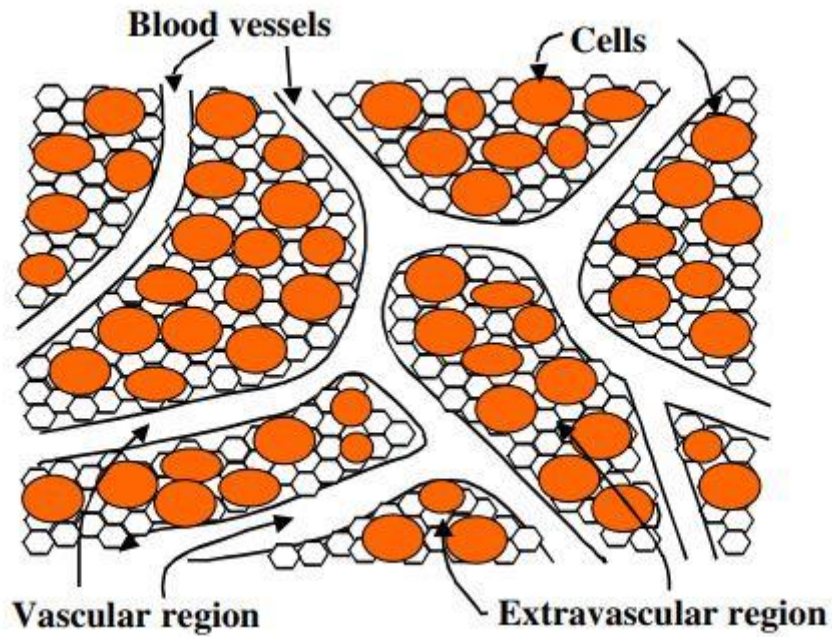


Figure 2.1. Representation of Biological Tissue [78]

The energy equation can be derived separately for these two regions. These equations are microscale and take into account the microstructure effects. In order to apply the equation in general and to use macroscopic properties, these equations must be valid in macroscale. For this reason, the equations written in microscale must be scaled up to the macroscale. This process can be made by the applied volume averaging method.

2.1.1 Volume –Averaging Theory

A control volume that considers fluid saturated porous media is defined for this operation, as shown in Figure 2.2. This volume needs to be a very large volume from a microscopic point of view and a very small volume from a macroscopic point of view.

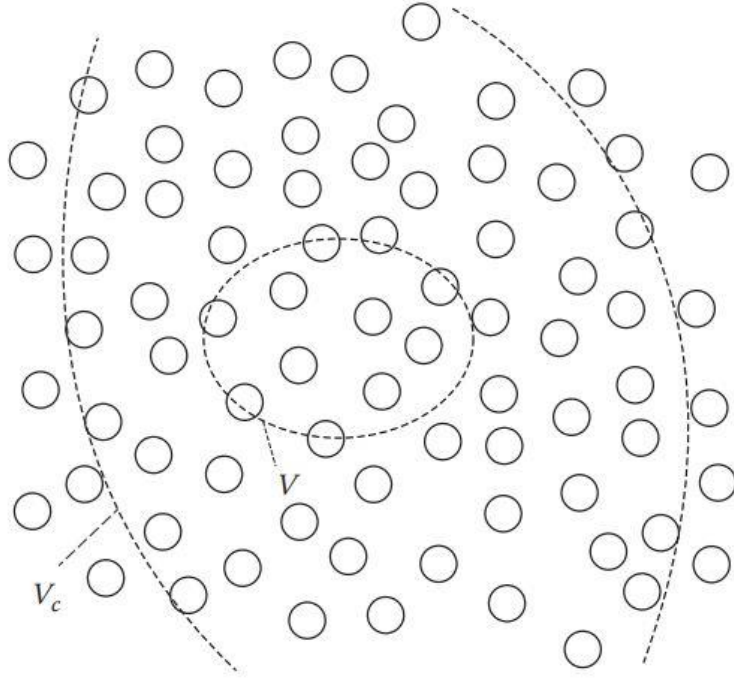


Figure 2.2. Example of Control Volume in Porous Media [79]

Volume average of a variable ϕ is defined as [79]

$$\langle \phi \rangle = \frac{1}{V} \int_V \phi dV \quad (2.3)$$

Intrinsic average on the other hand, which is another type average, is defined as [79]

$$\langle \phi \rangle^f = \frac{1}{V_f} \int_{V_f} \phi dV \quad (2.4)$$

Porosity and relation of two averages are [79]

$$\langle \phi \rangle = \varepsilon \langle \phi \rangle^f \quad (2.5a)$$

$$\text{where } \varepsilon = V_f / V \quad (2.5b)$$

A variable can be expressed as intrinsic average and the spatial deviation of it [79]:

$$\phi = \langle \phi \rangle^f + \tilde{\phi} \quad (2.6)$$

Spatial average relationships can be represented as following [79],

$$\langle \varphi_1 \varphi_2 \rangle^f = \langle \varphi_1 \rangle^f \langle \varphi_2 \rangle^f + \langle \tilde{\varphi}_1 \tilde{\varphi}_2 \rangle^f \quad (2.7)$$

$$\langle \nabla \varphi \rangle = \nabla \langle \varphi \rangle + \frac{1}{V} \int_{A_{int}} \varphi \, ndA \quad (2.8)$$

$$\langle \nabla \cdot \varphi \rangle = \nabla \cdot \langle \varphi \rangle + \frac{1}{V} \int_{A_{int}} \varphi \, ndA \quad (2.9)$$

$$\langle \nabla \varphi \rangle^f = \frac{1}{\varepsilon} \nabla (\varepsilon \langle \varphi \rangle^f) + \frac{1}{V^f} \int_{A_{int}} \varphi \, ndA \quad (2.10)$$

$$\left\langle \frac{\partial \varphi}{\partial t} \right\rangle = \frac{\partial \langle \varphi \rangle}{\partial t} \quad (2.11)$$

Although separate equations are created for the intravascular region and the extravascular region, these two regions are in interaction. Microscopically, local thermal equilibrium conditions provide various limitations. As a result of this interaction, two conditions may occur. One of them is the formation of local thermal equilibrium condition. Another one is the formation of local thermal nonequilibrium condition. From the microscopic point of view, local thermal equilibrium conditions are limited to certain situations [80]. For instance, the local thermal equilibrium condition does not hold when there is a high heat generation [81]. Another limitation is that this assumption is not correct when the liquid having the high Reynold number is present [82]. Therefore, mathematical model is derived under the assumption of local thermal nonequilibrium to obtain a more general model that is applicable for wider range of circumstances.

Based on the approach explained above, a general mathematical model can be written describing the heat transfer mechanism within the tissue. The laser interaction can be incorporated to this model by taking into account the optical properties of the tissue. There are two main approaches can be followed; one is the assumption that the tissue has a highly absorbing behavior. The other approach is the assumption that the tissue behaves as a medium with strongly scattering property.

For the highly absorbing case, it is assumed that the incident radiation is absorbed in the tissue at a very small depth and the scattering within the tissue is neglected. The amount of the fluence rate calculated by using Beer-Lambert's law [83].

$$\vartheta(z) = (1 - R_s)\vartheta_{in}e^{-\mu_t z} \cong (1 - R_s)\vartheta_{in}e^{-\mu_a z} \quad (2.12)$$

where $\vartheta(z)$ is the fluence rate in tissue, R_s is specular reflectance, ϑ_{in} is laser irradiance, μ_t is attenuation coefficient, μ_a is absorption coefficient. In the strongly scattering case, the radiation increases the temperature of the tissue by penetrating into the tissue. The fluence rate can be calculated by the diffusion theory [73,74].

$$\vartheta(z) = \vartheta_{in} \left[C_1 e^{\left(-\frac{D_1 z}{\delta}\right)} - C_2 e^{\left(-\frac{D_2 z}{\delta}\right)} \right] \quad (2.13)$$

$$\text{where} \quad \delta = \frac{1}{\sqrt{3\mu_a[\mu_a + \mu_s']}} \quad \text{for } \mu_a \ll \mu_s \quad (2.14)$$

C_1 , D_1 , C_2 , and D_2 are unknown coefficients of diffusion theory, δ is effective optical penetration depth, μ_s is scattering coefficient, μ_s' is reduced scattering coefficient. Monte Carlo simulations can be used to determine unknown coefficients of this theory. Gardner et al. [84] determined these unknown coefficients for laser tissue interaction case by using Monte Carlo simulation. The determined empirical expressions of unknown coefficients are as follows.

$$C_1 = 3.09 + 5.44R_d - 2.12e^{(-21.5R_d)} \quad (2.15)$$

$$D_1 = 1 - \left(1 - \frac{1}{\sqrt{3}}\right) e^{(-20.1R_d)} \quad (2.16)$$

$$C_2 = 2.09 - 1.47R_d - 2.12e^{(-21.5R_d)} \quad (2.17)$$

$$D_2 = 1.63e^{(3.4R_d)} \quad (2.18)$$

Heat generation due to Laser irradiance is added to the equation as a volumetric heat source for both highly absorbed and strongly scattering cases. The value of the heat source depends on the absorption coefficient and the fluence rate.

$$Q(z) = \mu_a \vartheta(z) \quad (2.19)$$

2.2 Governing Equations

Living tissue can be described with two separate regions, intravascular and extravascular. At this point, fluid is assumed incompressible and Newtonian, and all properties are assumed constant. In addition to these, metabolic heat generation for blood is neglected. As a result of these assumptions, thermal energy equations for these regions are obtained by using equation (2.2).

$$\rho_i c_{p,i} \left(\frac{\partial T_i}{\partial t} + \nabla \cdot (u_i \cdot T_i) \right) = k_i \nabla^2 T_i + Q \quad (2.20)$$

$$\rho_e c_{p,e} \left(\frac{\partial T_e}{\partial t} + \nabla \cdot (u_e \cdot T_e) \right) = k_e \nabla^2 T_e + Q + Q_m \quad (2.21)$$

These two regions have different characteristics. For this reason, it is necessary to consider them separately in derivation of valid equations in the microscale. The equations (2.20) and (2.21) that take microscopic features into account can scale up to the macroscale using volume average theory.

Taking integral of equation (2.20) for applying volume averaging method to intravascular region;

$$\frac{1}{V} \int_V \rho_i c_{p,i} \frac{\partial T_i}{\partial t} + \frac{1}{V} \int_V \rho_i c_{p,i} \nabla \cdot (u_i \cdot T_i) = \frac{1}{V} \int_V k_i \nabla^2 T_i + \frac{1}{V} \int_V Q_i \quad (2.22)$$

Using relations in the equation (2.3) and (2.5a), equation (2.22) can be expressed as;

$$\langle \rho_i c_{p,i} \frac{\partial T_i}{\partial t} \rangle + \langle \rho_i c_{p,i} \nabla \cdot (u_i \cdot T_i) \rangle = \langle k_i \nabla^2 T_i \rangle + \langle Q_i \rangle \quad (2.23)$$

This derivation can be reached more easily by examining the terms separately in equation (2.23). Firstly, using the equation (2.11), the first term in the left hand side of equation (2.23) can be expressed as following;

$$\langle \rho_i c_{p,i} \frac{\partial T_i}{\partial t} \rangle = \varepsilon \rho_i c_{p,i} \frac{\partial \langle T_i \rangle^i}{\partial t} \quad (2.24)$$

Secondly, the second term in the left hand side of equation (2.24) can be simplified by using relations presented in the equations (2.5a), (2.7) and (2.9).

$$\begin{aligned} \langle \rho_i c_{p,i} \nabla \cdot (u_i \cdot T_i) \rangle &= \rho_i c_{p,i} \varepsilon \nabla \cdot \langle u_i \cdot T_i \rangle^i + \frac{1}{V} \int_{A_{int}} \rho_i c_{p,i} (u_i T_i) n dA \\ &= \rho_i c_{p,i} \varepsilon \nabla \cdot \langle u_i \rangle^i \langle T_i \rangle^i + \rho_i c_{p,i} \varepsilon \nabla \cdot \langle \tilde{u}_i \cdot \tilde{T}_i \rangle^i + \frac{1}{V} \int_{A_{int}} \rho_i c_{p,i} (u_i T_i) n dA \end{aligned} \quad (2.25)$$

When the terms of equation (2.25) are evaluated individually, the second term at the right hand side is dispersion heat flux. Although it increases thermal conductivity of tissue at deep layers, effect on temperature is very low. This effect is shown in the Figure 2.3. Thermal dispersion term can be neglected [66].

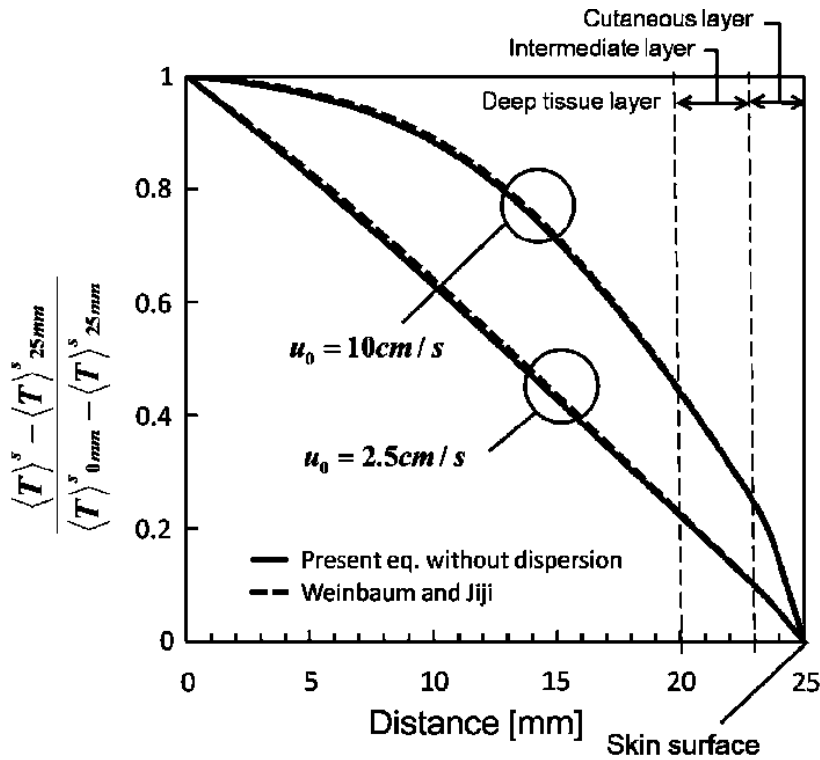


Figure 2.3 Thermal dispersion effect on the other models in literature [66].

$$\rho_i c_{p,i} \varepsilon \nabla \cdot \langle \tilde{u}_i \cdot \tilde{T}_i \rangle^i \cong 0 \quad (2.26)$$

Fluid transfer in the circulatory system occurs between intravascular and extravascular region. The amount of fluid leaving and entering the intravascular region is in equilibrium. At the same time, it can be assumed that the temperature of blood entering the intravascular region is equation to the temperature of the extravascular region. Hence, the third term on the right hand side of the equation can be expressed by blood perfusion [61].

$$\frac{1}{V} \int_{A_{int}} \rho_i c_{p,i} (u_i T_i) n dA = \rho_i c_{p,i} \omega (\langle T_i \rangle^i - \langle T_e \rangle^e) \quad (2.27)$$

Consequent of these, final version of equation (2.24) will be;

$$\langle \rho_i c_{p,i} \nabla \cdot (u_i \cdot T_i) \rangle = \rho_i c_{p,i} \varepsilon \nabla \cdot \langle u_i \rangle^i \langle T_i \rangle^i + \rho_i c_{p,i} \omega (\langle T_i \rangle^i - \langle T_e \rangle^e) \quad (2.28)$$

Thirdly, using relations in the equations (2.5a) and (2.8), the first term in the right hand side of equation (2.23) will be;

$$\begin{aligned} \langle k_i \nabla^2 T_i \rangle &= \varepsilon k_i \nabla \cdot \langle \nabla T_i \rangle^i + \frac{1}{V} \int_{A_{int}} k_i (\nabla T_i) n dA \\ &= \varepsilon k_i \nabla \cdot \left(\langle \nabla T_i \rangle^i + \frac{1}{V} \int_{A_{int}} T_i n dA \right) + \frac{1}{V} \int_{A_{int}} k_i (\nabla T_i) n dA \end{aligned} \quad (2.29)$$

Second term at the right hand side of equation (2.29) is called tortuosity heat flux. This term refers to the tendency of the heat flux to circulation. It is small enough to neglect when convection is much higher to compare with conduction [85]. Third term at the right hand side of equation (2.29) expresses interfacial heat transfer and it can be evaluated by Newton's law of cooling.

$$\frac{1}{V} \int_{A_{int}} k_i (\nabla T_i) n dA = a_i h_i (\langle T_e \rangle^e - \langle T_i \rangle^i) \quad (2.30)$$

Consequent of these manipulations, the final version of equation (2.29) will be;

$$\langle k_i \nabla^2 T_i \rangle = \varepsilon k_i \nabla^2 \langle T_i \rangle^i + a_i h_i (\langle T_e \rangle^e - \langle T_i \rangle^i) \quad (2.31)$$

For the intravascular region, the macroscale energy equation can be obtained by substituting equations (2.24), (2.28) and (2.31) into the equation (2.23).

$$\varepsilon \rho_i c_{p,i} \frac{\partial \langle T_i \rangle^i}{\partial t} + \rho_i c_{p,i} \varepsilon \nabla \cdot \langle u_i \rangle^i \langle T_i \rangle^i = k_{eff,i} \nabla^2 \langle T_i \rangle^i + G (\langle T_e \rangle^e - \langle T_i \rangle^i) + \varepsilon \langle Q_i \rangle^i \quad (2.32)$$

$$\text{where} \quad k_{eff,i} = \varepsilon k_i \quad (2.33a)$$

$$G = \rho_i c_{p,i} \omega + a_i h_i \quad (2.33b)$$

The same procedure can be applied to the extravascular region. For this region, porosity could be expressed in terms of porosity intravascular region.

$$\varepsilon_e = 1 - \varepsilon \quad (2.34)$$

$$\text{where} \quad \varepsilon_i + \varepsilon_e = 1 \quad (2.35)$$

Taking the integral of equation (2.22) for applying volume averaging method to extravascular region;

$$\frac{1}{V} \int_V \rho_e c_{p,e} \frac{\partial T_e}{\partial t} + \frac{1}{V} \int_V \rho_e c_{p,e} \nabla \cdot (u_e \cdot T_e) = \frac{1}{V} \int_V k_e \nabla^2 T_e + \frac{1}{V} \int_V Q_e + \frac{1}{V} \int_V Q_{m,e} \quad (2.36)$$

Using relations in equations (2.3) and (2.5a), equation (2.36) can be expressed as;

$$\langle \rho_e c_{p,e} \frac{\partial T_e}{\partial t} \rangle + \langle \rho_e c_{p,e} \nabla \cdot (u_e \cdot T_e) \rangle = \langle k_e \nabla^2 T_e \rangle + \langle Q_e \rangle + \langle Q_{m,e} \rangle \quad (2.37)$$

The derivation for extravascular region can be obtained more easily by examining the terms separately in equation (2.37). Firstly, using the relation presented in equation (2.11), the first term in the left hand side of equation (2.37) can be expressed as following;

$$\langle \rho_e c_{p,e} \frac{\partial T_e}{\partial t} \rangle = (1 - \varepsilon) \rho_e c_{p,e} \frac{\partial \langle T_e \rangle^e}{\partial t} \quad (2.38)$$

Secondly, the second term in the left hand side of equation (2.37) can be simplified by using relations given in equations (2.5a), (2.7) and (2.9).

$$\begin{aligned}
\langle \rho_e c_{p,e} \nabla \cdot (u_e \cdot T_e) \rangle &= \rho_e c_{p,e} (1 - \varepsilon) \nabla \cdot \langle u_e \cdot T_e \rangle^e + \frac{1}{V} \int_{A_{int}} \rho_e c_{p,e} (u_e T_e) n dA \\
&= \rho_e c_{p,e} (1 - \varepsilon) \nabla \cdot \langle u_e \rangle^e \langle T_e \rangle^e + \rho_e c_{p,e} \varepsilon \nabla \cdot \langle \tilde{u}_e \cdot \tilde{T}_e \rangle^e + \frac{1}{V} \int_{A_{int}} \rho_e c_{p,e} (u_e T_e) n dA
\end{aligned} \tag{2.39}$$

First term at the right hand side of equation (2.39) is a convection term. Since the flow is steady and incompressible, it is assumed that the inlet and outlet flow rates are equal to each other. For extravascular region, this term can be neglected because intrinsic average of velocity is zero. Second term at the right hand side of equation (2.39) is dispersion heat flux. It also can be neglected due to intrinsic average of velocity is zero.

The third term in the right hand side of equation (2.39) has the same characteristic with the third term in the right hand side of equation (2.25). Therefore, the same assumption can be made [61]. Using this assumption, third term in the right hand side of equation (2.39) will be;

$$\frac{1}{V} \int_{A_{int}} \rho_e c_{p,e} (u_e T_e) n dA = \rho_i c_{p,i} \omega (\langle T_e \rangle^e - \langle T_i \rangle^i) \tag{2.40}$$

Consequent of these, the final version of equation (2.39) will be;

$$\langle \rho_e c_{p,e} \nabla \cdot (u_e \cdot T_e) \rangle = \rho_i c_{p,i} \omega (\langle T_e \rangle^e - \langle T_i \rangle^i) \tag{2.41}$$

Thirdly, using relations in equations (2.5a) and (2.8), the first term in the right hand side of equation (2.37) will be;

$$\begin{aligned}
\langle k_e \nabla^2 T_e \rangle &= (1 - \varepsilon) k_e \nabla \cdot \langle \nabla T_e \rangle^e + \frac{1}{V} \int_{A_{int}} k_e (\nabla T_e) n dA \\
&= \varepsilon k_e \nabla \cdot \left(\langle \nabla T_e \rangle^e + \frac{1}{V} \int_{A_{int}} T_e n dA \right) + \frac{1}{V} \int_{A_{int}} k_e (\nabla T_e) n dA
\end{aligned} \tag{2.42}$$

The second term at the right hand side of equation (2.42) is tortuosity heat flux. The situation for the intravascular region is valid within this region. Therefore it is neglected [85]. The third term at the right hand side of equation (2.42) expresses interfacial heat transfer and it can be evaluated by Newton's law of cooling.

$$\frac{1}{V} \int_{A_{int}} k_e (\nabla T_e) n dA = a_i h_i (\langle T_i \rangle^i - \langle T_e \rangle^e) \quad (2.43)$$

After these mathematical manipulations, the final version of equation (2.42) will be;

$$\langle k_e \nabla^2 T_e \rangle = (1 - \varepsilon) k_e \nabla^2 \langle T_e \rangle^e + a_i h_i (\langle T_i \rangle^i - \langle T_e \rangle^e) \quad (2.44)$$

For the extravascular region, the macro-scale energy equation can be obtained by substituting equations (2.38), (2.41) and (2.44) into equation (2.37).

$$(1 - \varepsilon) \rho_e c_{p,e} \frac{\partial \langle T_e \rangle^e}{\partial t} = k_{eff,e} \nabla^2 \langle T_e \rangle^e + G (\langle T_i \rangle^i - \langle T_e \rangle^e) \\ + (1 - \varepsilon) \langle Q_e \rangle^e + (1 - \varepsilon) \langle Q_{m,e} \rangle^e \quad (2.45)$$

$$\text{where } k_{eff,e} = (1 - \varepsilon) k_e \quad (2.46a)$$

$$G = \rho_i c_{p,i} \omega + a_i h_i \quad (2.46b)$$

Coupling factor between blood and tissue, G, consists of interfacial heat transfer and blood perfusion term. Interfacial heat transfer can be calculated by Nusselt number and vessel properties [61].

$$a_i h_i = \frac{4\varepsilon k_b}{(2R)^2} Nu \quad (2.47)$$

When it is assumed that blood flow is in fully developed flow regime, Nusselt number can be approximated as 4.93 based on the Darcy flow model in porous media [86,87]. Using this assumption and equation (2.47) the coupling factor will be;

$$G = \rho_i c_{p,i} \omega + 4.93 \frac{4\varepsilon k_b}{(2D)^2} \quad (2.48)$$

As a result of two separate reviews, energy equation for intravascular and extravascular region can be written in macroscale perspective as following;

For intravascular region,

$$\varepsilon\rho_i c_{p,i} \frac{\partial T_i}{\partial t} + \varepsilon\rho_i c_{p,i} u_i \cdot \nabla T_i = k_{eff,i} \nabla^2 T_i + G(T_e - T_i) + \varepsilon Q_i \quad (2.49)$$

For extravascular region,

$$(1 - \varepsilon)\rho_e c_{p,e} \frac{\partial T_e}{\partial t} = k_{eff,e} \nabla^2 T_e + G(T_i - T_e) + (1 - \varepsilon)Q_e + (1 - \varepsilon)Q_{m,e} \quad (2.50)$$

To create a general form of equation, it is required to combine two equations. Under local thermal nonequilibrium condition, these equations can be combined. For this propose, rearranging equation (2.50);

$$T_i = \frac{(1 - \varepsilon)\rho_e c_{p,e} \partial T_e}{G} - \frac{k_{eff,e} \nabla^2 T_e}{G} + T_e - \frac{(1 - \varepsilon)}{G} Q_e - \frac{(1 - \varepsilon)}{G} Q_{m,e} \quad (2.51)$$

Substituting equation (2.51) in equation (2.49);

$$\begin{aligned} & \frac{\varepsilon\rho_i c_{p,i}(1 - \varepsilon)\rho_e c_{p,e} \partial^2 T_e}{G} - \frac{\varepsilon\rho_i c_{p,i} k_{eff,e} \partial}{G} (\nabla^2 T_e) + \varepsilon\rho_i c_{p,i} \frac{\partial T_e}{\partial t} - \frac{\varepsilon\rho_i c_{p,i}(1 - \varepsilon)}{G} \frac{\partial Q_e}{\partial t} \\ & - \frac{\varepsilon\rho_i c_{p,i}(1 - \varepsilon)}{G} \frac{\partial Q_{m,e}}{\partial t} + \frac{\varepsilon\rho_i c_{p,i}(1 - \varepsilon)\rho_e c_{p,e} u_i \cdot \nabla \left(\frac{\partial T_e}{\partial t} \right) - \frac{\varepsilon\rho_i c_{p,i} k_{eff,e} u_i \cdot \nabla^3 T_e + \varepsilon\rho_i c_{p,i} u_i \cdot \nabla T_e}{G} \\ & - \frac{\varepsilon\rho_i c_{p,i}(1 - \varepsilon)}{G} u_i \cdot \nabla Q_e - \frac{\varepsilon\rho_i c_{p,i}(1 - \varepsilon)}{G} u_i \cdot \nabla Q_{m,e} = \frac{(1 - \varepsilon)\rho_e c_{p,e} k_{eff,i} \nabla^2 \left(\frac{\partial T_e}{\partial t} \right) - \frac{k_{eff,e} k_{eff,i} \nabla^4 T_e}{G} \\ & + k_{eff,i} \nabla^2 T_e - \frac{(1 - \varepsilon)k_{eff,i} \nabla^2 Q_e - (1 - \varepsilon)k_{eff,i} \nabla^2 Q_{m,e} + G T_e - (1 - \varepsilon)\rho_e c_{p,e} \frac{\partial T_e}{\partial t} + k_{eff,e} \nabla^2 T_e}{G} \\ & - G T_e + (1 - \varepsilon)Q_e + (1 - \varepsilon)Q_{m,e} + \varepsilon Q_i \end{aligned} \quad (2.52)$$

Rearranging equation (2.52);

$$\begin{aligned} & \frac{\varepsilon\rho_i c_{p,i}(1 - \varepsilon)\rho_e c_{p,e} \partial^2 T_e}{G} + (\varepsilon\rho_i c_{p,i} + (1 - \varepsilon)\rho_e c_{p,e}) \frac{\partial T_e}{\partial t} = - \frac{k_{eff,e} k_{eff,i} \nabla^4 T_e}{G} \\ & + \frac{\varepsilon\rho_i c_{p,i} k_{eff,e} u_i \cdot \nabla^3 T_e + (k_{eff,e} + k_{eff,i}) \nabla^2 T_e + \left(\frac{\varepsilon\rho_i c_{p,i} k_{eff,e} + (1 - \varepsilon)\rho_e c_{p,e} k_{eff,i}}{G} \right) \frac{\partial}{\partial t} (\nabla^2 T_e)}{G} \\ & - \frac{\varepsilon\rho_i c_{p,i}(1 - \varepsilon)\rho_e c_{p,e} u_i \cdot \nabla \left(\frac{\partial T_e}{\partial t} \right) - \varepsilon\rho_i c_{p,i} u_i \cdot \nabla T_e - \frac{(1 - \varepsilon)k_{eff,i} \nabla^2 Q_e - \frac{(1 - \varepsilon)k_{eff,i} \nabla^2 Q_{m,e}}{G}}{G}}{G} \\ & + \frac{\varepsilon\rho_i c_{p,i}(1 - \varepsilon)}{G} u_i \cdot \nabla Q_e + \frac{\varepsilon\rho_i c_{p,i}(1 - \varepsilon)}{G} u_i \cdot \nabla Q_{m,e} + \frac{\varepsilon\rho_i c_{p,i}(1 - \varepsilon)}{G} \frac{\partial Q_e}{\partial t} + \frac{\varepsilon\rho_i c_{p,i}(1 - \varepsilon)}{G} \frac{\partial Q_{m,e}}{\partial t} \\ & + (1 - \varepsilon)Q_e + (1 - \varepsilon)Q_{m,e} + \varepsilon Q_i \end{aligned} \quad (2.53)$$

The final form of the obtained equation has several complicated terms. Some terms in the equation (2.53) can be simplified by making some assumptions and applying algebraic relations. First of all, the first term at the right hand side of equation (2.54) is a bi-harmonic term. This term is very small compared to other terms in the equation (2.53), so that it can be neglected [88].

It can be assumed that extravascular region is tissue and intravascular region is blood. So that, the final version of equation based on porous media approach under local thermal nonequilibrium conditions is found as;

$$\begin{aligned}
& \frac{\varepsilon\rho_b c_{p,b}(1-\varepsilon)\rho_t c_{p,t}}{G} \frac{\partial^2 T_t}{\partial t^2} + (\varepsilon\rho_b c_{p,b} + (1-\varepsilon)\rho_t c_{p,t}) \frac{\partial T_t}{\partial t} = (k_{eff,t} + k_{eff,b}) \nabla^2 T_t \\
& + \frac{\varepsilon\rho_b c_{p,b} k_{eff,t}}{G} u_b \cdot \nabla^3 T_t + \left(\frac{\varepsilon\rho_b c_{p,b} k_{eff,t} + (1-\varepsilon)\rho_t c_{p,t} k_{eff,b}}{G} \right) \frac{\partial}{\partial t} (\nabla^2 T_t) \\
& - \frac{\varepsilon\rho_b c_{p,b}(1-\varepsilon)\rho_t c_{p,t}}{G} u_b \cdot \nabla \left(\frac{\partial T_t}{\partial t} \right) - \varepsilon\rho_b c_{p,b} u_b \cdot \nabla T_t - \frac{(1-\varepsilon)k_{eff,b}}{G} \nabla^2 Q_t \\
& - \frac{(1-\varepsilon)k_{eff,b}}{G} \nabla^2 Q_{m,t} + \frac{\varepsilon\rho_b c_{p,b}(1-\varepsilon)}{G} u_b \cdot \nabla Q_t + \frac{\varepsilon\rho_b c_{p,b}(1-\varepsilon)}{G} u_b \cdot \nabla Q_{m,t} \\
& + \frac{\varepsilon\rho_b c_{p,b}(1-\varepsilon)}{G} \frac{\partial Q_t}{\partial t} + \frac{\varepsilon\rho_b c_{p,b}(1-\varepsilon)}{G} \frac{\partial Q_{m,t}}{\partial t} + (1-\varepsilon)Q_t + (1-\varepsilon)Q_{m,t} \\
& + \varepsilon Q_b
\end{aligned} \tag{2.54}$$

CHAPTER 3

SOLUTION METHODOLOGY

Mathematical models explaining the heat transfer on the tissue can be solved by analytical and numerical methods. Since equation (2.54) has a complex structure, it would be more appropriate to solve it with numerical methods. There are several approaches in numerical methods. One of these approaches is the finite volume method. For the finite volume method, the control volume is divided into very small volumes. The governing equations are written for each volume and these equations are solved simultaneously. As a result, the desired values are calculated for all small volumes. Owing to this method, conservation properties of the equations, which is the energy equation for this study, are ensured as flux balance is satisfied for all small volumes as well as the complete domain. It is one of the advantages of the finite volume method over other discretization methods.

In this study, one-dimensional analysis will be made. A simpler and faster solution can be created with one-dimensional analysis. When the size of the laser beam is greater than the area where the laser is intended to be applied, a one-dimensional model provides an adequate solution.

3.1 Numerical Solution Procedure

Before discretization process, the equation (2.54) can be simplified by using some assumptions. Firstly, in some cases, the volumetric heat source values occurred by laser irradiance can be accepted to be the same for tissue and blood regions. Secondly, it can be assumed that the metabolic heat source has a fixed value. Thirdly, it can be accepted that the vessels in the tissue are arranged parallel to the tissue surface, as shown Figure 3.1. This causes the blood velocity vector to be perpendicular to the temperature gradient vector and laser irradiance vector. As a result, the second, fourth, fifth and eighth terms on the right in equation (2.54) becomes zero. Finally, the coefficient of the second-order derivative of this volumetric heat source has a very small value for the case of strong scattering case compared to the coefficients of other terms. On the other hand, this coefficient has a very high value for the highly absorbed case compared to the coefficient of other terms. It is physically unreasonable that this value is so high for the highly absorbed case. Therefore the sixth term on the right in equation (2.54) is ignored.

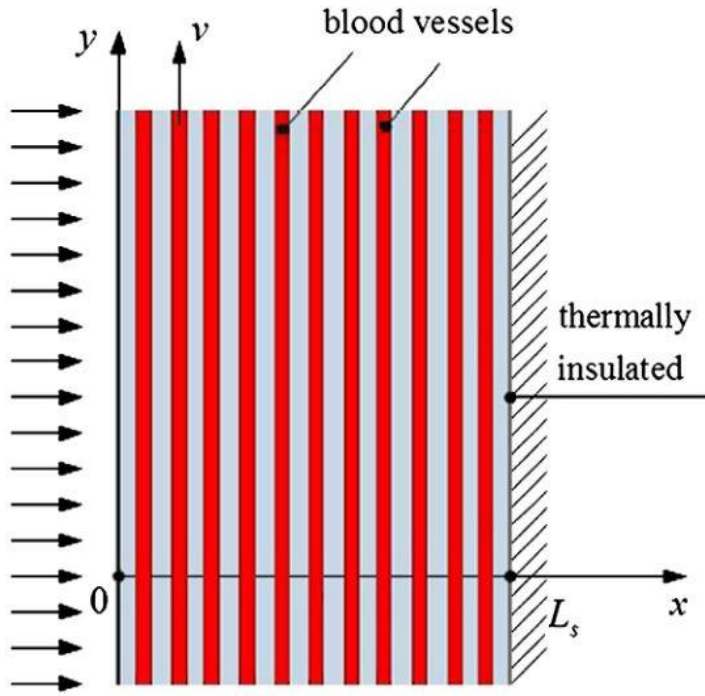


Figure 3.1. Blood Vessel Alignment in Tissue[89]

Consequent of these assumptions, equation (2.54) is simplified as follows.

$$\begin{aligned}
 & \frac{\varepsilon\rho_b c_{p,b}(1-\varepsilon)\rho_t c_{p,t}}{G} \frac{\partial^2 T_t}{\partial t^2} + (\varepsilon\rho_b c_{p,b} + (1-\varepsilon)\rho_t c_{p,t}) \frac{\partial T_t}{\partial t} = (k_{eff,t} + k_{eff,b}) \nabla^2 T_t \\
 & + \left(\frac{\varepsilon\rho_b c_{p,b} k_{eff,t} + (1-\varepsilon)\rho_t c_{p,t} k_{eff,b}}{G} \right) \frac{\partial}{\partial t} (\nabla^2 T_t) + \frac{\varepsilon\rho_b c_{p,b}(1-\varepsilon)}{G} \frac{\partial Q}{\partial t} + Q \\
 & (1-\varepsilon)Q_m
 \end{aligned} \tag{3.1}$$

3.1.1 Discretization of Governing Equations

In one-dimensional analysis, as seen in figure 3.2, the tissue can be defined as a control volume with L length. Laser irradiance is considered to be applied to the left surface whereas the right surface is considered thermally isolated.

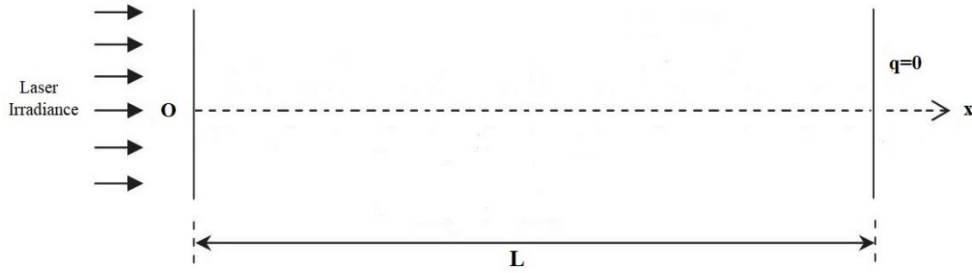


Figure 3.2. Physical Model of 1D Analysis

For discretization process, control volume is divided into $n+1$ number cell volume. Cells at both ends have the half size of cell volume. Except for the first and last cell, grid points are placed at the center of these volumes. For the first and last cell, grid point is located at their boundary. Neighbors of grid point P are named as E and W which means east and west neighbor, respectively. Faces of grid point P also are named as e and w which means east and west face, respectively. First and last cell length are half of Δx whereas other cell's length are Δx , as shown figure 3.3.

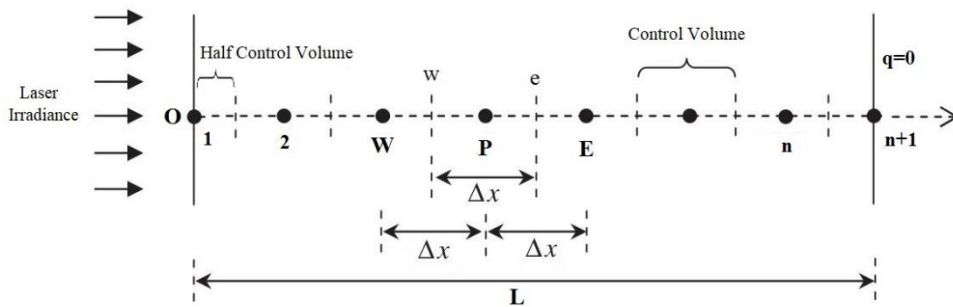


Figure 3.3. Grid System of 1D Analysis

In the solution phase of Equation (3.1), appropriate initial and boundary condition are required. In this study, the initial temperature is considered constant.

$$\text{When } t = 0 \quad T_t = \text{constant} \quad \text{for } 0 \leq x \leq L \quad (3.2)$$

Laser irradiance effect for highly absorbed and strongly scattering cases is added to the equation as a volumetric heat source. Therefore; The boundary conditions are defined independently of the laser irradiance. However, natural convection, surface radiation and evaporative cooling affect the left surface of the control volume. Heat losses due to

radiation and evaporative cooling at the surface are ignored. Convection heat transfer can be found using Newton's Cooling law. As a result, boundary conditions are as follows.

$$-k_{eff} \frac{\partial T_t}{\partial x} = h_e(T_\infty - T_t) \quad \text{When } 0 \leq t \leq t_{total} \quad \text{at } x = 0 \quad (3.3)$$

$$-k_{eff} \frac{\partial T_t}{\partial x} = 0 \quad \text{When } 0 \leq t \leq t_{total} \quad \text{at } x = L \quad (3.4)$$

where h_e is coefficient of convection heat transfer [W/m²K], T_∞ is ambient temperature [C°], T_t is tissue temperature at left surface [C°].

For applying finite volume method, integration of equation (3.1) is made over control volume of grid P with time step from t to t+Δt. Then, Crank Nicolson method is applied to this equation to obtain the discretized form of the equation. Details of this procedure is given in Appendix A. To find the temperature, the discretized equation must be simultaneously solved for all cells. The obtained equations can be solved by using Gauss elimination method. Using this method, the temperature values of each time step in all cells are calculated.

3.2 Convergence Study

In this study, an numerical method is used for the solution. Therefore, the convergence of the results must be checked. A two-stage test is applied to control the approach of the results. In the first stage, the convergence test is made by taking into account the grid dimensions. The time step to be used at this stage will be selected taking into account similar studies in the literature. In the second step, the effect of the time step is examined by using the grid size specified in the previous stage.

This convergence studies will be done through working cases. In this study, results obtained from the derived model are compared with the results of the experimental study conducted with pig skin by Museux et al. [90]. In the study of Museux et al., the heat values on the tissue are calculated mathematically as well as the experimental study. Due to similarity of the properties of pig skin with properties of human skin, Museux et al. use properties of human skin. Although human skin shows similar properties with pig skin, slight differences are observed. In this study, pig skin properties are used to obtain better results. Therefore, the values used in this study and the values in the study of Museux et

al. differ. However, in the case of incomplete or inconsistent properties of pig skin in the literature, the properties of human skin are used.

First, the general characteristics of the skin should be evaluated. The skin has a multi-layered structure with different properties. For a simpler solution, it can be assumed that the tissue has a single-layer structure [91–94]. Therefore, a single-layer skin model is used in this study. In the literature, the values of the skin are given for multi-layer skin or single-layer skin. In order to apply the properties of multi-layer leather in a single layer structure, the values must be modified. The method of weighted average based on the thickness of layers is applied for this modification. The values obtained by this method are used when the properties of the single-layer structure were missing or to support the properties of the single-layer structure. The thermophysical properties used in this study are given in the Table 3.1.

Table 3.1 Thermophysical properties.

Parameters	Values	Unit	References
Tissue Density	1081.6	kg/m^3	[95–97]
Tissue Specific Heat	3238.5	$J/kg.K$	[95,96,98]
Thermal Conductivity of Tissue	0.4108	$W/m.K$	[95–100]
Blood Density	1060	kg/m^3	[101–105]
Blood Specific Heat	3770	$J/kg.K$	[101–104]
Thermal Conductivity of Blood	0.5066	$W/m.K$	[100,102,105–107]
Blood Perfusion	0.00112	$m^3 / m^3.s$	[37,101,103,108,109]
Diameter of Blood Vessel	1.14	mm	[102,110–112]
Porosity	0.0060	-	[102,110,112–114]
Metabolic Heat Generation	368.1	W/m^3	[104,115–119]
Coefficient of Convection Heat Transfer	10	W/m^2K	[90]
Ambient Temperature	22.35	C^0	[90]

Skin tissue shows different optical properties in the laser of different wavelengths. In study of Museux et al., two different laser irradiation beams are used at 808 nm and 1940 nm wavelengths. The tissue exhibits strong scattering properties at a wavelength of 808 nm, while it exhibits high absorbing properties at a wavelength of 1940 nm [91,115,120,121]. Therefore, the effect of 808 nm laser is added to the equation using diffusion theory. On the other hand, the effect of the 1940 nm laser is added using the Beer-Lambert's law. The optical properties of tissue used in this study are given in the Table 3.2.

Table 3.2 Optical properties of tissue.

Parameters	Values	Unit	References
<i>At 808 nm wavelength</i>			
Diffusive Reflectance	0.05	-	[122,123]
Absorption Coefficient	78	m^{-1}	[124,125]
Reduced Scattering Coefficient	2104	m^{-1}	[124,125]
<i>At 1940 nm wavelength</i>			
Specular Reflectance	0.0475	-	[122,126]
Absorption Coefficient	5643	m^{-1}	[90,121,126]

For the analysis, laser exposures for 10-second with 14 kW/m^2 irradiance on the skin for the wavelengths of 808 nm and 1940 nm are chosen. In the one-dimensional analysis, the skin tissue is accepted as a 5 cm slab. The initial temperature of the skin is 33.2 degrees in 808 nm wavelength laser application and 32.9 degrees in 1940 nm wavelength laser application

3.2.1 Grid Convergence Study

The mechanism of each case is different. Therefore, a grid convergence study should be performed separately for each case. The solutions are performed by dividing the control volume to a different number of grids. Maximum temperature values occurred in these solutions are compared with each other to obtain an optimum number of the grid. For this study, the time step is chosen as 0.01 second [127]. Firstly, the control volume with 100 grid points is examined. Then the number of grids in the control volume is gradually increased. The amount of increase is chosen as 10. In this way, maximum temperature values in 808 nm and 1940 nm laser application are given in the Figure 3.4 and 3.5, respectively.

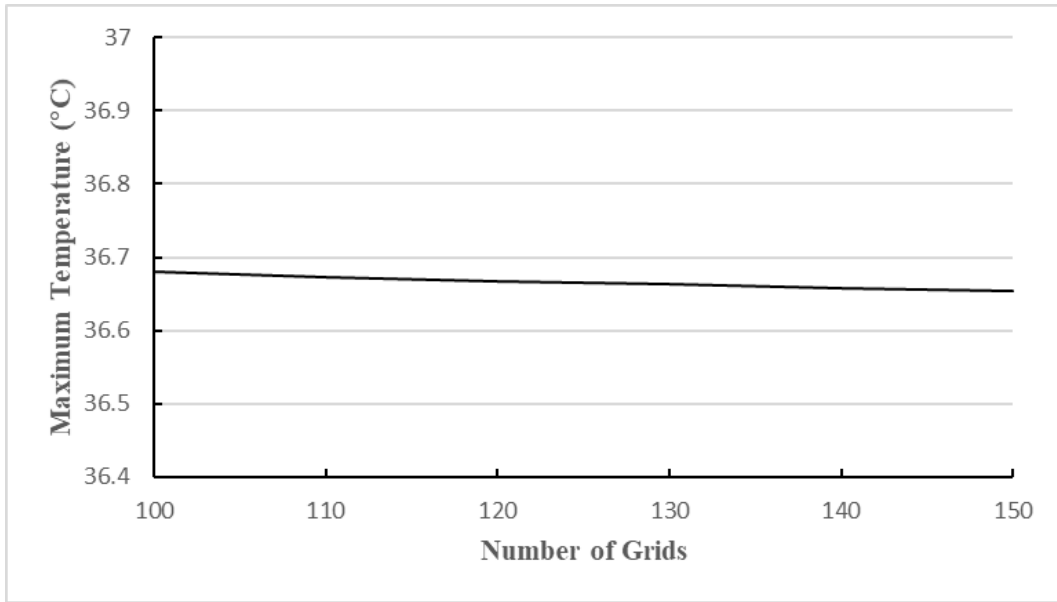


Figure 3.4 The maximum temperature with respect of the number of grids in 808nm laser application (strongly scattering case).

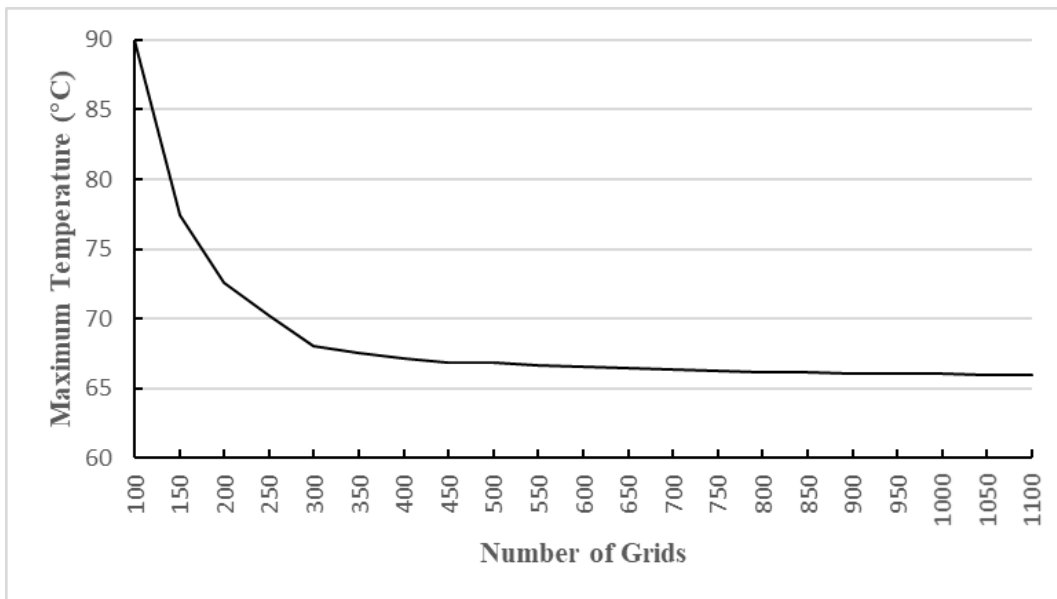


Figure 3.5 The maximum temperature with respect of the number of grids in 1940 nm laser application (highly absorbed case).

When the results are examined, the solution using the 120 grid number gives satisfactory results. If the number of grids is increased further, the decrease in the maximum temperature value is less than 0.005 degrees. On the other hand, the effect of the grid numbers has more at in 1940 nm laser application than the 808 nm laser application. In the 1940 nm laser application, the number of grids is chosen as 1050.

3.2.2 Time Step Convergence Study

The study performed for the number of grids should also be performed for the time step. The optimum time step will be chosen using the grid numbers determined in the previous stage. This study is performed separately for both wavelength laser applications. Tissue properties, initial conditions and boundary conditions are the same as the previous study. This study is performed using five different time steps, which are 0.1, 0.05, 0.01, 0.005 and 0.001 seconds. The maximum temperature values in 808 nm and 1940 nm laser application are given in the Figure 3.6 and 3.7, respectively.

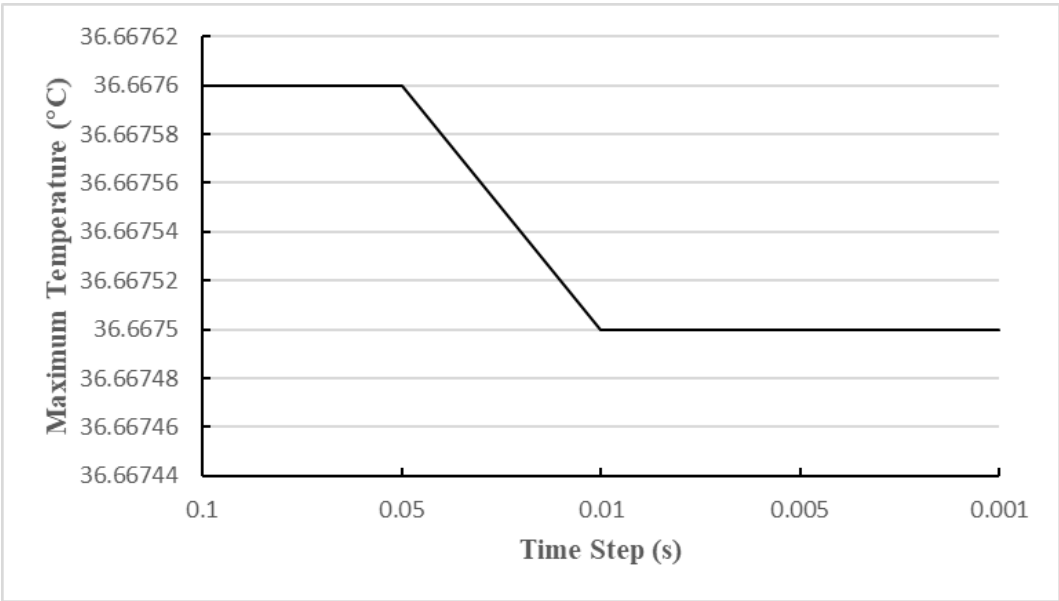


Figure 3.6 The maximum temperature with respect of the time step in 808 nm laser application (strongly scattering case).

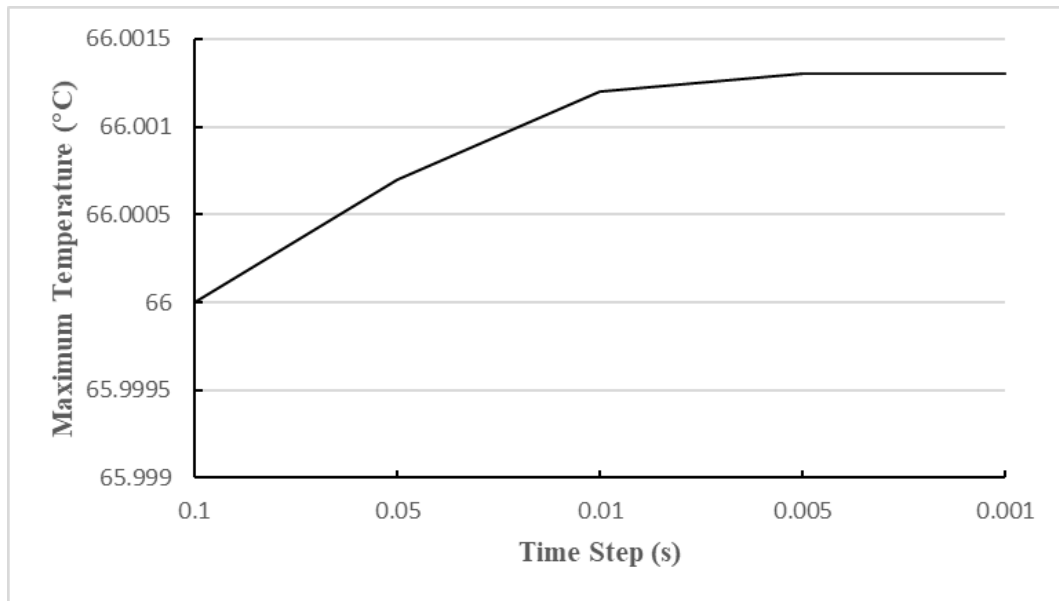


Figure 3.7 The maximum temperature with respect of the time step in 1940 nm laser application (highly absorbed case).

Selecting a time step of fewer than 0.01 seconds has a very low impact on the maximum temperature. Therefore, 0.01 seconds will be selected as the time step for both applications.

3.3 Code Validation

The validity of the solution of the mathematical model obtained in this study should be checked. Moreover, the validity of the solution of the DPL and Pennes models to be used for comparison purposes should be checked.

Model in this study is solved using the numerical procedure in section 3.1. At the same time, this numerical procedure is also applied to Pennes and DPL models. The details about discretization of Pennes and DPL models are given in Appendix B and C, respectively. In addition, MATLAB codes for the three models to be used in this study are given in appendix D, E and F. It is compared with the solution made by Tzou [128] to check the validity. All parameters and geometrical properties are chosen the same as in Tzou's study in order to make the comparison accurate. All parameters and geometric properties are chosen so that the same parameters in Tzou's study are obtained to make the comparison accurate. In addition, as in Tzou's study, the parameters to be used in its solution are dimensionless. The MATLAB code for Tzou's study is given in Appendix G.

In order to compare the results with Tzou's results, metabolic heat source and blood perfusion are taken as zero. The values of some parameters to be used differ according to the mathematical model. In the Pennes equation, thermal diffusivity is considered to be 1. In addition, the solution of the Pennes model is obtained by using zero for values of phase lags in Tzou's solution. The thermal diffusivity for the DPL equation is also 1. For this equation, the heat flux and temperature phase lag values are 0.05 and 0.001 respectively. In order to solve the equation obtained in this study, the coefficients of the equation are changed. The values of these coefficients are selected as follows.

$$\left(\frac{\varepsilon \rho_b c_{p,b} (1 - \varepsilon) \rho_t c_{p,t}}{G(\varepsilon \rho_b c_{p,b} + (1 - \varepsilon) \rho_t c_{p,t})} \right) = 0.05 \quad (3.17)$$

$$\frac{(k_{eff,t} + k_{eff,b})}{(\varepsilon \rho_b c_{p,b} + (1 - \varepsilon) \rho_t c_{p,t})} = 1 \quad (3.18)$$

$$\left(\frac{\varepsilon \rho_b c_{p,b} k_{eff,t} + (1 - \varepsilon) \rho_t c_{p,t} k_{eff,b}}{G(\varepsilon \rho_b c_{p,b} + (1 - \varepsilon) \rho_t c_{p,t})} \right) = 0.01 \quad (3.19)$$

For study of code validation, the control volume is a slab with a length of 1. Initially, the temperature and temperature gradient of the plate is zero. The left surface temperature of the control volume is then increased to 1. The temperature gradient of the right surface is considered as zero. For the validation study, temperature values are examined along the length of the slab at time 0.05 second. The comparison of results of Pennes, DPL and the equation used in this study with Tzou's results are given in Figure 3.8, Figure 3.9 and Figure 3.10, respectively.

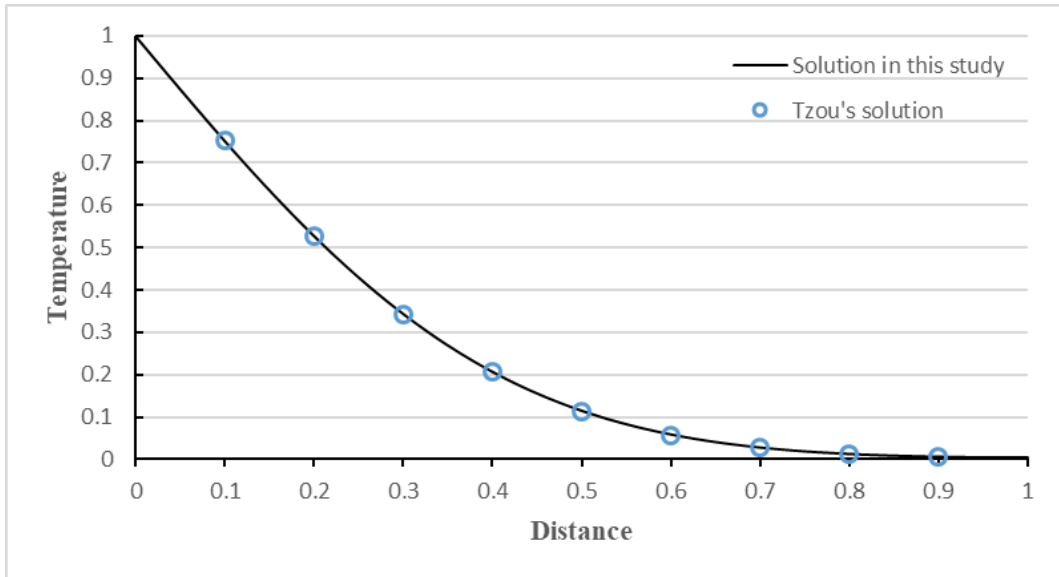


Figure 3.8. The temperature distribution using Pennes equation.

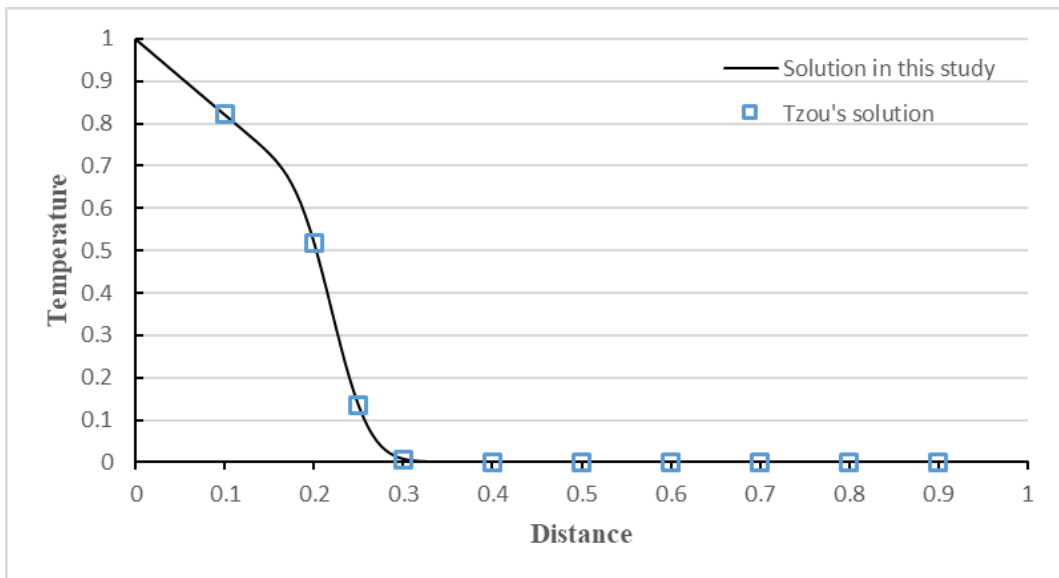


Figure 3.9. The temperature distribution using DPL equation.

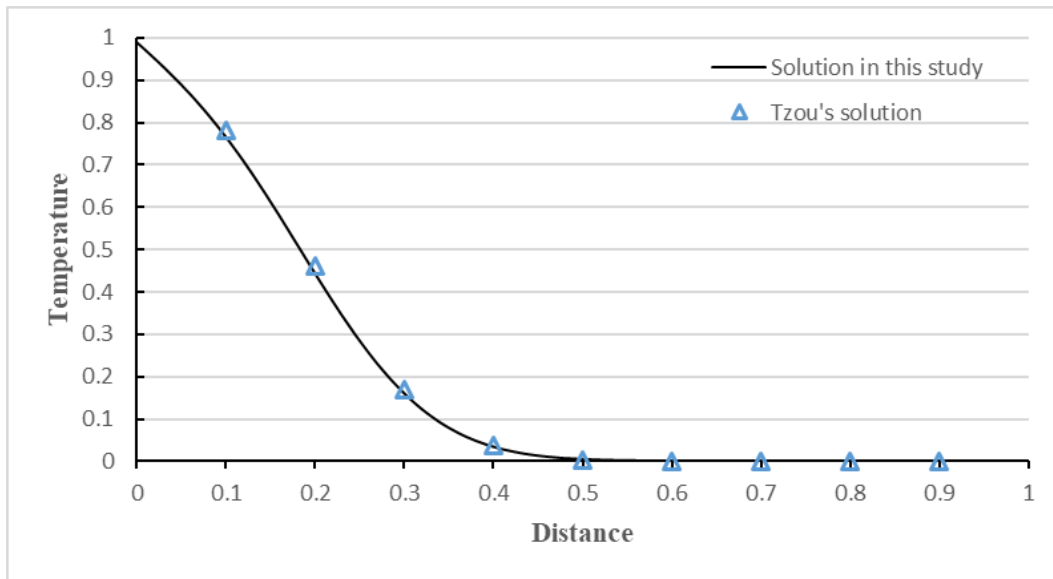


Figure 3.10. The temperature distribution using the mathematical model developed in this study.

When the results of these mathematical models in one-dimensional analysis are examined, numerical results are consistent with result of Tzou's solution.

CHAPTER 4

RESULTS AND DISCUSSION

In this study, the derived model will be compared with experimental results and the two models commonly used for laser tissue interaction in the literature. One of the selected models is the Pennes model, the other is the dual phase lag model. The reason for choosing the Pennes equation is that it is one of the fundamental equations in the literature and is widely used. The reason for choosing the DPL model is that it can explain microstructural effects like thermalization behavior better than other models. In order to understand the laser-tissue interaction, the effects of the laser beams having wavelengths of 808 nm and 1940 nm are examined.

4.1 Comparison of Models

In this study, the derived model is compared with the other models and experimental results by examining the time-dependent temperature values of the skin surface. In this comparison, thermophysical and optical properties are used presented in Table 3.1 and Table 3.2, respectively. For the solution of Pennes and DPL models, there is no need for values such as thermal conductivity of blood and the diameter of blood vessel. On the other hand, blood temperature is required for Pennes and DPL models. It is assumed that blood temperature equals to initial skin temperature. In addition, phase lag values are required for the DPL model. In this study, the heat flux and temperature phase lag values are chosen as 16 seconds and 0.05 seconds, respectively. Other properties are used in this analysis are as follows. For both applications, the magnitude of laser irradiance is 14 kW and the exposure time is 10 seconds. In the one-dimensional analysis, the tissue is accepted as a 5 cm slab. The initial temperature of the skin is 33.2 degrees in 808 nm laser application and 32.9 degrees in 1940 nm laser application

The temperature of cell 1 corresponds to the temperature value of the laser-irradiated surface. In the 808 nm laser application, the temperature values obtained by Pennes and DPL approaches as well as the presented model, which is derived in this study, are shown in Figure 4.1.

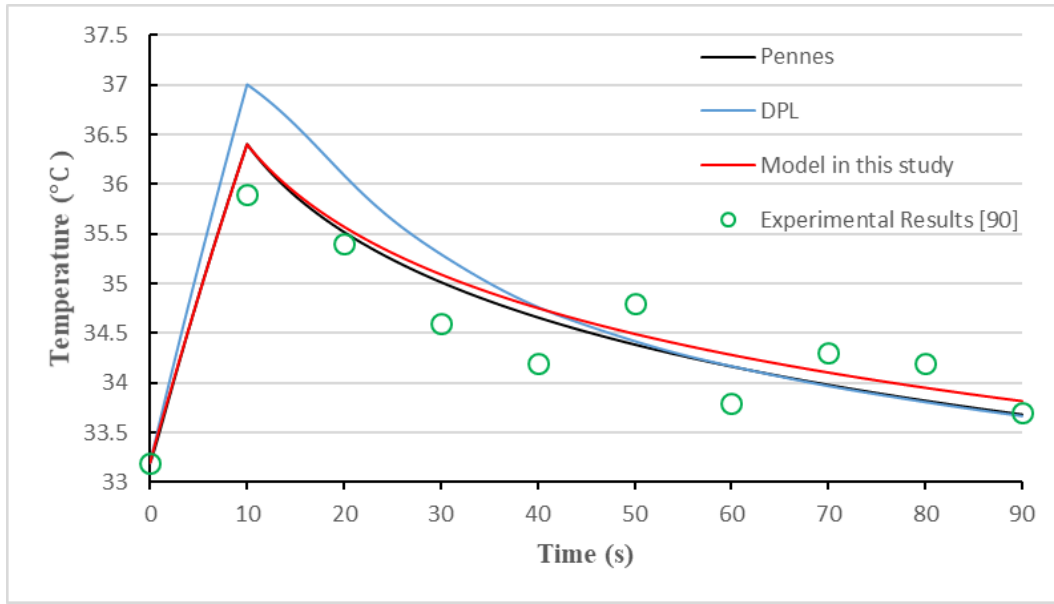


Figure 4.1. Evolution of temperature at the irradiated surface in 808 nm laser application (strongly scattering case).

The model derived in this study and the Pennes model, show shows similar trends for the evolution of temperature. Furthermore, the results of these two models are close to the experimental results. However, a higher increase in temperature occurs in the DPL model during the exposure period, because there is a high phase lag for the heat flux and a very low phase lag for the temperature. The high phase delay for the heat flux causes a delay in transferring heat to deeper regions. In addition to that, a very low phase lag for temperature allows the temperature to change suddenly. A similar phenomenon is observed after the end of the exposure time. This time, this causes a higher drop in temperature. The model in this study has terms which are not exist in Fourier's law of conduction ($\partial^2 T_t / \partial t^2$ and $\partial(\partial T_t^2 / \partial x^2) / \partial t$) like the ones in the DPL model. However, because of the fact that the coefficients of these terms are low, no sudden temperature changes occur as in the DPL model. For example, in this solution, coefficients of $\partial^2 T_t / \partial t^2$ and $\partial(\partial T_t^2 / \partial x^2) / \partial t$ are 0.4677 and 1.1414×10^{-7} , respectively.

In the 1940 nm laser application, the temperature values obtained by Pennes and DPL models and the presented one, which is derived in this study, are given in Figure 4.2.

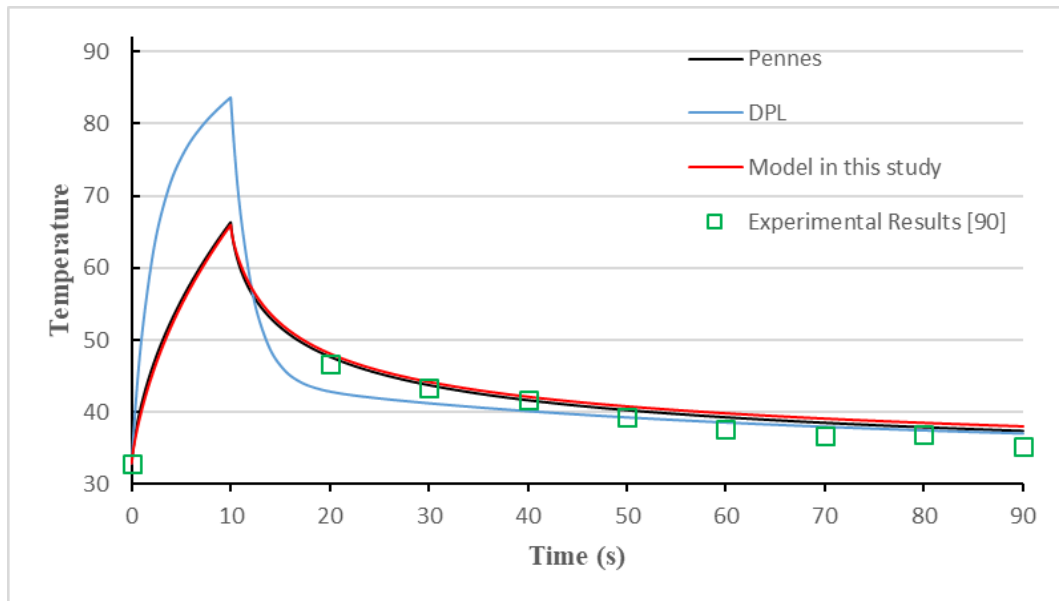


Figure 4.2. Evolution of temperature at the irradiated surface in 1940 nm laser application (highly absorbed case).

Similar to the 808 nm wavelength laser beam application, the Pennes model and the model derived in this study give similar results when the laser wavelength is 1940 nm. However, since the tissue exhibits a higher absorbance under the influence of the 1940 nm laser, the maximum temperatures are higher than in the previous application. The results obtained from these two models are consistent with the experimental results. On the other hand, sudden temperature rise and drop are observed in the DPL model. This rate of increase and decrease in temperature are higher compared to the one in the previous application.

4.2 Effect of Porosity

There are different parameters affecting the model in this study. One of them is porosity. The porosity value differs depending on the location of tissue. Therefore, the effect of different porosity values on the temperature value should be examined. The effect of porosity will be examined using 3 different values. Besides, vessel radius values are proportional to porosity. When the porosity is changed, the vessel radius also changes. The porosity and the vessel radii values used in the presented model are given in table 4.1. The other parameters are the same as the previous calculation.

Table 4. 1 Porosity and diameter of blood vessel.

	Parameters	Values	Unit	References
1	Porosity	0.0060	-	[102,112]
	Diameter of Blood Vessel	1.14	<i>mm</i>	[102,112]
2	Porosity	0.019	-	[102,112]
	Diameter of Blood Vessel	2.28	<i>mm</i>	[102,112]
3	Porosity	0.066	-	[102,112]
	Diameter of Blood Vessel	4.56	<i>mm</i>	[102,112]

In 808 nm laser application, the temperature values obtained by using different porosity values are given in Figure 4.3.

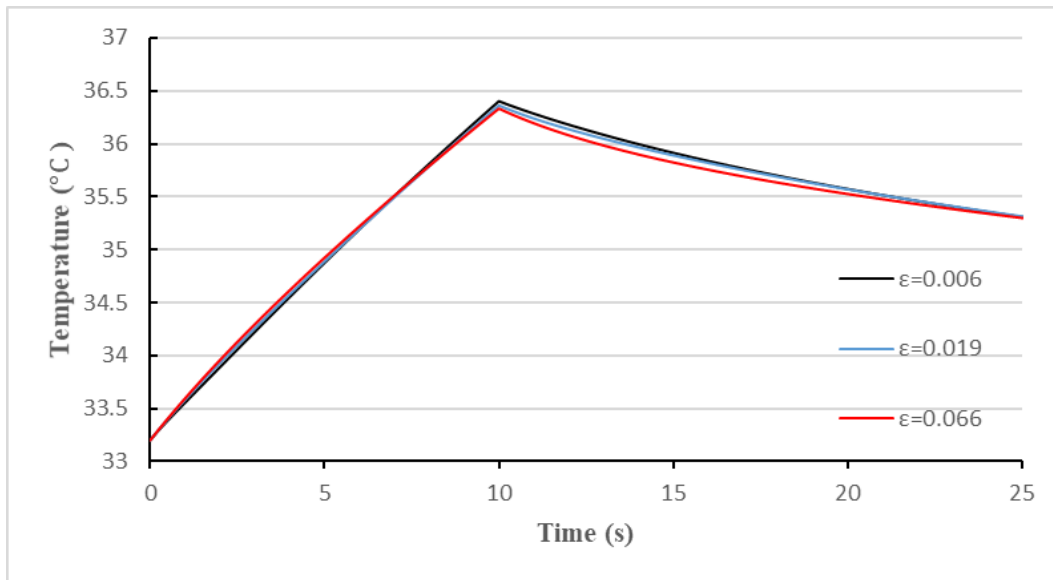


Figure 4.3. In 808 nm laser application (strongly scattering case), the effect of porosity on the temperature at the irradiated surface.

The effect of porosity on the temperature is very low in 808 nm laser application. As the porosity value increases, the maximum observed temperature decreases. the same examination is performed in the 1940 nm laser application. In the 1940 nm laser application, the temperature values obtained by using different porosity values are given in Figure 4.4.

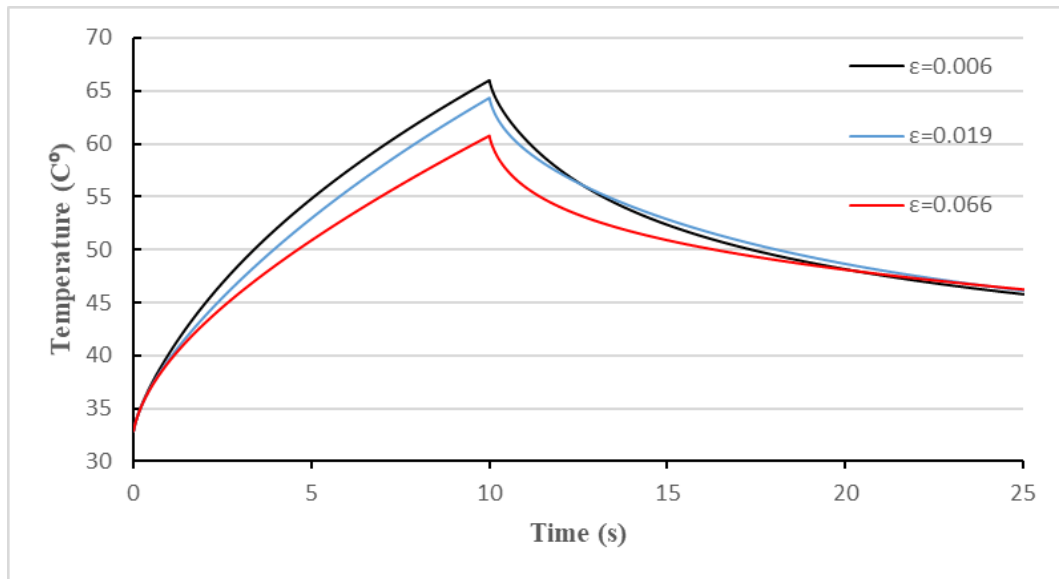


Figure 4.4. In the 1940 nm laser application (highly absorbed case), the effect of porosity on the temperature at the irradiated surface.

The lowest temperature increase during the laser irradiance is observed on tissue with high porosity. On the other hand, the highest temperature decrease is observed on tissue with low porosity after laser irradiance is ended. The reason is that the coupling factor is high. Porosity directly affects the coupling factor. When the porosity increases, the coupling factor is reduced. For example, in this calculation, when the porosity values are 0.0060, 0.019 and 0.066, while the corresponding coupling factors are 50918, 41309 and 36505, respectively. When the value of the coupling factor increases, the speeds of the heating and cooling processes increase.

Although the coupling factor is high in both applications, the effect of the porosity on the tissue is significantly lower in the 808 nm laser application. The reason for that, the optical properties of the tissue vary depending on the wavelength of the laser. Under the influence of the 1940 nm wavelength laser, the laser irradiance is absorbed near the surface. Therefore, a temperature difference occurs between this region and the deeper regions. However, under the influence of the laser with 808 nm wavelength, the absorption rate in the tissue is lower. In this case, the temperature difference between the region close to the surface and the deep regions is low. Therefore, the increase in heat transfer in the 1940 nm laser application is greater than the increase in heat transfer in the 808 nm laser application.

4.3 Effect of Laser Irradiance and Exposure Time

In laser applications, the magnitude of laser radiation and exposure time vary depending on the purpose of the application. Therefore, the effects of different laser irradiance and exposure times should be examined. For this examination, laser irradiance powers and exposure time are changed provided that the applied energy is kept constant. The values to be used for this analysis are given in Table 4.2. The other parameters are the same as in the chapter 4.1.

Table 4.2. The exposure time and intensity of laser irradiance

	Parameters	Values	Unit
1	Exposure Time	2	s
	Magnitude of Laser Irradiance	70	kW/m^2
2	Exposure Time	10	s
	Magnitude of Laser Irradiance	14	kW/m^2
3	Exposure Time	40	s
	Magnitude of Laser Irradiance	3.5	kW/m^2

In 808 nm laser application, the temperature values obtained by using different laser irradiances and exposure times are given in Figure 4.5.

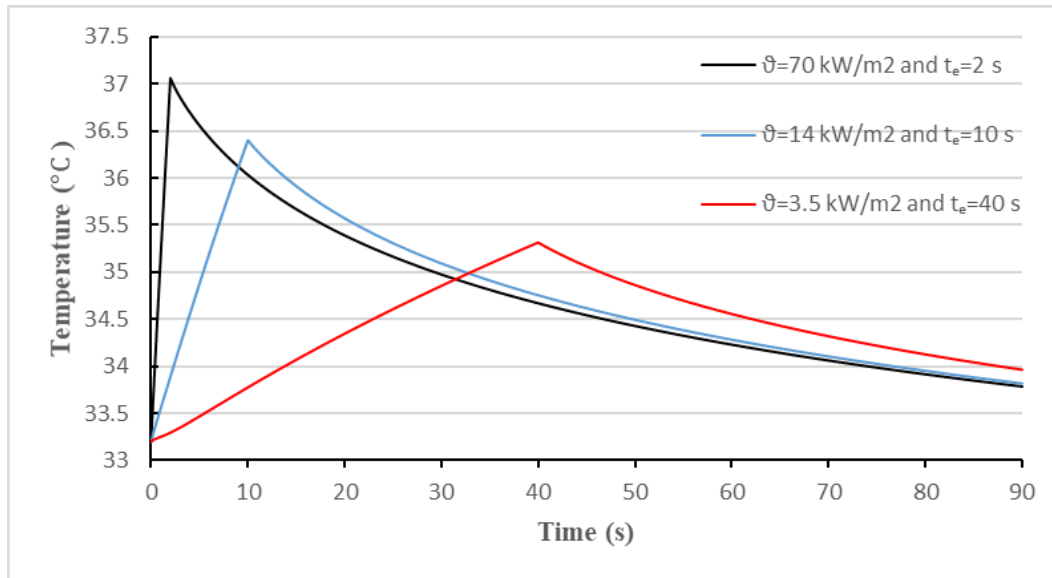


Figure 4.5. In 808 nm laser application (strongly scattering case), the effect of laser irradiance and exposure time on the temperature at the irradiated surface.

In 808 nm laser application, the effect of change in laser irradiance on temperature is less than the one obtained for 1940 nm laser application. Because the laser irradiance is absorbed low rate at the regions, near the surface and transmitted to deeper regions of the

tissue. Moreover, the increase in laser irradiance causes an increase in the maximum temperature, although it is not as high as the 1940 nm laser application. After the laser irradiation has finished, temperature values reach to similar values.

In 1940 nm laser application, the temperature values obtained by using different laser irradiances and exposure times are given in Figure 4.6.

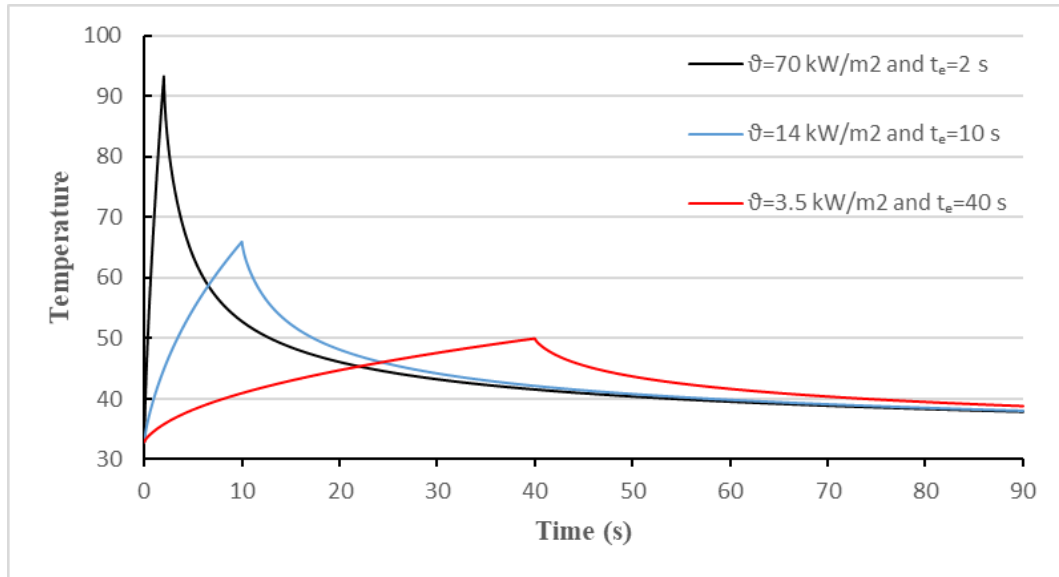


Figure 4.6. In 1940 nm laser application (highly absorbed case), the effect of laser irradiance and exposure time on the temperature at the irradiated surface.

The effect of laser irradiance on the temperature is high in 1940 nm laser application. The reason is that the laser irradiance is absorbed in the tissue at a very small depth. The increase in laser irradiance raises the amount of heat entering into the cell. This leads that the difference between the amount of heat entering and leaving the cell is increased. Therefore, the highest temperature rise occurs in the highest laser irradiance. After the laser irradiation has ended, similar temperatures are obtained in three cases.

CHAPTER 5

CONCLUSIONS AND FUTURE WORK

In this study, a mathematical model is formed to understand the thermal effect of laser on tissue. Laser radiation is included in the equation using two different formulas. One of these is Beer-Lambert's law. The other is diffusion theory. The model is solved numerically under these two assumptions. In this study, the one-dimensional analysis is performed. Models are evaluated by examining the evolution of temperature at the irradiated surface. For comparison, the Pennes and DPL models are solved under the same conditions. Then, the results of three models compared with experimental results.

Similar results are obtained from the model derived in this study with the Pennes model in laser applications with wavelengths of 808 nm and 1940 nm. But there is a small difference. In the Pennes model, the temperature values are slightly higher. On the other hand, a different temperature evolution is observed with the DPL model. In this study, while the phase lag for heat flux used for the DPL model is high, the phase lag for temperature is low. This situation allows for sudden temperature rise or drop. On the other hand, in the model in this study, sudden temperature rise or drop does not occur due to the coefficients of this model. The increase in the laser irradiance causes the maximum temperature at the surface to increase.

The model in this study is examined in different porosity values. Generally, when the porosity decreases, faster temperature rise and fall are observed. Furthermore, the effect of laser irradiance and exposure time are also examined. The effect of change in the magnitude of laser irradiance is greater in the 1940 nm laser application than in the 808 nm laser application.

The study on the model can be expanded in several ways.

- By changing the solution domain, the solution can perform for the axisymmetric case.
- In this study, tissue is considered as a uniform structure. The tissue can be divided into regions with different properties and the solution can be performed by considering the characteristics of these regions. For

example, the effect of the laser on the skin can be examined by considering the multi-layered skin structure. Moreover, by defining the tumor region within the tissue, the solution can be performed taking into account the characteristics of the tumor.

- It can be solved with using variable laser irradiance instead of constant laser irradiance.

REFERENCES

- [1] M.H. Niemz, *Laser-tissue interactions: fundamentals and applications*, Springer Science & Business Media, 2013.
- [2] J.M. Hermens, M.J. Bennett, C.A. Hirshman, Anesthesia for laser surgery., *Anesth. Analg.* 62 (1983) 218–229.
- [3] A.L. Mckenzie, *Physics in Medicine & Biology* Physics of thermal processes in laser-tissue interaction Physics of thermal processes in laser-tissue interaction, *Phys. Med. Biol.* 35 (1990) 1175–1209.
<http://iopscience.iop.org/article/10.1088/0031-9155/35/9/001/pdf>.
- [4] I. Ishikawa, A. Aoki, A.A. Takasaki, Potential applications of Erbium: YAG laser in periodontics, *J. Periodontal Res.* 39 (2004) 275–285.
- [5] A.C. Steger, W.R. Lees, K. Walmsley, S.G. Bown, Interstitial laser hyperthermia: a new approach to local destruction of tumours., *Bmj.* 299 (1989) 362–365.
- [6] M.D. A. R. Moritz, P.D. F. C. Henriques, JR., The relative importance of time and surface temperature in the causation of cutaneous burns, *Am J Pathol.* (1947). doi:10.1097/DAD.0b013e31820d15f0.
- [7] F.H. Sakamoto, H.R. Jalian, R.R. Anderson, *Understanding lasers, lights, and tissue interactions*, 2016. doi:10.1016/B978-1-4557-2783-4.00001-6.
- [8] H.H. Pennes, Analysis of tissue and arterial blood temperatures in the resting human forearm, *J. Appl. Physiol.* 1 (1948) 93–122.
- [9] H.W. Huang, C.L. Chan, R.B. Roemer, Analytical solutions of Pennes bio-heat transfer equation with a blood vessel, *J. Biomech. Eng.* 116 (1994) 208–212.
- [10] T.-C. Shih, P. Yuan, W.-L. Lin, H.-S. Kou, Analytical analysis of the Pennes bioheat transfer equation with sinusoidal heat flux condition on skin surface, *Med. Eng. Phys.* 29 (2007) 946–953.
- [11] Z.-S. Deng, J. Liu, Analytical study on bioheat transfer problems with spatial or transient heating on skin surface or inside biological bodies, *J. Biomech. Eng.* 124 (2002) 638–649.
- [12] J.J. Zhao, J. Zhang, N. Kang, F. Yang, A two level finite difference scheme for one dimensional Pennes' bioheat equation, *Appl. Math. Comput.* 171 (2005) 320–331.
- [13] K. Yue, X. Zhang, F. Yu, An analytic solution of one-dimensional steady-state Pennes' bioheat transfer equation in cylindrical coordinates, *J. Therm. Sci.* 13 (2004) 255–258.
- [14] M. Dehghan, M. Sabouri, A spectral element method for solving the Pennes bioheat transfer equation by using triangular and quadrilateral elements, *Appl.*

- Math. Model. 36 (2012) 6031–6049.
- [15] W. Wulff, The energy conservation equation for living tissue, *IEEE Trans. Biomed. Eng.* (1974) 494–495.
- [16] K. Das, S.C. Mishra, Study of thermal behavior of a biological tissue: An equivalence of Pennes bioheat equation and Wulff continuum model, *J. Therm. Biol.* 45 (2014) 103–109.
- [17] W. Wulff, DISCUSSION PAPER: ALTERNATIVES TO THE BIO-HEAT TRANSFER EQUATION, *Ann. N. Y. Acad. Sci.* 335 (1980) 151–154.
- [18] H.G. Klinger, Heat transfer in perfused biological tissue—I: General theory, *Bull. Math. Biol.* 36 (1974) 403–415.
- [19] M. Chaichanyut, S. Tungjitkusolmun, Microwave ablation using four-tine antenna: effects of blood flow velocity, vessel location, and total displacement on porous hepatic cancer tissue, *Comput. Math. Methods Med.* 2016 (2016).
- [20] P. Revathy, V. Sadasivam, Analysis on the Healthy Pixels in the Region of Tumor and the Untreated Tumor Pixels in the Boundary during High Intensity Focused Ultrasound Interventions., in: *Recent Adv. Comput. Sci. Proc. 14th Int. Conf. Appl. Comput. Appl. Comput. Sci.*, 2015: pp. 65–69.
- [21] M.M. Chen, K.R. Holmes, Microvascular contributions in tissue heat transfer, *Ann. N. Y. Acad. Sci.* 335 (1980) 137–150.
- [22] X. Xu, The evaluation of heat transfer equations in the pig renal cortex, (1991).
- [23] W. Zhu, F. Tian, P. Ran, ANALYTICAL SOLUTIONS OF NON-FOURIER PENNES AND CHEN–HOLMES EQUATIONS, *Int. J. Biomath.* 5 (2012) 1250022.
- [24] G. Chenhua, C. Ruixian, An analytical solution of non-Fourier Chen-Holmes bioheat transfer equation, *Chinese Sci. Bull.* 50 (2005) 2791–2792.
- [25] R. Cai, N. Zhang, Unsteady one-dimensional analytical solutions for bioheat transfer equations, *Prog. Nat. Sci.* 8 (1998) 733–739.
- [26] S. Weinbaum, L.M. Jiji, D.E. Lemons, Theory and experiment for the effect of vascular microstructure on surface tissue heat transfer—Part I: Anatomical foundation and model conceptualization, *J. Biomech. Eng.* 106 (1984) 321–330.
- [27] L.M. Jiji, S. Weinbaum, D.E. Lemons, Theory and experiment for the effect of vascular microstructure on surface tissue heat transfer—part II: model formulation and solution, *J. Biomech. Eng.* 106 (1984) 331–341.
- [28] S. Weinbaum, L.M. Jiji, A new simplified bioheat equation for the effect of blood flow on local average tissue temperature, *ASME J. Biomech. Eng.* 107 (1985) 131–139.
- [29] J.W. Valvano, S. Nho, G.T. Anderson, Analysis of the Weinbaum-Jiji model of blood flow in the Canine Kidney cortex for self-heated thermistors, *J. Biomech.*

Eng. 116 (1994) 201–207.

- [30] S. Weinbaum, L.M. Jiji, D.E. Lemons, The bleed off perfusion term in the Weinbaum-Jiji bioheat equation, *J. Biomech. Eng.* 114 (1992) 539–542.
- [31] C.K. Charny, S. Weinbaum, R.L. Levin, An evaluation of the Weinbaum-Jiji bioheat equation for normal and hyperthermic conditions, *J. Biomech. Eng.* 112 (1990) 80–87.
- [32] R.B. Roemer, J.R. Oleson, T.C. Cetas, Oscillatory temperature response to constant power applied to canine muscle, *Am. J. Physiol. Integr. Comp. Physiol.* 249 (1985) R153–R158.
- [33] K. Mitra, S. Kumar, A. Vedevarz, M.K. Moallemi, Experimental evidence of hyperbolic heat conduction in processed meat, *J. Heat Transfer.* 117 (1995) 568–573.
- [34] D.Y. Tzou, *Macro-to microscale heat transfer: the lagging behavior*, John Wiley & Sons, 2014.
- [35] C. Cattaneo, A form of heat-conduction equations which eliminates the paradox of instantaneous propagation, *Comptes Rendus.* 247 (1958) 431.
- [36] P. Vernotte, Les paradoxes de la theorie continue de l'equation de la chaleur, *Compt. Rendu.* 246 (1958) 3154–3155.
- [37] J. Liu, X. Chen, L.X. Xu, New thermal wave aspects on burn evaluation of skin subjected to instantaneous heating, *IEEE Trans. Biomed. Eng.* 46 (1999) 420–428.
- [38] H. Ahmadikia, R. Fazlali, A. Moradi, Analytical solution of the parabolic and hyperbolic heat transfer equations with constant and transient heat flux conditions on skin tissue, *Int. Commun. Heat Mass Transf.* 39 (2012) 121–130.
- [39] K.-C. Liu, Thermal propagation analysis for living tissue with surface heating, *Int. J. Therm. Sci.* 47 (2008) 507–513.
- [40] S. Kumar, S. Singh, Numerical Study on Biological Tissue Freezing Using Dual Phase Lag Bio-Heat Equation, in: *Trends Biomath. Model. Optim. Comput. Probl.*, Springer, 2018: pp. 283–300.
- [41] S.C. Mishra, R.K. Chaurasia, Analysis of dual-phase-lag non-Fourier conduction and radiation heat transfer in a planar slab, *Numer. Heat Transf. Part A Appl.* 68 (2015) 1010–1022.
- [42] H. Askarizadeh, H. Ahmadikia, Analytical analysis of the dual-phase-lag model of bioheat transfer equation during transient heating of skin tissue, *Heat Mass Transf.* 50 (2014) 1673–1684.
- [43] K.-C. Liu, Y.-N. Wang, Y.-S. Chen, Investigation on the bio-heat transfer with the dual-phase-lag effect, *Int. J. Therm. Sci.* 58 (2012) 29–35.
- [44] J. Zhou, J.K. Chen, Y. Zhang, Dual-phase lag effects on thermal damage to

- biological tissues caused by laser irradiation, *Comput. Biol. Med.* 39 (2009) 286–293.
- [45] Y. Zhang, Generalized dual-phase lag bioheat equations based on nonequilibrium heat transfer in living biological tissues, *Int. J. Heat Mass Transf.* 52 (2009) 4829–4834.
- [46] A.R.A. Khaled, K. Vafai, The role of porous media in modeling flow and heat transfer in biological tissues, *Int. J. Heat Mass Transf.* 46 (2003) 4989–5003. doi:10.1016/S0017-9310(03)00301-6.
- [47] K.-C. Liu, H.-T. Chen, Analysis of the bioheat transfer problem with pulse boundary heat flux using a generalized dual-phase-lag model, *Int. Commun. Heat Mass Transf.* 65 (2015) 31–36.
- [48] M. Jasiński, E. Majchrzak, L. Turchan, Numerical analysis of the interactions between laser and soft tissues using generalized dual-phase lag equation, *Appl. Math. Model.* 40 (2016) 750–762.
- [49] E. Majchrzak, Ł. Turchan, J. Dziatkiewicz, Modeling of skin tissue heating using the generalized dual phase-lag equation., *Arch. Mech.* 67 (2015).
- [50] N. Afrin, J. Zhou, Y. Zhang, D.Y. Tzou, J.K. Chen, Numerical simulation of thermal damage to living biological tissues induced by laser irradiation based on a generalized dual phase lag model, *Numer. Heat Transf. Part A Appl.* 61 (2012) 483–501.
- [51] M.A. Ezzat, N.S. AlSowayan, Z.I.A. Al-Muhiameed, S.M. Ezzat, Fractional modelling of Pennes’ bioheat transfer equation, *Heat Mass Transf.* 50 (2014) 907–914.
- [52] R.S. Damor, S. Kumar, A.K. Shukla, Numerical solution of fractional bioheat equation with constant and sinusoidal heat flux coindition on skin tissue, *Am. J. Math. Anal.* 1 (2013) 20–24.
- [53] R.S. Damor, S. Kumar, A.K. Shukla, Solution of fractional bioheat equation in terms of Fox’s H-function, *Springerplus.* 5 (2016) 111.
- [54] X. Jiang, H. Qi, Thermal wave model of bioheat transfer with modified Riemann–Liouville fractional derivative, *J. Phys. A Math. Theor.* 45 (2012) 485101.
- [55] X. Huan-Ying, J. Xiao-Yun, Time fractional dual-phase-lag heat conduction equation, *Chinese Phys. B.* 24 (2015) 34401.
- [56] B. Yu, X. Jiang, C. Wang, Numerical algorithms to estimate relaxation parameters and Caputo fractional derivative for a fractional thermal wave model in spherical composite medium, *Appl. Math. Comput.* 274 (2016) 106–118.
- [57] J. Fan, L. Wang, A general bioheat model at macroscale, *Int. J. Heat Mass Transf.* 54 (2011) 722–726.

- [58] P. Vadasz, Explicit conditions for local thermal equilibrium in porous media heat conduction, *Transp. Porous Media*. 59 (2005) 341–355.
- [59] P. Keangin, P. Rattanadecho, Analysis of heat transport on local thermal non-equilibrium in porous liver during microwave ablation, *Int. J. Heat Mass Transf.* 67 (2013) 46–60.
- [60] Y. Xuan, W. Roetzel, Bioheat equation of the human thermal system, *Chem. Eng. Technol.* 20 (1997) 268–276. doi:10.1002/ceat.270200407.
- [61] A. Nakayama, F. Kuwahara, A general bioheat transfer model based on the theory of porous media, *Int. J. Heat Mass Transf.* 51 (2008) 3190–3199. doi:10.1016/j.ijheatmasstransfer.2007.05.030.
- [62] E. Majchrzak, Turchan, A numerical analysis of heating tissue using the two-temperature model, *WIT Trans. Eng. Sci.* 83 (2014) 477–488. doi:10.2495/HT140411.
- [63] M. Shafahi, K. Vafai, Human Eye Response to Thermal Disturbances, *J. Heat Transfer*. 133 (2010) 011009. doi:10.1115/1.4002360.
- [64] S. Mahjoob, K. Vafai, Analysis of Heat Transfer in Consecutive Variable Cross-Sectional Domains: Applications in Biological Media and Thermal Management, *J. Heat Transfer*. 133 (2010) 011006. doi:10.1115/1.4002303.
- [65] J.C. Chato, Heat transfer to blood vessels, *J. Biomech. Eng.* 102 (1980) 110–118.
- [66] A. Nakayama, Y. Sano, K. Yoshikawa, A rigorous derivation of the bioheat equation for local tissue heat transfer based on a volume averaging theory, *Heat Mass Transf.* 46 (2010) 739–746.
- [67] S. Hassanpour, A. Saboonchi, Interstitial hyperthermia treatment of countercurrent vascular tissue: A comparison of Pennes, WJ and porous media bioheat models, *J. Therm. Biol.* 46 (2014) 47–55. doi:10.1016/j.jtherbio.2014.10.005.
- [68] E. Gabryś, M. Rybaczuk, A. Kędzia, Fractal models of circulatory system. Symmetrical and asymmetrical approach comparison, *Chaos, Solitons & Fractals*. 24 (2005) 707–715.
- [69] D. Shrivastava, *Theory and Applications of Heat Transfer in Humans*, Wiley Online Library, 2018.
- [70] C. Orndorff, W. Dai, Numerical hyperthermia simulation for a 3-d triplelayered skin structure with embedded vascular countercurrent network and nanoparticles, *Int. J. Heat Technol.* 34 (2016) s179–s184.
- [71] J. Zhou, J.K. Chen, Y. Zhang, Dual-phase lag effects on thermal damage to biological tissues caused by laser irradiation, *Comput. Biol. Med.* 39 (2009) 286–293. doi:10.1016/j.combiomed.2009.01.002.
- [72] K.-C. Liu, J.-C. Wang, Analysis of thermal damage to laser irradiated tissue

- based on the dual-phase-lag model, *Int. J. Heat Mass Transf.* 70 (2014) 621–628.
- [73] S. Patidar, S. Kumar, A. Srivastava, S. Singh, Dual phase lag model-based thermal analysis of tissue phantoms using lattice Boltzmann method, *Int. J. Therm. Sci.* 103 (2016) 41–56.
- [74] K.-C. Liu, Y.-S. Chen, Analysis of heat transfer and burn damage in a laser irradiated living tissue with the generalized dual-phase-lag model, *Int. J. Therm. Sci.* 103 (2016) 1–9.
- [75] P. Hooshmand, A. Moradi, B. Khezry, Bioheat transfer analysis of biological tissues induced by laser irradiation, *Int. J. Therm. Sci.* 90 (2015) 214–223.
- [76] S. Whitaker, S. Whitaker, 5 – The Basic Equations of Momentum and Energy Transfer, in: *Fundam. Princ. Heat Transf.*, Elsevier, 1977: pp. 192–271. doi:10.1016/B978-0-08-017866-0.50011-3.
- [77] Y. Xuan, W. Roetzel, Bioheat equation of the human thermal system, *Chem. Eng. Technol. Ind. Chem. Equipment-Process Eng.* 20 (1997) 268–276.
- [78] A. Nakayama, F. Kuwahara, A general bioheat transfer model based on the theory of porous media, *Int. J. Heat Mass Transf.* 51 (2008) 3190–3199.
- [79] A. Nakayama, Y. Sano, K. Nagase, T. Nishimura, Porous media theory for membrane transport phenomena, in: *Handb. Porous Media*, Third Ed., 2015: pp. 321–356. doi:10.1201/b18614.
- [80] F. Duval, F. Fichot, M. Quintard, A local thermal non-equilibrium model for two-phase flows with phase-change in porous media, *Int. J. Heat Mass Transf.* 47 (2004) 613–639.
- [81] M. Kaviany, *Principles of Heat Transfer in Porous Media*, Springer Science & Business Media, 1991. doi:10.1007/978-1-4684-0412-8.
- [82] K. Vafai, M. Sozen, Analysis of energy and momentum transport for fluid flow through a porous bed, *J. Heat Transfer.* 112 (1990) 690–699.
- [83] R.W. Waynant, *Lasers in medicine*, CRC press, 2001.
- [84] C.M. Gardner, S.L. Jacques, A.J. Welch, Light transport in tissue: Accurate expressions for one-dimensional fluence rate and escape function based upon Monte Carlo simulation, *Lasers Surg. Med. Off. J. Am. Soc. Laser Med. Surg.* 18 (1996) 129–138.
- [85] A. Nakayama, F. Kuwahara, M. Sugiyama, G. Xu, A two-energy equation model for conduction and convection in porous media, *Int. J. Heat Mass Transf.* 44 (2001) 4375–4379. doi:10.1016/S0017-9310(01)00069-2.
- [86] C.-L. Tien, K. Vafai, Convective and radiative heat transfer in porous media, in: *Adv. Appl. Mech.*, Elsevier, 1989: pp. 225–281.
- [87] W. Roetzel, Y. Xuan, Transient response of the human limb to an external stimulant, *Int. J. Heat Mass Transf.* 41 (1998) 229–239.

- [88] F. de Monte, A. Haji-Sheikh, Bio-heat diffusion under local thermal non-equilibrium conditions using dual-phase lag-based Green's functions, *Int. J. Heat Mass Transf.* 113 (2017) 1291–1305.
- [89] F. de Monte, A. Haji-Sheikh, Micro-Scale Bio-Heat Diffusion Using Green's Functions, in: *Model. Microscale Transp. Biol. Process.*, Elsevier, 2017: pp. 261–310.
- [90] N. Museux, L. Perez, L. Autrique, D. Agay, Skin burns after laser exposure: Histological analysis and predictive simulation, *Burns*. 38 (2012) 658–667.
- [91] J. Steketee, M.J. Van Der Hoek, Thermal recovery of the skin after cooling, *Phys. Med. Biol.* 24 (1979) 583.
- [92] K.M. Shurrab, M.S. El-Daher, Simulation and Study of Temperature Distribution in Living Biological Tissues under Laser Irradiation, *J. Lasers Med. Sci.* 5 (2014) 135.
- [93] M.J. Simpson, S. McInerney, E.J. Carr, L. Cuttle, Quantifying the efficacy of first aid treatments for burn injuries using mathematical modelling and in vivo porcine experiments, *Sci. Rep.* 7 (2017) 10925.
- [94] R. Marchesini, C. Clemente, E. Pignoli, M. Brambilla, Optical properties of in vitro epidermis and their possible relationship with optical properties of in vivo skin, *J. Photochem. Photobiol. B Biol.* 16 (1992) 127–140.
- [95] J.Y. Lee, S. Jung, H. Kwon, In vitro burn model illustrating heat conduction patterns using compressed thermal papers, *Wound Repair Regen.* 23 (2015) 124–131.
- [96] F.S. Knox III, T.L. Wachtel, G.R. McCahan, S.C. Knapp, Thermal properties calculated from measured water content as a function of depth in porcine skin, *Burns*. 12 (1986) 556–562.
- [97] J. Ruminski, M. Kaczmarek, A. Renkielska, A. Nowakowski, Thermal parametric imaging in the evaluation of skin burn depth, *IEEE Trans. Biomed. Eng.* 54 (2007) 303–312.
- [98] F.C. Henriques Jr, A.R. Moritz, Studies of thermal injury: I. The conduction of heat to and through skin and the temperatures attained therein. A theoretical and an experimental investigation, *Am. J. Pathol.* 23 (1947) 530.
- [99] T.P. Davis, A Theoretical and Experimental Investigation of the Temperature Response of Pig Skin Exposed to Thermal Radiation, Rochester, NY Univ. Atomic Energy Project, 1959.
- [100] H.F. Bowman, E.G. Cravalho, M. Woods, Theory, measurement, and application of thermal properties of biomaterials, *Annu. Rev. Biophys. Bioeng.* 4 (1975) 43–80.
- [101] K.-C. Liu, P.-J. Cheng, Finite propagation of heat transfer in a multilayer tissue, *J. Thermophys. Heat Transf.* 22 (2008) 775–782.

- [102] P. Yuan, Numerical analysis of an equivalent heat transfer coefficient in a porous model for simulating a biological tissue in a hyperthermia therapy, *Int. J. Heat Mass Transf.* 52 (2009) 1734–1740.
- [103] D.A. Torvi, J.D. Dale, A finite element model of skin subjected to a flash fire, *J. Biomech. Eng.* 116 (1994) 250–255.
- [104] M. Ciesielski, B. Mochnicki, Hyperbolic model of thermal interactions in a system biological tissue—protective clothing subjected to an external heat source, *Numer. Heat Transf. Part A Appl.* 74 (2018) 1685–1700.
- [105] H.F. Poppendiek, R. Randall, J.A. Breeden, J.E. Chambers, J.R. Murphy, Thermal conductivity measurements and predictions for biological fluids and tissues, *Cryobiology.* 3 (1967) 318–327.
- [106] K.E. Spells, The thermal conductivities of some biological fluids, *Phys. Med. Biol.* 5 (1960) 139.
- [107] A. Dumas, G.S. Barozzi, Laminar heat transfer to blood flowing in a circular duct, *Int. J. Heat Mass Transf.* 27 (1984) 391–398.
- [108] N.N. Johnson, J.P. Abraham, Z.I. Helgeson, W.J. Minkowycz, E.M. Sparrow, An archive of skin-layer thicknesses and properties and calculations of scald burns with comparisons to experimental observations, *J. Therm. Sci. Eng. Appl.* 3 (2011) 11003.
- [109] S.C. Jiang, N. Ma, H.J. Li, X.X. Zhang, Effects of thermal properties and geometrical dimensions on skin burn injuries, *Burns.* 28 (2002) 713–717.
- [110] J.W. Baish, K.R. Foster, P.S. Ayyaswamy, Perfused phantom models of microwave irradiated tissue, *J. Biomech. Eng.* 108 (1986) 239–245.
- [111] F. de Monte, A. Haji-Sheikh, Bio-heat diffusion under local thermal non-equilibrium conditions using dual-phase lag-based Green’s functions, *Int. J. Heat Mass Transf.* 113 (2017) 1291–1305.
doi:10.1016/j.ijheatmasstransfer.2017.06.006.
- [112] Y. Zhang, Generalized dual-phase lag bioheat equations based on nonequilibrium heat transfer in living biological tissues, *Int. J. Heat Mass Transf.* 52 (2009) 4829–4834. doi:10.1016/j.ijheatmasstransfer.2009.06.007.
- [113] C.W. Song, M.S. Kang, J.G. Rhee, S.H. Levitt, Effect of hyperthermia on vascular function in normal and neoplastic tissues, *Ann. N. Y. Acad. Sci.* 335 (1980) 35–47.
- [114] C.W. Song, J.H. Kim, J.G. Rhee, S.H. Levitt, Effect of X irradiation and hyperthermia on vascular function in skin and muscle, *Radiat. Res.* 94 (1983) 404–415.
- [115] F. Xu, T.J. Lu, K.A. Seffen, E.Y.K. Ng, Mathematical modeling of skin bioheat transfer, *Appl. Mech. Rev.* 62 (2009) 50801.

- [116] M.P. Çetingül, C. Herman, A heat transfer model of skin tissue for the detection of lesions: sensitivity analysis, *Phys. Med. Biol.* 55 (2010) 5933.
- [117] J. Dutta, B. Kundu, Thermal wave propagation in blood perfused tissues under hyperthermia treatment for unique oscillatory heat flux at skin surface and appropriate initial condition, *Heat Mass Transf.* 54 (2018) 3199–3217.
- [118] A. Chanmugam, R. Hatwar, C. Herman, Thermal analysis of cancerous breast model, in: *ASME 2012 Int. Mech. Eng. Congr. Expo.*, American Society of Mechanical Engineers, 2012: pp. 135–143.
- [119] F. Xu, T. Wen, T.J. Lu, K.A. Seffen, Modeling of nociceptor transduction in skin thermal pain sensation, *J. Biomech. Eng.* 130 (2008) 41013.
- [120] F. Xu, T. Lu, Skin bioheat transfer and skin thermal damage, in: *Introd. to Ski. Biothermomechanics Therm. Pain*, Springer, 2011: pp. 23–68.
- [121] B. Chen, D.C. O’Dell, S.L. Thomsen, B.A. Rockwell, A.J. Welch, Porcine skin ED50 damage thresholds for 2,000 nm laser irradiation, *Lasers Surg. Med. Off. J. Am. Soc. Laser Med. Surg.* 37 (2005) 373–381.
- [122] R.R. Anderson, J.A. Parrish, The optics of human skin, *J. Invest. Dermatol.* 77 (1981) 13–19.
- [123] F.A. Duck, Optical properties of tissue including ultraviolet and infrared radiation, *Phys. Prop. Tissue.* 19 (1990) 43–71.
- [124] C.R. Simpson, M. Kohl, M. Essenpreis, M. Cope, Near-infrared optical properties of ex vivo human skin and subcutaneous tissues measured using the Monte Carlo inversion technique, *Phys. Med. Biol.* 43 (1998) 2465.
- [125] T.L. Troy, D.L. Page, E.M. Sevick-Muraca, Optical properties of normal and diseased breast tissues: prognosis for optical mammography, *J. Biomed. Opt.* 1 (1996) 342–356.
- [126] B. Chen, S.L. Thomsen, R.J. Thomas, A.J. Welch, Modeling thermal damage in skin from 2000-nm laser irradiation, *J. Biomed. Opt.* 11 (2006) 64028.
- [127] J. Zhou, Y. Zhang, J.K. Chen, An axisymmetric dual-phase-lag bioheat model for laser heating of living tissues, *Int. J. Therm. Sci.* 48 (2009) 1477–1485.
- [128] D.Y. Tzou, A unified field approach for heat conduction from macro-to micro-scales, *J. Heat Transfer.* 117 (1995) 8–16.
- [129] S. Patankar, *Numerical heat transfer and fluid flow*, CRC press, 2018.

APPENDIX A

Discretization of Model in This Study

To make calculations clearer and simplify, equation (3.1) can be represented by using some coefficients.

$$a_1 \frac{\partial^2 T}{\partial t^2} + \frac{\partial T}{\partial t} = a_2 \nabla^2 T + a_3 \frac{\partial}{\partial t} (\nabla^2 T) + a_4 \left(\frac{\partial Q}{\partial t} \right) + a_5 Q + a_6 Q_m \quad (\text{A.1})$$

where

$$a_1 = \left(\frac{\varepsilon \rho_b c_{p,b} (1 - \varepsilon) \rho_t c_{p,t}}{G(\varepsilon \rho_b c_{p,b} + (1 - \varepsilon) \rho_t c_{p,t})} \right) \quad (\text{A.2})$$

$$a_2 = \frac{(k_{eff,t} + k_{eff,b})}{(\varepsilon \rho_b c_{p,b} + (1 - \varepsilon) \rho_t c_{p,t})} \quad (\text{A.3})$$

$$a_3 = \left(\frac{\varepsilon \rho_b c_{p,b} k_{eff,t} + (1 - \varepsilon) \rho_t c_{p,t} k_{eff,b}}{G(\varepsilon \rho_b c_{p,b} + (1 - \varepsilon) \rho_t c_{p,t})} \right) \quad (\text{A.4})$$

$$a_4 = \frac{\varepsilon \rho_b c_{p,b} (1 - \varepsilon)}{G(\varepsilon \rho_b c_{p,b} + (1 - \varepsilon) \rho_t c_{p,t})} \quad (\text{A.5})$$

$$a_5 = \frac{1}{(\varepsilon \rho_b c_{p,b} + (1 - \varepsilon) \rho_t c_{p,t})} \quad (\text{A.6})$$

$$a_6 = \frac{(1 - \varepsilon)}{(\varepsilon \rho_b c_{p,b} + (1 - \varepsilon) \rho_t c_{p,t})} \quad (\text{A.7})$$

Same expression in equation (A.1) can be made for equation (3.5). Hence, equation (3.5) is represented as follows.

$$a_1 \frac{\partial^2 T}{\partial t^2} + \frac{\partial T}{\partial t} = a_2 \frac{\partial^2 T}{\partial x^2} + a_3 \frac{\partial}{\partial t} \left(\frac{\partial^2 T}{\partial x^2} \right) + a_4 \left(\frac{\partial Q}{\partial t} \right) + a_5 Q + a_6 Q_m \quad (\text{A.8})$$

For applying FVM, integration of equation (A.8) can be made over control volume of grid P with time step from t to $t+\Delta t$.

$$\begin{aligned} & \int_w^e \int_t^{t+\Delta t} \left(a_1 \frac{\partial^2 T}{\partial t^2} + \frac{\partial T}{\partial t} \right) dt dx \\ &= \int_w^e \int_t^{t+\Delta t} \left(a_2 \frac{\partial^2 T}{\partial x^2} + a_3 \frac{\partial}{\partial t} \left(\frac{\partial^2 T}{\partial x^2} \right) + a_4 \left(\frac{\partial Q}{\partial t} \right) + a_5 Q + a_6 Q_m \right) dt dx \end{aligned} \quad (A.9)$$

The algebraic equation for temperature is obtained with applying Crank Nicolson method to equation (A.9).

$$\begin{aligned} & a_{1,p} \frac{T_P^{(1)} - 2T_P^{(0)} + T_P^{(-1)}}{\Delta t^2} \Delta x + \frac{T_P^{(1)} - T_P^{(0)}}{\Delta t} \Delta x = \frac{1}{2} \left\{ \frac{a_{2,e} \frac{T_E^{(1)} - T_P^{(1)}}{\Delta x} - a_{2,w} \frac{T_P^{(1)} - T_W^{(1)}}{\Delta x}}{\Delta x} \right\} \Delta x \\ & + \frac{1}{2} \left\{ \frac{a_{3,e} \left[\frac{T_E^{(1)} - T_P^{(1)}}{\Delta x \Delta t} - \frac{T_E^{(0)} - T_P^{(0)}}{\Delta x \Delta t} \right] - a_{3,w} \left[\frac{T_P^{(1)} - T_W^{(1)}}{\Delta x \Delta t} - \frac{T_P^{(0)} - T_W^{(0)}}{\Delta x \Delta t} \right]}{\Delta x} \right\} \Delta x \\ & + \frac{1}{2} \left\{ \frac{a_{2,e} \frac{T_E^{(0)} - T_P^{(0)}}{\Delta x} - a_{2,w} \frac{T_P^{(0)} - T_W^{(0)}}{\Delta x}}{\Delta x} \right\} \Delta x \\ & + \frac{1}{2} \left\{ \frac{a_{3,e} \left[\frac{T_E^{(0)} - T_P^{(0)}}{\Delta x \Delta t} - \frac{T_E^{(-1)} - T_P^{(-1)}}{\Delta x \Delta t} \right] - a_{3,w} \left[\frac{T_P^{(0)} - T_W^{(0)}}{\Delta x \Delta t} - \frac{T_P^{(-1)} - T_W^{(-1)}}{\Delta x \Delta t} \right]}{\Delta x} \right\} \Delta x \\ & + a_{4,p} \mu_a \left(\frac{\vartheta_{in,sc}^{(1)} - \vartheta_{in,sc}^{(0)}}{\Delta t} \right) \left[C_1 e^{-\frac{D_1 x}{\delta}} - C_2 e^{-\frac{D_2 x}{\delta}} \right] \Delta x \\ & + a_{5,p} \mu_a \vartheta_{in,sc}^{(1)} \left[C_1 e^{-\frac{D_1 x}{\delta}} - C_2 e^{-\frac{D_2 x}{\delta}} \right] \Delta x \\ & + a_{4,p} \mu_a (1 - R_s) \left(\frac{\vartheta_{in,ab}^{(1)} - \vartheta_{in,ab}^{(0)}}{\Delta t} \right) e^{-\mu_a x} \Delta x \\ & + a_{5,p} \mu_a (1 - R_s) \vartheta_{in,ab}^{(1)} e^{-\mu_a x} \Delta x + a_{6,p} Q_{m,e} \Delta x \end{aligned} \quad (A.10)$$

It is assumed that the control volume has uniform properties. Then, equation (A.10) can be arranged as follows.

$$a_P T_P^{(1)} + a_E T_E^{(1)} + a_W T_W^{(1)} = b \quad (A.11)$$

where

$$a_E = -\frac{1}{2} \left(\frac{a_2 \Delta t}{\Delta x} + \frac{a_3}{\Delta x} \right) \quad (\text{A. 12})$$

$$a_W = -\frac{1}{2} \left(\frac{a_2 \Delta t}{\Delta x} + \frac{a_3}{\Delta x} \right) \quad (\text{A. 13})$$

$$a_P = \frac{a_1 \Delta x}{\Delta t} + \Delta x - a_E - a_W \quad (\text{A. 14})$$

$$\begin{aligned} b = & \left(\frac{2a_1 \Delta x}{\Delta t} + \Delta x \right) T_P^{(0)} - \frac{a_1 \Delta x}{\Delta t} T_P^{(-1)} - \frac{1}{2} \left(\frac{a_3}{\Delta x} \right) (T_E^{(0)} - T_P^{(0)}) \\ & + \frac{1}{2} \left(\frac{a_3}{\Delta x} \right) (T_P^{(0)} - T_W^{(0)}) + \frac{1}{2} \left(\frac{a_2 \Delta t}{\Delta x} + \frac{a_3}{\Delta x} \right) (T_E^{(0)} - T_P^{(0)}) \\ & - \frac{1}{2} \left(\frac{a_2 \Delta t}{\Delta x} + \frac{a_3}{\Delta x} \right) (T_P^{(0)} - T_W^{(0)}) - \frac{1}{2} \left(\frac{a_3}{\Delta x} \right) (T_E^{(-1)} - T_P^{(-1)}) \\ & + \frac{1}{2} \left(\frac{a_3}{\Delta x} \right) (T_P^{(-1)} - T_W^{(-1)}) \\ & + a_4 \mu_a (\vartheta_{in,sc}^{(1)} - \vartheta_{in,sc}^{(0)}) \left[C_1 e^{-\frac{D_1 x}{\delta}} - C_2 e^{-\frac{D_2 x}{\delta}} \right] \Delta x \\ & + a_5 \mu_a \vartheta_{in,sc}^{(1)} \left[C_1 e^{-\frac{D_1 x}{\delta}} - C_2 e^{-\frac{D_2 x}{\delta}} \right] \Delta x \Delta t \\ & + a_4 \mu_a (1 - R_s) (\vartheta_{in,ab}^{(1)} - \vartheta_{in,ab}^{(0)}) e^{-\mu_a x} \Delta x \\ & + a_5 \mu_a (1 - R_s) \vartheta_{in,ab}^{(1)} e^{-\mu_a x} \Delta x \Delta t + a_6 Q_{m,e} \Delta x \Delta t \end{aligned} \quad (\text{A. 15})$$

Half cell volume methodology is used for cells in boundary conditions [129]. The algebraic equation obtained with applying Crank Nicolson method to boundary cells follows as.

For cell at the left boundary;

$$a_{1,p} \frac{T_P^{(1)} - 2T_P^{(0)} + T_P^{(-1)} \Delta x}{\Delta t^2} + \frac{T_P^{(1)} - T_P^{(0)} \Delta x}{\Delta t} = \frac{1}{2} \left\{ \frac{a_{2,e} \frac{T_E^{(1)} - T_P^{(1)}}{\Delta x} + \frac{a_{2,p} h}{k_{eff}} (T_\infty^{(1)} - T_P^{(1)})}{\frac{\Delta x}{2}} \right\} \frac{\Delta x}{2}$$

$$\begin{aligned}
& + \frac{1}{2} \left\{ \frac{a_{3,e} \left[\frac{T_E^{(1)} - T_P^{(1)}}{\Delta x \Delta t} - \frac{T_E^{(0)} - T_P^{(0)}}{\Delta x \Delta t} \right] - \frac{a_{3,p} h}{k_{eff}} \left[\frac{-(T_\infty^{(1)} - T_P^{(1)})}{\Delta t} + \frac{(T_\infty^{(0)} - T_P^{(0)})}{\Delta t} \right]}{\frac{\Delta x}{2}} \right\} \frac{\Delta x}{2} \\
& + \frac{1}{2} \left\{ \frac{a_{2,e} \frac{T_E^{(0)} - T_P^{(0)}}{\Delta x} + \frac{a_{2,p} h}{k_{eff}} (T_\infty^{(0)} - T_P^{(0)})}{\frac{\Delta x}{2}} \right\} \frac{\Delta x}{2} \\
& + \frac{1}{2} \left\{ + \frac{a_{3,e} \left[\frac{T_E^{(0)} - T_P^{(0)}}{\Delta x \Delta t} - \frac{T_E^{(-1)} - T_P^{(-1)}}{\Delta x \Delta t} \right] - \frac{a_{3,p} h}{k_{eff}} \left[\frac{-(T_\infty^{(0)} - T_P^{(0)})}{\Delta t} + \frac{(T_\infty^{(-1)} - T_P^{(-1)})}{\Delta t} \right]}{\frac{\Delta x}{2}} \right\} \frac{\Delta x}{2} \\
& + a_{4,p} \mu_a \left(\frac{\vartheta_{in,sc}^{(1)} - \vartheta_{in,sc}^{(0)}}{\Delta t} \right) \left[C_1 e^{-\left(\frac{D_1 x}{\delta}\right)} - C_2 e^{-\left(\frac{D_2 x}{\delta}\right)} \right] \frac{\Delta x}{2} \\
& + a_{5,p} \mu_a \vartheta_{in,sc}^{(1)} \left[C_1 e^{-\left(\frac{D_1 x}{\delta}\right)} - C_2 e^{-\left(\frac{D_2 x}{\delta}\right)} \right] \frac{\Delta x}{2} \\
& + a_{4,p} \mu_a (1 - R_s) \left(\frac{\vartheta_{in,ab}^{(1)} - \vartheta_{in,ab}^{(0)}}{\Delta t} \right) e^{-\mu_a x} \frac{\Delta x}{2} \\
& + a_{5,p} \mu_a (1 - R_s) \vartheta_{in,ab}^{(1)} e^{-\mu_a x} \frac{\Delta x}{2} + a_{6,p} Q_{m,e} \frac{\Delta x}{2} \tag{A.16}
\end{aligned}$$

where $k_{eff} = (k_{eff,t} + k_{eff,b})$ (A.17)

It is assumed that the control volume has uniform properties. Then, equation (A.16) can be arranged as follows.

$$a_P T_P^{(1)} + a_E T_E^{(1)} + a_W T_W^{(1)} = b \tag{A.18}$$

where

$$a_E = -\frac{1}{2} \left(\frac{a_2 \Delta t}{\Delta x} + \frac{a_3}{\Delta x} \right) \tag{A.19}$$

$$a_W = 0 \tag{A.20}$$

$$a_P = \frac{a_{1,p} \Delta x}{2 \Delta t} + \frac{\Delta x}{2} - a_E + \frac{1}{2} \left(\frac{a_2 h \Delta t}{k_{eff}} \right) + \frac{1}{2} \left(\frac{a_3 h}{k_{eff}} \right) \tag{A.21}$$

$$\begin{aligned}
b = & \left(\frac{a_1 \Delta x}{\Delta t} + \frac{\Delta x}{2} - \frac{1}{2} \left(\frac{a_2 h \Delta t}{k_{eff}} \right) \right) T_P^{(0)} + \frac{1}{2} \left(\frac{a_3 h}{k_{eff}} - \frac{a_1 \Delta x}{\Delta t} \right) T_P^{(-1)} - \frac{1}{2} \left(\frac{a_3}{\Delta x} \right) (T_E^{(0)} - T_P^{(0)}) \\
& + \frac{1}{2} \left(\frac{a_2 \Delta t}{\Delta x} + \frac{a_3}{\Delta x} \right) (T_E^{(0)} - T_P^{(0)}) - \frac{1}{2} \left(\frac{a_3}{\Delta x} \right) (T_E^{(-1)} - T_P^{(-1)}) + \left(\frac{a_2 h \Delta t}{k_{eff}} \right) (T_\infty) \\
& + a_4 \mu_a (\vartheta_{in,sc}^{(1)} - \vartheta_{in,sc}^{(0)}) \left[C_1 e^{\left(-\frac{D_1 x}{\delta} \right)} - C_2 e^{\left(-\frac{D_2 x}{\delta} \right)} \right] \frac{\Delta x}{2} \\
& + a_5 \mu_a \vartheta_{in,sc}^{(1)} \left[C_1 e^{\left(-\frac{D_1 x}{\delta} \right)} - C_2 e^{\left(-\frac{D_2 x}{\delta} \right)} \right] \frac{\Delta x \Delta t}{2} \\
& + a_4 \mu_a (1 - R_s) (\vartheta_{in,ab}^{(1)} - \vartheta_{in,ab}^{(0)}) e^{(-\mu_a x)} \frac{\Delta x}{2} \\
& + a_5 \mu_a (1 - R_s) \vartheta_{in,ab}^{(1)} e^{(-\mu_a x)} \frac{\Delta x \Delta t}{2} + a_6 Q_{m,e} \frac{\Delta x \Delta t}{2} \tag{A.21}
\end{aligned}$$

For cell at the right boundary;

$$\begin{aligned}
a_{1,p} \frac{T_P^{(1)} - 2T_P^{(0)} + T_P^{(-1)}}{\Delta t^2} \frac{\Delta x}{2} + \frac{T_P^{(1)} - T_P^{(0)}}{\Delta t} \frac{\Delta x}{2} = & \frac{1}{2} \left\{ \frac{0 - a_{2,w} \frac{T_P^{(1)} - T_W^{(1)}}{\Delta x}}{\frac{\Delta x}{2}} \right\} \frac{\Delta x}{2} \\
& + \frac{1}{2} \left\{ \frac{0 - a_{3,w} \left[\frac{T_P^{(1)} - T_W^{(1)}}{\Delta x \Delta t} - \frac{T_P^{(0)} - T_W^{(0)}}{\Delta x \Delta t} \right]}{\frac{\Delta x}{2}} \right\} \frac{\Delta x}{2} + \frac{1}{2} \left\{ \frac{0 - a_{2,w} \frac{T_P^{(0)} - T_W^{(0)}}{\Delta x}}{\frac{\Delta x}{2}} \right\} \frac{\Delta x}{2} \\
& + \frac{1}{2} \left\{ \frac{0 - a_{3,w} \left[\frac{T_P^{(0)} - T_W^{(0)}}{\Delta x \Delta t} - \frac{T_P^{(-1)} - T_W^{(-1)}}{\Delta x \Delta t} \right]}{\frac{\Delta x}{2}} \right\} \frac{\Delta x}{2} \\
& + a_{4,p} \mu_a \left(\frac{\vartheta_{in,sc}^{(1)} - \vartheta_{in,sc}^{(0)}}{\Delta t} \right) \left[C_1 e^{\left(-\frac{D_1 x}{\delta} \right)} - C_2 e^{\left(-\frac{D_2 x}{\delta} \right)} \right] \frac{\Delta x}{2} \\
& + a_{5,p} \mu_a \vartheta_{in,sc}^{(1)} \left[C_1 e^{\left(-\frac{D_1 x}{\delta} \right)} - C_2 e^{\left(-\frac{D_2 x}{\delta} \right)} \right] \frac{\Delta x}{2} \\
& + a_{4,p} \mu_a (1 - R_s) \left(\frac{\vartheta_{in,ab}^{(1)} - \vartheta_{in,ab}^{(0)}}{\Delta t} \right) e^{(-\mu_a x)} \frac{\Delta x}{2} \\
& + a_{5,p} \mu_a (1 - R_s) \vartheta_{in,ab}^{(1)} e^{(-\mu_a x)} \frac{\Delta x}{2} + a_{6,p} Q_{m,e} \frac{\Delta x}{2} \tag{A.22}
\end{aligned}$$

It is assumed that the control volume has uniform properties. Then, equation (A.22) can be arranged as follows.

$$a_P T_P^{(1)} + a_E T_E^{(1)} + a_W T_W^{(1)} = b \quad (\text{A. 23})$$

where

$$a_E = 0 \quad (\text{A. 24})$$

$$a_W = -\frac{1}{2} \left(\frac{a_2 \Delta t}{\Delta x} + \frac{a_3}{\Delta x} \right) \quad (\text{A. 25})$$

$$a_P = \frac{a_{1,p} \Delta x}{2 \Delta t} + \frac{\Delta x}{2} - a_W \quad (\text{A. 26})$$

$$\begin{aligned} b = & \left(\frac{a_1 \Delta x}{\Delta t} + \frac{\Delta x}{2} \right) T_P^{(0)} - \frac{a_1 \Delta x}{2 \Delta t} T_P^{(-1)} + \frac{1}{2} \left(\frac{a_3}{\Delta x} \right) (T_P^{(0)} - T_W^{(0)}) \\ & - \frac{1}{2} \left(\frac{a_2 \Delta t}{\Delta x} + \frac{a_3}{\Delta x} \right) (T_P^{(0)} - T_W^{(0)}) + \frac{1}{2} \left(\frac{a_3}{\Delta x} \right) (T_P^{(-1)} - T_W^{(-1)}) \\ & + a_4 \mu_a (\vartheta_{in,sc}^{(1)} - \vartheta_{in,sc}^{(0)}) \left[C_1 e^{\left(-\frac{D_1 x}{\delta}\right)} - C_2 e^{\left(-\frac{D_2 x}{\delta}\right)} \right] \frac{\Delta x}{2} \\ & + a_5 \mu_a \vartheta_{in,sc}^{(1)} \left[C_1 e^{\left(-\frac{D_1 x}{\delta}\right)} - C_2 e^{\left(-\frac{D_2 x}{\delta}\right)} \right] \frac{\Delta x \Delta t}{2} \\ & + a_4 \mu_a (1 - R_s) (\vartheta_{in,ab}^{(1)} - \vartheta_{in,ab}^{(0)}) e^{(-\mu_a x)} \frac{\Delta x}{2} \\ & + a_5 \mu_a (1 - R_s) \vartheta_{in,ab}^{(1)} e^{(-\mu_a x)} \frac{\Delta x \Delta t}{2} + a_6 Q_{m,e} \frac{\Delta x \Delta t}{2} \end{aligned} \quad (\text{A. 27})$$

APPENDIX B

Discretization of The Pennes Model

The Pennes model for one dimension is as follows.

$$\rho c \frac{\partial T}{\partial t} = \alpha \frac{\partial^2 T}{\partial x^2} + Q + Q_m + w_b \rho_b c_b (T_b - T) \quad (B.1)$$

For applying FVM, integration of equation (B.1) can be made over control volume of grid P with time step from t to t+Δt.

$$\int_w^e \int_t^{t+\Delta t} \left(\rho c \frac{\partial T}{\partial t} \right) dt dx = \int_w^e \int_t^{t+\Delta t} \left(\alpha \frac{\partial^2 T}{\partial x^2} + Q + Q_m + w_b \rho_b c_b (T_b - T) \right) dt dx \quad (B.2)$$

The algebraic equation for heat flux is obtained with applying Crank Nicolson method to equation (B.2).

$$\begin{aligned} \frac{T_P^{(1)} - T_P^{(0)}}{\Delta t} \Delta x &= \frac{1}{2} \left\{ \frac{\alpha_e \frac{T_E^{(1)} - T_P^{(1)}}{\Delta x} - \alpha_w \frac{T_P^{(1)} - T_W^{(1)}}{\Delta x}}{\Delta x} \right\} \Delta x + \frac{1}{2} \left\{ \frac{\alpha_e \frac{T_E^{(0)} - T_P^{(0)}}{\Delta x} - \alpha_w \frac{T_P^{(0)} - T_W^{(0)}}{\Delta x}}{\Delta x} \right\} \Delta x \\ &+ \frac{1}{2} \left\{ \frac{w_b \rho_b c_b}{\rho_t c_{p,t}} (T_b - T_P^{(1)}) \Delta x \right\} + \frac{1}{2} \left\{ \frac{w_b \rho_b c_b}{\rho_t c_{p,t}} (T_b - T_P^{(0)}) \Delta x \right\} \\ &+ \frac{1}{\rho_t c_{p,t}} \mu_a \vartheta_{in,sc}^{(1)} \left[C_1 e^{\left(-\frac{D_1 x}{\delta}\right)} - C_2 e^{\left(-\frac{D_2 x}{\delta}\right)} \right] \Delta x \\ &+ \frac{1}{\rho_t c_{p,t}} \mu_a (1 - R_s) \vartheta_{in,ab}^{(1)} e^{(-\mu_a x)} \Delta x + \frac{1}{\rho_t c_{p,t}} Q_{m,e} \Delta x \end{aligned} \quad (B.3)$$

It is assumed that the control volume has uniform properties. Then, equation (B.3) can be arranged as follows.

$$a_P T_P^{(1)} + a_E T_E^{(1)} + a_W T_W^{(1)} = b \quad (B.4)$$

where

$$a_E = -\frac{1}{2} \left(\frac{\alpha \Delta t}{\Delta x} \right) \quad (\text{B. 5})$$

$$a_W = -\frac{1}{2} \left(\frac{\alpha \Delta t}{\Delta x} \right) \quad (\text{B. 6})$$

$$a_P = \Delta x - a_E - a_W + \frac{1}{2} \left(\frac{w_b \rho_b c_{p,b} \Delta x \Delta t}{\rho_t c_{p,t}} \right) \quad (\text{B. 7})$$

$$\begin{aligned} b &= \left(\Delta x - \frac{1}{2} \left(\frac{w_b \rho_b c_{p,b} \Delta x \Delta t}{\rho_t c_{p,t}} \right) \right) T_P^{(0)} + \frac{1}{2} \left(\frac{\alpha \Delta t}{\Delta x} \right) (T_E^{(0)} - T_P^{(0)}) \\ &- \frac{1}{2} \left(\frac{\alpha \Delta t}{\Delta x} \right) (T_P^{(0)} - T_W^{(0)}) + \frac{w_b \rho_b c_{p,b} \Delta x \Delta t}{\rho_t c_{p,t}} T_b \\ &+ \frac{1}{\rho_t c_{p,t}} \mu_a \vartheta_{in,sc}^{(1)} \left[C_1 e^{\left(-\frac{D_1 x}{\delta} \right)} - C_2 e^{\left(-\frac{D_2 x}{\delta} \right)} \right] \Delta x \Delta t \\ &+ \frac{1}{\rho_t c_{p,t}} \mu_a (1 - R_s) \vartheta_{in,ab}^{(1)} e^{(-\mu_a x)} \Delta x \Delta t + \frac{1}{\rho_t c_{p,t}} Q_{m,e} \Delta x \Delta t \end{aligned} \quad (\text{B. 8})$$

Half cell volume methodology is used for cells in boundary conditions [129]. The algebraic equation obtained with applying Crank Nicolson method to boundary cells follows as.

For cell at the left boundary;

$$\begin{aligned} \frac{T_P^{(1)} - T_P^{(0)} \Delta x}{\Delta t} \frac{\Delta x}{2} &= \frac{1}{2} \left\{ \frac{\alpha_e \frac{T_E^{(1)} - T_P^{(1)}}{\Delta x} + \frac{\alpha_w h}{k_{t,w}} (T_\infty^{(1)} - T_P^{(1)})}{\frac{\Delta x}{2}} \right\} \frac{\Delta x}{2} \\ &+ \frac{1}{2} \left\{ \frac{\alpha_e \frac{T_E^{(0)} - T_P^{(0)}}{\Delta x} + \frac{\alpha_w h}{k_{t,w}} (T_\infty^{(0)} - T_P^{(0)})}{\frac{\Delta x}{2}} \right\} \frac{\Delta x}{2} + \frac{1}{2} \left\{ \frac{w_b \rho_b c_{p,b}}{\rho_t c_{p,t}} (T_b - T_P^{(1)}) \frac{\Delta x}{2} \right\} \\ &+ \frac{1}{2} \left\{ \frac{w_b \rho_b c_{p,b}}{\rho_t c_{p,t}} (T_b - T_P^{(0)}) \frac{\Delta x}{2} \right\} + \frac{1}{\rho_t c_{p,t}} \mu_a \vartheta_{in,sc}^{(1)} \left[C_1 e^{\left(-\frac{D_1 x}{\delta} \right)} - C_2 e^{\left(-\frac{D_2 x}{\delta} \right)} \right] \frac{\Delta x}{2} \\ &+ \frac{1}{\rho_t c_{p,t}} \mu_a (1 - R_s) \vartheta_{in,ab}^{(1)} e^{(-\mu_a x)} \frac{\Delta x}{2} + \frac{1}{\rho_t c_{p,t}} Q_{m,e} \frac{\Delta x}{2} \end{aligned} \quad (\text{B. 9})$$

It is assumed that the control volume has uniform properties. Then, equation (B.9) can be arranged as follows.

$$a_P T_P^{(1)} + a_E T_E^{(1)} + a_W T_W^{(1)} = b \quad (\text{B.10})$$

Where

$$a_E = -\frac{1}{2} \left(\frac{\alpha \Delta t}{\Delta x} \right) \quad (\text{B.10})$$

$$a_W = 0 \quad (\text{B.11})$$

$$a_P = \frac{\Delta x}{2} - a_E + \frac{1}{2} \left(\frac{w_b \rho_b c_{p,b} \Delta x \Delta t}{2 \rho_t c_{p,t}} \right) + \frac{1}{2} \left(\frac{\alpha h \Delta t}{k_t} \right) \quad (\text{B.12})$$

$$\begin{aligned} b = & \left(\frac{\Delta x}{2} - \frac{1}{2} \left(\frac{w_b \rho_b c_{p,b} \Delta x \Delta t}{2 \rho_t c_{p,t}} \right) - \frac{1}{2} \left(\frac{\alpha h \Delta t}{k_t} \right) \right) T_P^{(0)} + \frac{1}{2} \left(\frac{\alpha \Delta t}{\Delta x} \right) (T_E^{(0)} - T_P^{(0)}) \\ & + \frac{w_b \rho_b c_{p,b} \Delta x \Delta t}{2 \rho_t c_{p,t}} T_b + \frac{\alpha h \Delta t}{k_t} T_\infty + \frac{1}{\rho_t c_{p,t}} \mu_a \vartheta_{in,sc}^{(1)} \left[C_1 e^{\left(-\frac{D_1 x}{\delta} \right)} - C_2 e^{\left(-\frac{D_2 x}{\delta} \right)} \right] \frac{\Delta x \Delta t}{2} \\ & + \frac{1}{\rho_t c_{p,t}} \mu_a (1 - R_s) \vartheta_{in,ab}^{(1)} e^{(-\mu_a x)} \frac{\Delta x \Delta t}{2} + \frac{1}{\rho_t c_{p,t}} Q_{m,e} \frac{\Delta x \Delta t}{2} \end{aligned} \quad (\text{B.13})$$

For cell at the right boundary;

$$\begin{aligned} \frac{T_P^{(1)} - T_P^{(0)}}{\Delta t} \frac{\Delta x}{2} = & \frac{1}{2} \left\{ \frac{0 - \alpha_w \frac{T_P^{(1)} - T_W^{(1)}}{\Delta x}}{\frac{\Delta x}{2}} \right\} \frac{\Delta x}{2} + \frac{1}{2} \left\{ \frac{0 - \alpha_w \frac{T_P^{(0)} - T_W^{(0)}}{\Delta x}}{\frac{\Delta x}{2}} \right\} \frac{\Delta x}{2} \\ & + \frac{1}{2} \left\{ \frac{w_b \rho_b c_{p,b}}{\rho_t c_{p,t}} (T_b - T_P^{(1)}) \frac{\Delta x}{2} \right\} + \frac{1}{2} \left\{ \frac{w_b \rho_b c_{p,b}}{\rho_t c_{p,t}} (T_b - T_P^{(0)}) \frac{\Delta x}{2} \right\} \\ & + \frac{1}{\rho_t c_{p,t}} \mu_a \vartheta_{in,sc}^{(1)} \left[C_1 e^{\left(-\frac{D_1 x}{\delta} \right)} - C_2 e^{\left(-\frac{D_2 x}{\delta} \right)} \right] \frac{\Delta x}{2} \\ & + \frac{1}{\rho_t c_{p,t}} \mu_a (1 - R_s) \vartheta_{in,ab}^{(1)} e^{(-\mu_a x)} \frac{\Delta x}{2} + \frac{1}{\rho_t c_{p,t}} Q_{m,e} \frac{\Delta x}{2} \end{aligned} \quad (\text{B.14})$$

It is assumed that the control volume has uniform properties. Then, equation (B.14) can be arranged as follows.

$$a_P T_P^{(1)} + a_E T_E^{(1)} + a_W T_W^{(1)} = b \quad (\text{B.15})$$

where

$$a_E = 0 \quad (\text{B.16})$$

$$a_W = -\frac{1}{2} \left(\frac{\alpha \Delta t}{\Delta x} \right) \quad (\text{B.17})$$

$$a_P = \frac{\Delta x}{2} - a_W + \frac{1}{2} \left(\frac{w_b \rho_b c_{p,b} \Delta x \Delta t}{2 \rho_t c_{p,t}} \right) \quad (\text{B.18})$$

$$\begin{aligned} b = & \left(\frac{\Delta x}{2} - \frac{1}{2} \left(\frac{w_b \rho_b c_{p,b} \Delta x \Delta t}{2 \rho_t c_{p,t}} \right) \right) T_P^{(0)} - \frac{1}{2} \left(\frac{\alpha \Delta t}{\Delta x} \right) (T_P^{(0)} - T_W^{(0)}) + \frac{w_b \rho_b c_{p,b} \Delta x \Delta t}{2 \rho_t c_{p,t}} T_b \\ & + \frac{1}{\rho_t c_{p,t}} \mu_a \vartheta_{in,sc}^{(1)} \left[C_1 e^{\left(-\frac{D_1 x}{\delta} \right)} - C_2 e^{\left(-\frac{D_2 x}{\delta} \right)} \right] \frac{\Delta x \Delta t}{2} \\ & + \frac{1}{\rho_t c_{p,t}} \mu_a (1 - R_s) \vartheta_{in,ab}^{(1)} e^{(-\mu_a x)} \frac{\Delta x \Delta t}{2} + \frac{1}{\rho_t c_{p,t}} Q_{m,e} \frac{\Delta x \Delta t}{2} \end{aligned} \quad (\text{B.19})$$

APPENDIX C

Discretization of DPL Model

DPL model is formed by combining the energy equation and non-Fourier heat conduction equation, which are given below.

$$\begin{aligned} \tau_q \frac{\partial^2 T}{\partial t^2} + \left(1 + \frac{\tau_q w_b \rho_b c_{p,b}}{\rho_t c_{p,t}}\right) \frac{\partial T}{\partial t} &= \alpha \frac{\partial^2 T}{\partial x^2} + \alpha \tau_T \frac{\partial}{\partial t} \left(\frac{\partial^2 T}{\partial x^2}\right) + \frac{w_b \rho_b c_{p,b}}{\rho_t c_{p,t}} (T_b - T) \\ + \frac{\tau_q}{\rho_t c_{p,t}} \left(\frac{\partial Q_m}{\partial t} + \frac{\partial Q}{\partial t}\right) + \frac{Q_m}{\rho_t c_{p,t}} + \frac{Q}{\rho_t c_{p,t}} \end{aligned} \quad (C.1)$$

For applying FVM, integration of equation (C.1) can be made over control volume of grid P with time step from t to t+Δt.

$$\begin{aligned} \int_w^e \int_t^{t+\Delta t} \left(\tau_q \frac{\partial^2 T}{\partial t^2} + \left(1 + \frac{\tau_q w_b \rho_b c_{p,b}}{\rho_t c_{p,t}}\right) \frac{\partial T}{\partial t} \right) dt dx \\ = \int_w^e \int_t^{t+\Delta t} \left(\alpha \frac{\partial^2 T}{\partial x^2} + \alpha \tau_T \frac{\partial}{\partial t} \left(\frac{\partial^2 T}{\partial x^2}\right) + \frac{w_b \rho_b c_{p,b}}{\rho_t c_{p,t}} (T_b - T) + \frac{\tau_q}{\rho_t c_{p,t}} \left(\frac{\partial Q_m}{\partial t} + \frac{\partial Q}{\partial t}\right) \right) dt dx \\ + \int_w^e \int_t^{t+\Delta t} \left(\frac{Q_m}{\rho_t c_{p,t}} + \frac{Q}{\rho_t c_{p,t}} \right) dt dx \end{aligned} \quad (C.2)$$

The algebraic equation for heat flux is obtained with applying Crank Nicolson method to equation (C.2).

$$\begin{aligned} \tau_q \frac{T_P^{(1)} - 2T_P^{(0)} + T_P^{(-1)}}{\Delta t^2} \Delta x + \left(1 + \frac{\tau_q w_b \rho_b c_{p,b}}{\rho_t c_{p,t}}\right) \frac{T_P^{(1)} - T_P^{(0)}}{\Delta t} \Delta x \\ = \frac{1}{2} \left\{ \frac{\alpha_e \frac{T_E^{(1)} - T_P^{(1)}}{\Delta x} - \alpha_w \frac{T_P^{(1)} - T_W^{(1)}}{\Delta x}}{\Delta x} \right\} \Delta x + \frac{1}{2} \left\{ \frac{\alpha_e \frac{T_E^{(0)} - T_P^{(0)}}{\Delta x} - \alpha_w \frac{T_P^{(0)} - T_W^{(0)}}{\Delta x}}{\Delta x} \right\} \Delta x \\ + \frac{1}{2} \left\{ \frac{\alpha_e \tau_T \left[\frac{T_E^{(1)} - T_P^{(1)}}{\Delta x \Delta t} - \frac{T_E^{(0)} - T_P^{(0)}}{\Delta x \Delta t} \right] - \alpha_w \tau_T \left[\frac{T_P^{(1)} - T_W^{(1)}}{\Delta x \Delta t} - \frac{T_P^{(0)} - T_W^{(0)}}{\Delta x \Delta t} \right]}{\Delta x} \right\} \Delta x \end{aligned}$$

$$\begin{aligned}
& + \frac{1}{2} \left\{ + \frac{\alpha_e \tau_T \left[\frac{T_E^{(0)} - T_P^{(0)}}{\Delta x \Delta t} - \frac{T_E^{(-1)} - T_P^{(-1)}}{\Delta x \Delta t} \right] - \alpha_w \tau_T \left[\frac{T_P^{(0)} - T_W^{(0)}}{\Delta x \Delta t} - \frac{T_P^{(-1)} - T_W^{(-1)}}{\Delta x \Delta t} \right]}{\Delta x} \right\} \Delta x \\
& + \frac{1}{2} \left\{ \frac{w_b \rho_b c_{p,b}}{\rho_t c_{p,t}} (T_b - T_P^{(1)}) \Delta x \right\} + \frac{1}{2} \left\{ \frac{w_b \rho_b c_{p,b}}{\rho_t c_{p,t}} (T_b - T_P^{(0)}) \Delta x \right\} \\
& + \frac{\tau_q}{\rho_t c_{p,t}} \mu_a \left(\frac{\vartheta_{in,sc}^{(1)} - \vartheta_{in,sc}^{(0)}}{\Delta t} \right) \left[C_1 e^{\left(-\frac{D_1 x}{\delta} \right)} - C_2 e^{\left(-\frac{D_2 x}{\delta} \right)} \right] \Delta x \\
& + \frac{1}{\rho_t c_{p,t}} \mu_a \vartheta_{in,sc}^{(1)} \left[C_1 e^{\left(-\frac{D_1 x}{\delta} \right)} - C_2 e^{\left(-\frac{D_2 x}{\delta} \right)} \right] \Delta x \\
& + \frac{\tau_q}{\rho_t c_{p,t}} \mu_a (1 - R_s) \left(\frac{\vartheta_{in,ab}^{(1)} - \vartheta_{in,ab}^{(0)}}{\Delta t} \right) e^{(-\mu_a x)} \Delta x \\
& + \frac{1}{\rho_t c_{p,t}} \mu_a (1 - R_s) \vartheta_{in,ab}^{(1)} e^{(-\mu_a x)} \Delta x + \frac{1}{\rho_t c_{p,t}} Q_{m,e} \Delta x \tag{C.3}
\end{aligned}$$

It is assumed that the control volume has uniform properties. Then, equation (C.3) can be arranged as follows.

$$a_P T_P^{(1)} + a_E T_E^{(1)} + a_W T_W^{(1)} = b \tag{C.4}$$

where

$$a_E = -\frac{1}{2} \left(\frac{\alpha \Delta t}{\Delta x} + \frac{\alpha \tau_T}{\Delta x} \right) \tag{C.5}$$

$$a_W = -\frac{1}{2} \left(\frac{\alpha \Delta t}{\Delta x} + \frac{\alpha \tau_T}{\Delta x} \right) \tag{C.6}$$

$$a_P = \frac{\tau_q \Delta x}{\Delta t} + \Delta x + \frac{\tau_q w_b \rho_b c_{p,b} \Delta x}{\rho_t c_{p,t}} - a_E - a_W + \frac{1}{2} \left(\frac{w_b \rho_b c_{p,b} \Delta x \Delta t}{\rho_t c_{p,t}} \right) \tag{C.7}$$

$$\begin{aligned}
b & = \left(\frac{2\tau_q \Delta x}{\Delta t} + \Delta x + \frac{\tau_q w_b \rho_b c_{p,b} \Delta x}{\rho_t c_{p,t}} - \frac{1}{2} \left(\frac{w_b \rho_b c_{p,b} \Delta x \Delta t}{\rho_t c_{p,t}} \right) \right) T_P^{(0)} - \frac{\tau_q \Delta x}{\Delta t} T_P^{(-1)} \\
& + \frac{1}{2} \left(\frac{\alpha \Delta t}{\Delta x} \right) (T_E^{(0)} - T_P^{(0)}) - \frac{1}{2} \left(\frac{\alpha \Delta t}{\Delta x} \right) (T_P^{(0)} - T_W^{(0)}) \\
& - \frac{1}{2} \left(\frac{\alpha \tau_T}{\Delta x} \right) (T_E^{(-1)} - T_P^{(-1)}) + \frac{1}{2} \left(\frac{\alpha \tau_T}{\Delta x} \right) (T_P^{(-1)} - T_W^{(-1)}) + \frac{w_b \rho_b c_{p,b} \Delta x \Delta t}{\rho_t c_{p,t}} T_b \\
& + \frac{\tau_q}{\rho_t c_{p,t}} \mu_a (\vartheta_{in,sc}^{(1)} - \vartheta_{in,sc}^{(0)}) \left[C_1 e^{\left(-\frac{D_1 x}{\delta} \right)} - C_2 e^{\left(-\frac{D_2 x}{\delta} \right)} \right] \Delta x
\end{aligned}$$

$$\begin{aligned}
& + \frac{1}{\rho_t c_{p,t}} \mu_a \vartheta_{in,sc}^{(1)} \left[C_1 e^{\left(-\frac{D_1 x}{\delta}\right)} - C_2 e^{\left(-\frac{D_2 x}{\delta}\right)} \right] \Delta x \Delta t \\
& + \frac{\tau_q}{\rho_t c_{p,t}} \mu_a (1 - R_s) (\vartheta_{in,ab}^{(1)} - \vartheta_{in,ab}^{(1)}) e^{(-\mu_a x)} \Delta x \\
& + \frac{1}{\rho_t c_{p,t}} \mu_a (1 - R_s) \vartheta_{in,ab}^{(1)} e^{(-\mu_a x)} \Delta x \Delta t + \frac{1}{\rho_t c_{p,t}} Q_{m,e} \Delta x \Delta t \tag{C.8}
\end{aligned}$$

Half cell volume methodology is used for cells in boundary conditions [129]. The algebraic equation obtained with applying Crank Nicolson method to boundary cells follows as.

For cell at the left boundary;

$$\begin{aligned}
& \tau_q \frac{T_P^{(1)} - 2T_P^{(0)} + T_P^{(-1)} \Delta x}{\Delta t^2} + \left(1 + \frac{\tau_q w_b \rho_b c_{p,b}}{\rho_t c_{p,t}} \right) \frac{T_P^{(1)} - T_P^{(0)} \Delta x}{\Delta t} \\
& = \frac{1}{2} \left\{ \frac{\alpha_e \frac{T_E^{(1)} - T_P^{(1)}}{\Delta x} + \frac{\alpha_w h}{k_{t,w}} (T_\infty^{(1)} - T_P^{(1)})}{\frac{\Delta x}{2}} \right\} \frac{\Delta x}{2} + \frac{1}{2} \left\{ \frac{\alpha_e \frac{T_E^{(0)} - T_P^{(0)}}{\Delta x} + \frac{\alpha_w h}{k_{t,w}} (T_\infty^{(0)} - T_P^{(0)})}{\frac{\Delta x}{2}} \right\} \frac{\Delta x}{2} \\
& + \frac{1}{2} \left\{ \frac{\alpha_e \tau_T \left[\frac{T_E^{(1)} - T_P^{(1)}}{\Delta x \Delta t} - \frac{T_E^{(0)} - T_P^{(0)}}{\Delta x \Delta t} \right] - \frac{\alpha_w \tau_T h}{k_{t,w}} \left[\frac{-(T_\infty^{(1)} - T_P^{(1)})}{\Delta t} + \frac{(T_\infty^{(0)} - T_P^{(0)})}{\Delta t} \right]}{\frac{\Delta x}{2}} \right\} \frac{\Delta x}{2} \\
& + \frac{1}{2} \left\{ \frac{\alpha_e \tau_T \left[\frac{T_E^{(0)} - T_P^{(0)}}{\Delta x \Delta t} - \frac{T_E^{(-1)} - T_P^{(-1)}}{\Delta x \Delta t} \right] - \frac{\alpha_w \tau_T h}{k_{t,w}} \left[\frac{-(T_\infty^{(0)} - T_P^{(0)})}{\Delta t} + \frac{(T_\infty^{(-1)} - T_P^{(-1)})}{\Delta t} \right]}{\frac{\Delta x}{2}} \right\} \frac{\Delta x}{2} \\
& + \frac{1}{2} \left\{ \frac{w_b \rho_b c_{p,b}}{\rho_t c_{p,t}} (T_b - T_P^{(1)}) \frac{\Delta x}{2} \right\} + \frac{1}{2} \left\{ \frac{w_b \rho_b c_{p,b}}{\rho_t c_{p,t}} (T_b - T_P^{(0)}) \frac{\Delta x}{2} \right\} \\
& + \frac{\tau_q}{\rho_t c_{p,t}} \mu_a \left(\frac{\vartheta_{in,sc}^{(1)} - \vartheta_{in,sc}^{(0)}}{\Delta t} \right) \left[C_1 e^{\left(-\frac{D_1 x}{\delta}\right)} - C_2 e^{\left(-\frac{D_2 x}{\delta}\right)} \right] \frac{\Delta x}{2} \\
& + \frac{1}{\rho_t c_{p,t}} \mu_a \vartheta_{in,sc}^{(1)} \left[C_1 e^{\left(-\frac{D_1 x}{\delta}\right)} - C_2 e^{\left(-\frac{D_2 x}{\delta}\right)} \right] \frac{\Delta x}{2} \\
& + \frac{\tau_q}{\rho_t c_{p,t}} \mu_a (1 - R_s) \left(\frac{\vartheta_{in,ab}^{(1)} - \vartheta_{in,ab}^{(1)}}{\Delta t} \right) e^{(-\mu_a x)} \frac{\Delta x}{2} \\
& + \frac{1}{\rho_t c_{p,t}} \mu_a (1 - R_s) \vartheta_{in,ab}^{(1)} e^{(-\mu_a x)} \frac{\Delta x}{2} + \frac{1}{\rho_t c_{p,t}} Q_{m,e} \frac{\Delta x}{2} \tag{C.9}
\end{aligned}$$

It is assumed that the control volume has uniform properties. Then, equation (C.9) can be arranged as follows.

$$a_P T_P^{(1)} + a_E T_E^{(1)} + a_W T_W^{(1)} = b \quad (\text{C.10})$$

where

$$a_E = -\frac{1}{2} \left(\frac{\alpha \Delta t}{\Delta x} + \frac{\alpha \tau_T}{\Delta x} \right) \quad (\text{C.11})$$

$$a_W = 0 \quad (\text{C.12})$$

$$\begin{aligned} a_P &= \frac{\tau_q \Delta x}{2 \Delta t} + \frac{\Delta x}{2} + \frac{\tau_q w_b \rho_b c_{p,b} \Delta x}{2 \rho_t c_{p,t}} - a_E + \frac{1}{2} \left(\frac{w_b \rho_b c_{p,b} \Delta x \Delta t}{2 \rho_t c_{p,t}} \right) \\ &+ \frac{1}{2} \left(\frac{\alpha h \Delta t}{k_t} \right) + \frac{1}{2} \left(\frac{\alpha \tau_T h}{k_t} \right) \end{aligned} \quad (\text{C.13})$$

$$\begin{aligned} b &= \left(\frac{\tau_q \Delta x}{\Delta t} + \frac{\Delta x}{2} + \frac{\tau_q w_b \rho_b c_{p,b} \Delta x}{2 \rho_t c_{p,t}} - \frac{1}{2} \left(\frac{w_b \rho_b c_{p,b} \Delta x \Delta t}{2 \rho_t c_{p,t}} \right) - \frac{1}{2} \left(\frac{\alpha h \Delta t}{k_t} \right) \right) T_P^{(0)} \\ &+ \frac{1}{2} \left(\frac{\alpha \tau_T h}{k_t} - \frac{\tau_q \Delta x}{2 \Delta t} \right) T_P^{(-1)} + \frac{1}{2} \left(\frac{\alpha \Delta t}{\Delta x} \right) (T_E^{(0)} - T_P^{(0)}) - \frac{1}{2} \left(\frac{\alpha \tau_T}{\Delta x} \right) (T_E^{(-1)} - T_P^{(-1)}) \\ &+ \frac{w_b \rho_b c_{p,b} \Delta x \Delta t}{2 \rho_t c_{p,t}} T_b + \frac{\alpha h \Delta t}{k_t} T_\infty \\ &+ \frac{\tau_q}{\rho_t c_{p,t}} \mu_a (\vartheta_{in,sc}^{(1)} - \vartheta_{in,sc}^{(0)}) \left[C_1 e^{\left(-\frac{D_1 x}{\delta}\right)} - C_2 e^{\left(-\frac{D_2 x}{\delta}\right)} \right] \frac{\Delta x}{2} \\ &+ \frac{1}{\rho_t c_{p,t}} \mu_a \vartheta_{in,sc}^{(1)} \left[C_1 e^{\left(-\frac{D_1 x}{\delta}\right)} - C_2 e^{\left(-\frac{D_2 x}{\delta}\right)} \right] \frac{\Delta x \Delta t}{2} \\ &+ \frac{\tau_q}{\rho_t c_{p,t}} \mu_a (1 - 6R_s) (\vartheta_{in,ab}^{(1)} - \vartheta_{in,ab}^{(0)}) e^{(-\mu_a x)} \frac{\Delta x}{2} \\ &+ \frac{1}{\rho_t c_{p,t}} \mu_a (1 - R_s) \vartheta_{in,ab}^{(1)} e^{(-\mu_a x)} \frac{\Delta x \Delta t}{2} + \frac{1}{\rho_t c_{p,t}} Q_{m,e} \frac{\Delta x \Delta t}{2} \end{aligned} \quad (\text{C.14})$$

For cell at the right boundary;

$$\tau_q \frac{T_P^{(1)} - 2T_P^{(0)} + T_P^{(-1)} \Delta x}{\Delta t^2} + \left(1 + \frac{\tau_q w_b \rho_b c_{p,b}}{\rho_t c_{p,t}} \right) \frac{T_P^{(1)} - T_P^{(0)} \Delta x}{\Delta t} = \frac{1}{2} \left\{ \frac{0 - \alpha_w \frac{T_P^{(1)} - T_W^{(1)}}{\Delta x}}{\frac{\Delta x}{2}} \right\} \frac{\Delta x}{2}$$

$$\begin{aligned}
& + \frac{1}{2} \left\{ \frac{0 - \alpha_w \tau_T \left[\frac{T_P^{(1)} - T_W^{(1)}}{\Delta x \Delta t} - \frac{T_P^{(0)} - T_W^{(0)}}{\Delta x \Delta t} \right]}{\frac{\Delta x}{2}} \right\} \frac{\Delta x}{2} + \frac{1}{2} \left\{ \frac{0 - \alpha_w \frac{T_P^{(0)} - T_W^{(0)}}{\Delta x}}{\frac{\Delta x}{2}} \right\} \frac{\Delta x}{2} \\
& + \frac{1}{2} \left\{ \frac{0 - \alpha_w \tau_T \left[\frac{T_P^{(0)} - T_W^{(0)}}{\Delta x \Delta t} - \frac{T_P^{(-1)} - T_W^{(-1)}}{\Delta x \Delta t} \right]}{\frac{\Delta x}{2}} \right\} \frac{\Delta x}{2} + \frac{1}{2} \left\{ \frac{w_b \rho_b c_{p,b}}{\rho_t c_{p,t}} (T_b - T_P^{(1)}) \frac{\Delta x}{2} \right\} \\
& + \frac{1}{2} \left\{ \frac{w_b \rho_b c_{p,b}}{\rho_t c_{p,t}} (T_b - T_P^{(0)}) \frac{\Delta x}{2} \right\} + \frac{\tau_q}{\rho_t c_{p,t}} \mu_a \left(\frac{\vartheta_{in,sc}^{(1)} - \vartheta_{in,sc}^{(0)}}{\Delta t} \right) \left[C_1 e^{(-\frac{D_1 x}{\delta})} - C_2 e^{(-\frac{D_2 x}{\delta})} \right] \frac{\Delta x}{2} \\
& + \frac{1}{\rho_t c_{p,t}} \mu_a \vartheta_{in,sc}^{(1)} \left[C_1 e^{(-\frac{D_1 x}{\delta})} - C_2 e^{(-\frac{D_2 x}{\delta})} \right] \frac{\Delta x}{2} + \frac{\tau_q}{\rho_t c_{p,t}} \mu_a (1 - R_s) \left(\frac{\vartheta_{in,ab}^{(1)} - \vartheta_{in,ab}^{(1)}}{\Delta t} \right) e^{(-\mu_a x)} \frac{\Delta x}{2} \\
& + \frac{1}{\rho_t c_{p,t}} \mu_a (1 - R_s) \vartheta_{in,ab}^{(1)} e^{(-\mu_a x)} \frac{\Delta x}{2} + \frac{1}{\rho_t c_{p,t}} Q_{m,e} \frac{\Delta x}{2} \tag{C.15}
\end{aligned}$$

It is assumed that the control volume has uniform properties. Then, equation (C.15) can be arranged as follows.

$$a_P T_P^{(1)} + a_E T_E^{(1)} + a_W T_W^{(1)} = b \tag{C.16}$$

Where

$$a_E = 0 \tag{C.17}$$

$$a_W = -\frac{1}{2} \left(\frac{\alpha \Delta t}{\Delta x} + \frac{\alpha \tau_T}{\Delta x} \right) \tag{C.18}$$

$$a_P = \frac{\tau_q \Delta x}{2 \Delta t} + \frac{\Delta x}{2} + \frac{\tau_q w_b \rho_b c_{p,b} \Delta x}{2 \rho_t c_{p,t}} - a_W + \frac{1}{2} \left(\frac{w_b \rho_b c_{p,b} \Delta x \Delta t}{2 \rho_t c_{p,t}} \right) \tag{C.19}$$

$$\begin{aligned}
b & = \left(\frac{\tau_q \Delta x}{\Delta t} + \frac{\Delta x}{2} + \frac{\tau_q w_b \rho_b c_{p,b} \Delta x}{2 \rho_t c_{p,t}} - \frac{1}{2} \left(\frac{w_b \rho_b c_{p,b} \Delta x \Delta t}{2 \rho_t c_{p,t}} \right) \right) T_P^{(0)} - \frac{\tau_q \Delta x}{2 \Delta t} T_P^{(-1)} \\
& - \frac{1}{2} \left(\frac{\alpha \Delta t}{\Delta x} \right) (T_P^{(0)} - T_W^{(0)}) + \frac{1}{2} \left(\frac{\alpha \tau_T}{\Delta x} \right) (T_P^{(-1)} - T_W^{(-1)}) + \frac{w_b \rho_b c_{p,b} \Delta x \Delta t}{2 \rho_t c_{p,t}} T_b \\
& + \frac{\tau_q}{\rho_t c_{p,t}} \mu_a (\vartheta_{in,sc}^{(1)} - \vartheta_{in,sc}^{(0)}) \left[C_1 e^{(-\frac{D_1 x}{\delta})} - C_2 e^{(-\frac{D_2 x}{\delta})} \right] \frac{\Delta x}{2} \\
& + \frac{1}{\rho_t c_{p,t}} \mu_a \vartheta_{in,sc}^{(1)} \left[C_1 e^{(-\frac{D_1 x}{\delta})} - C_2 e^{(-\frac{D_2 x}{\delta})} \right] \frac{\Delta x \Delta t}{2}
\end{aligned}$$

$$\begin{aligned}
& + \frac{\tau_q}{\rho_t c_{p,t}} \mu_a (1 - R_s) (\vartheta_{in,ab}^{(1)} - \vartheta_{in,ab}^{(1)}) e^{(-\mu_a x)} \frac{\Delta x}{2} \\
& + \frac{1}{\rho_t c_{p,t}} \mu_a (1 - R_s) \vartheta_{in,ab}^{(1)} e^{(-\mu_a x)} \frac{\Delta x \Delta t}{2} + \frac{1}{\rho_t c_{p,t}} Q_{m,e} \frac{\Delta x \Delta t}{2}
\end{aligned} \tag{C.20}$$

APPENDIX D

MATLAB Code for Model in This Study

```
clear all;
clc;
close all;

%%%%%%%%%%%%%%%%%%%%%%%%%%%%%%%%%%%%%%%%%%%%%%%%%%%%%%%%%%%%%%%%%%%%%%%%
%%%%%%%%%%%%%%%%%%%%%%%%%%%%%%%%%%%%%%%%%%%%%%%%%%%%%%%%%%%%%%%%%%%%%%%% Problem Definition %%%%%%%%%
%%%%%%%%%%%%%%%%%%%%%%%%%%%%%%%%%%%%%%%%%%%%%%%%%%%%%%%%%%%%%%%%%%%%%%%%

tic; % Used for measuring run time
tTotal =90; % Total time [s]
tin =10; % Exposure time [s]
dt =0.01; % Constant time step [s]
Nx =120; % Number of cells in x direction
L =0.05; % Length [m]
dx =L/(Nx); % Constant cell size in x direction
IterN =tTotal/dt; % Iteration number
IterNb =tin/dt; % Iteration number for heat flux exposure time
ms =3*Nx+1;

% Arrays and matrices %

T =zeros(Nx+1,1); % Temperature components at nodes
Ts =zeros(1,IterN); % Temperature values at Cell (1)
ii =zeros(ms,1); % Row number of aT sparse matrix
jj =zeros(ms,1); % Column number of aT sparse matrix
cc =zeros(ms,1); % Values of aT sparse matrix
aT =zeros(Nx+1,1); % Coefficients of new heat flux values
aTold1 =zeros(Nx+1,1); % Coefficients of previous heat flux values
aTold2 =zeros(Nx+1,1); % Coefficients of one before previous heat flux values
rhsa =zeros(Nx+1,1); % Right hand side vector of the energy equation
Tn =zeros(Nx+1,1); % New temperature values at nodes
```

```
Told =zeros(Nx+1,1); % Previous values at nodes
Told2 =zeros(Nx+1,1); % One before previous temperature values at nodes
```

```
% Optical properties %
```

```
% For 808 nm laser
```

```
Rd =0.05; % Diffuse reflectance
mu_a =78; % Absorption coefficient [m^-1]
mu_sr =2104; % Reduced scattering coefficient [m^-1]
```

```
delta =1/sqrt(3*mu_a*(mu_a+mu_sr)); % Effective optical penetration depth [m]
```

```
% Coefficients of diffusion theory equation
```

```
C1=3.09+5.44*Rd-2.12*exp(-21.5*Rd);
D1=1-(1-(1/sqrt(3)))*exp(-20.1*Rd);
C2=2.09-1.47*Rd-2.12*exp(-21.5*Rd);
D2=1.63*exp(3.40*Rd);
```

```
% For 1940 nm laser
```

```
Rs =0.0475; % Specular reflectance
mu_a_a =5643; % Absorption coefficient [m^-1]
```

```
% Boundary Conditions %
```

```
qin_A =0; % Laser intensity for 1940 nm laser [W/m^2]
qin_S =14000; % Laser intensity for 808 nm laser [W/m^2]
```

```
%%%%%%%%%%%%%%%%%%%%%%%%%%%%%%%%%%%%%%%%%%%%%%%%%%%%%%%%%%%%%%%%%%%%%%%%
%%%%%%%%%%%%%%%%%%%%%%%%%%%%%%%%%%%%%%%%%%%%%%%%%%%%%%%%%%%%%%%%%%%%%%%% Initial values and boundary conditions %%%%%%%%%
%%%%%%%%%%%%%%%%%%%%%%%%%%%%%%%%%%%%%%%%%%%%%%%%%%%%%%%%%%%%%%%%%%%%%%%%
```

```
h =10; % Heat convection [W/mK]
T_Inf =22.35; % Room temperature [C]
qm =368.1; % Constant metabolic heat generation [W/m^3]
```

```

Tn(1:Nx+1,1)      =33.2;          % Temperature values at nodes
Told(1:Nx+1,1)    =33.2;          % Previous Temperature values at nodes
Told2(1:Nx+1,1)   =33.2;          % One before previous temperature values at nodes
qin_s_old          =0;            % Previous laser irradiance values [W/m^2]
qin_a_old          =0;            % Previous laser irradiance values [W/m^2]
rho_t              =1081.6;        % Density of tissue [kg/m^3]
rho_b              =1060;          % Density of blood [kg/m^3]
k_t                =0.4108;        % Thermal Conductivity for tissue [W/m*k]
k_b                =0.5066;        % Thermal Conductivity for blood [W/m*k]
c_t                =3238.5;        % Heat Capacity of tissue [J/kg*K]
c_b                =3770;          % Heat Capacity of blood [J/kg*K]
w                  =0.0012;        % Blood perfusion rate [m^3/m^3*s]
eps                =0.0060;        % Porosity
D                  =0.00114;       % Vessel Diameter [m]

```

```

% Coupling factor %

```

```

G      =rho_b*c_b*w+4.93*((4*eps*k_b)/(D^2));

```

```

% Effective heat capacity [J/kg*K]

```

```

pc     =(eps*rho_b*c_b+(1-eps)*rho_t*c_t);

```

```

% Effective thermal conductivity for tissue [W/m*k]

```

```

k_t_eff =(1-eps)*k_t;

```

```

% Effective thermal conductivity for blood [W/m*k]

```

```

k_b_eff =eps*(k_b);

```

```

% Effective thermal conductivity [W/m*k]

```

```

k_eff   =k_t_eff+k_b_eff;

```

```

% Coefficients of Model %

```

```

a1 =(eps*rho_b*c_b*(1-eps)*rho_t*c_t)/(G*pc);

```

```

a2 =(k_t_eff+k_b_eff)/pc;

```

```
a3 =(eps*rho_b*c_b*k_t_eff+(1-eps)*rho_t*c_t*k_b_eff)/(G*pc);
```

```
a4 =(eps*rho_b*c_b*(1-eps))/(G*pc);
```

```
a5 =1/pc;
```

```
a6 =(1-eps)/pc;
```

```
%%%%%%%%%%%%%%%%%%%%%%%%%%%%%%%%%%%%%%%%%%%%%%%%%%%%%%%%%%%%%%%%%%%%%%%%  
%%%%%%%%%%%%%%%%%%%%%%%%%%%%%%%%%%%%%%%%%%%%%%%%%%%%%%%%%%%%%%%%%%%%%%%% End of problem definition %%%%%%%%%  
%%%%%%%%%%%%%%%%%%%%%%%%%%%%%%%%%%%%%%%%%%%%%%%%%%%%%%%%%%%%%%%%%%%%%%%%
```

```
%%%%%%%%%%%%%%%%%%%%%%%%%%%%%%%%%%%%%%%%%%%%%%%%%%%%%%%%%%%%%%%%%%%%%%%%  
%%%%%%%%%%%%%%%%%%%%%%%%%%%%%%%%%%%%%%%%%%%%%%%%%%%%%%%%%%%%%%%%%%%%%%%% Solution Process %%%%%%%%%  
%%%%%%%%%%%%%%%%%%%%%%%%%%%%%%%%%%%%%%%%%%%%%%%%%%%%%%%%%%%%%%%%%%%%%%%%
```

```
for lter=1:lterN;
```

```
ww=0;
```

```
tol=10;
```

```
if (lter<=lterNb);
```

```
    qin_s    =qin_S;        % Source term
```

```
    qin_a    =qin_A;        % Source term
```

```
else
```

```
    qin_s    =0;           % Source term
```

```
    qin_a    =0;           % Source term
```

```
end
```

```
k    =0;                  % Counter for sparse matrix
```

```
%%%%%%%%%%%%%%%%%%%%%%%%%%%%%%%%%%%%%%%%%%%%%%%%%%%%%%%%%%%%%%%%%%%%%%%%  
% Energy equation
```

```
%%%%%%%%%%%%%%%%%%%%%%%%%%%%%%%%%%%%%%%%%%%%%%%%%%%%%%%%%%%%%%%%%%%%%%%%
```

```
%%%%%%%%%%%%%%%%%%%%%%%%%%%%%%%%%%%%%%%%%%%%%%%%%%%%%%%%%%%%%%%%%%%%%%%% Cell (1) %%%%%%%%%
```

```
i=1;          % Indices
```

```

cP    =i;           %Cell number of cell (i,j),i.e cell P
cE    =cP+1;       %Cell number of East neighbor

aTold2(cP)    =((a3*h)/(2*k_eff)-(a1*(dx/2))/dt);    % One before previous P coeff.

aTold1(cE)    =-0.5*(a3/dx);                        % Previous E coeff.

aTold1(cP)    =(a1*dx)/dt+(dx/2)-(a2*h*dt)/(2*k_eff); % Previous P coeff.

aT(cE)       =-0.5*((a2*dt)/dx+a3/dx);              % E coeff.

% E coeff. for sparse form
k        =k+1;
ii(k)    =cP;
jj(k)    =cE;
cc(k)    =aT(cE);

% Distance from the boundary layer %
xb       =(i-1)*dx;

% Part of heat source for 808 nm laser %
qrs1     =((a4*mu_a*(dx/2))*(C1*exp((-D1*xb)/delta)
           -C2*exp((-D2*xb)/delta)))*(qin_s-qin_s_old);
% Part of heat source for 808 nm laser
qrs2     =(a5*mu_a*dt*(dx/2)*qin_s)*(C1*exp((-D1*xb)/delta)-C2*exp((-D2*xb)/delta));

% Part of heat source for 1940 nm laser
qra1     =a4*mu_a_a*(dx/2)*(1-Rs)*exp(-mu_a_a*xb)*(qin_a-qin_a_old);

% Part of heat source for 1940 nm laser
qra2     =a5*mu_a_a*dt*(dx/2)*qin_a*(1-Rs)*exp(-mu_a_a*xb);

Sr       =qra2+qra1+qrs2+qrs1; % Heat Source for laser irradiance

```

```
Sm      =a6*qm*(dx/2)*dt;    % Heat Source due to metabolic heat generation
```

```
S      =Sr+Sm;              % Heat Source.
```

```
% P coeff. for sparse form
```

```
k      =k+1;
```

```
ii(k)  =cP;
```

```
jj(k)  =cP;
```

```
cc(k)  =(a1*(dx/2))/dt+(dx/2)-aT(cE)+(a2*h*dt)/(2*k_eff)+(a3*h)/(2*k_eff);
```

```
% Parts of RHS value
```

```
b1      =aTold1(cP)*Told(cP)+aTold2(cP)*Told2(cP)+S;
```

```
b2      =aTold1(cE)*(Told(cE)-Told(cP));
```

```
b3      =(0.5*((a2*dt)/dx+a3/dx)*(Told(cE)-Told(cP)))+(aTold1(cE)*(Told2(cE)-Told2(cP)));
```

```
b4      =((a2*h*dt)/k_eff)*T_Inf;
```

```
% RHS value
```

```
rhsa(cP) =b1+b2+b3+b4;
```

```
%%%%%%%%%% Cell (2) to (Nx)%%%%%%%%%%
```

```
for i=2:(Nx)
```

```
cP      =i;                %Cell number of cell (i,j),i.e cell P
```

```
cE      =cP+1;            %Cell number of East neighbor
```

```
cW      =cP-1;            %Cell number of West neighbor
```

```
aTold2(cP)  =-((a1*dx)/dt);          % One before previous P coeff.
```

```
aTold1(cE)  =-0.5*(a3/dx);          % Previous E coeff.
```

```
aTold1(cW)  =-0.5*(a3/dx);          % Previous W coeff.
```

```
aTold1(cP)  =(2*a1*dx)/dt+dx;       % Previous P coeff.
```

```

aT(cE)      =-0.5*((a2*dt)/dx+a3/dx);    % E coeff.
aT(cW)      =-0.5*((a2*dt)/dx+a3/dx);    % W coeff.

% E coeff. for sparse form
k          =k+1;
ii(k)     =cP;
jj(k)     =cE;
cc(k)     =aT(cE);

% W coeff. for sparse form
k          =k+1;
ii(k)     =cP;
jj(k)     =cW;
cc(k)     =aT(cW);

% Distance from the boundary layer %
xb        =(i-1)*dx;

% Part of heat source for 808 nm laser
qrs1      =((a4*mu_a*dx)*(C1*exp((-D1*xb)/delta)
            -C2*exp((-D2*xb)/delta)))*(qin_s-qin_s_old);
% Part of heat source for 808 nm laser
qrs2      =(a5*mu_a*dt*dx*qin_s)*(C1*exp((-D1*xb)/delta)-C2*exp((-D2*xb)/delta));

% Part of heat source for 1940 nm laser
qra1      =a4*mu_a_a*dx*(1-Rs)*exp(-mu_a_a*xb)*(qin_a-qin_a_old);

% Part of heat source for 1940 nm laser
qra2      =a5*mu_a_a*dt*dx*qin_a*(1-Rs)*exp(-mu_a_a*xb);

Sr        =qra2+qra1+qrs2+qrs1;    % Heat Source for laser irradiance.
Sm        =a6*qm*dx*dt;           % Heat Source due to metabolic heat generation.

S         =Sr+Sm;                 % Heat Source.

```

% P coeff. for sparse form

```
k      =k+1;
ii(k)  =cP;
jj(k)  =cP;
cc(k)  =(a1*dx)/dt+dx-aT(cE)-aT(cW);
```

% Parts of RHS value

```
b1      =aTold1(cP)*Told(cP)+aTold2(cP)*Told2(cP)+S;
b2      =(aTold1(cE)*(Told(cE)-Told(cP))+aTold1(cW)*(Told(cW)-Told(cP)));
b3      =(0.5*((a2*dt)/dx+a3/dx)*(Told(cE)-Told(cP)))
        +(0.5*((a2*dt)/dx+a3/dx)*(Told(cW)-Told(cP)));
b4      =(aTold1(cE)*(Told2(cE)-Told2(cP)))+(aTold1(cW)*(Told2(cW)-Told2(cP)));
```

% RHS value

```
rhsa(cP) =b1+b2+b3+b4;
```

end

%%%%%%%%%% Cell (Nx+1) %%%%%%%%%%

```
i=Nx+1;      % Indices
```

```
cP      =i;          %Cell number of cell (i,j),i.e cell P
```

```
cW      =cP-1;      %Cell number of West neighbor
```

```
aTold2(cP)  =-((a1*dx)/(2*dt));          % One before previous P coeff.
```

```
aTold1(cW)  =-0.5*(a3/dx);              % Previous W coeff.
```

```
aTold1(cP)  =(a1*dx)/dt+(dx/2);        % Previous P coeff.
```

```
aT(cW)      =-0.5*((a2*dt)/dx+a3/dx);  % W coeff.
```

% W coeff. for sparse form

```
k      =k+1;
```



```

ii(k) =cP;
jj(k) =cW;
cc(k) =aT(cW);

% Distance from the boundary layer %
xb      =(i-1)*dx;

% Part of heat source for 808 nm laser
qrs1     =((a4*mu_a*(dx/2))*(C1*exp((-D1*xb)/delta)
          --C2*exp((-D2*xb)/delta)))*(qin_s-qin_s_old);
% Part of heat source for 808 nm laser
qrs2     =(a5*mu_a*dt*(dx/2)*qin_s)*(C1*exp((-D1*xb)/delta)-C2*exp((-D2*xb)/delta));

% Part of heat source for 1940 nm laser
qra1     =a4*mu_a*(dx/2)*(1-Rs)*exp(-mu_a*xb)*(qin_a-qin_a_old);

% Part of heat source for 1940 nm laser
qra2     =a5*mu_a*dt*(dx/2)*qin_a*(1-Rs)*exp(-mu_a*xb);

Sr       =qra2+qra1+qrs2+qrs1; % Heat Source for laser irradiance.
Sm       =a6*qm*(dx/2)*dt; % Heat Source due to metabolic heat generation.

S        =Sr+Sm; % Heat Source.

% P coeff. for sparse form
k        =k+1;
ii(k)    =cP;
jj(k)    =cP;
cc(k)    =(a1*dx)/(2*dt)+(dx/2)-aT(cW);

% Parts of RHS value
b1       =aTold1(cP)*Told(cP)+aTold2(cP)*Told2(cP)+S;
b2       =aTold1(cW)*(Told(cW)-Told(cP));
b3       =(0.5*((a2*dt)/dx+a3/dx)*(Told(cW)-Told(cP)));
b4       =(aTold1(cW)*(Told2(cW)-Told2(cP)));

```

```

% RHS value
rhsa(cP) =b1+b2+b3+b4;

% Creating Sparse matrix %

aTnew=sparse(ii,jj,cc,Nx+1,Nx+1);

% New heat flux values after the time step

Tn=aTnew\rhsa;

% Stored values
qin_s_old =qin_s; % Stored laser irradiance value
qin_a_old =qin_a; % Stored laser irradiance value

Told2      =Told; % Stored one before previous temperature values
Told       =Tn; % Stored previous temperature values

Ts(iter)=Tn(1); % Temperature values at cell (1)

end

toc;

```

APPENDIX E

MATLAB Code for Pennes Model

```

clear all;
clc;
close all;

%%%%%%%%%%%%%%%%%%%%%%%%%%%%%%%%%%%%%%%%%%%%%%%%%%%%%%%%%%%%%%%%%%%%%%%%
%%%%%%%%%%%%%%%%%%%%%%%%%%%%%%%%%%%%%%%%%%%%%%%%%%%%%%%%%%%%%%%%%%%%%%%% Problem Definition %%%%%%%%%%%%%%%%%%%%%%%%%%%%%%%%%%%%%%%%%%%%%%%%%%%%%%%%%%%%%%%%%%%%%%%%%
%%%%%%%%%%%%%%%%%%%%%%%%%%%%%%%%%%%%%%%%%%%%%%%%%%%%%%%%%%%%%%%%%%%%%%%%

tic;                                % Used for measuring run time
tTotal    =90;                       % Total time [s]
tin       =10;                       % Exposure time [s]
dt        =0.01;                     % Constant time step [s]
Nx        =120;                      % Number of cells in x direction
L         =0.05;                     % Length [m]
dx        =L/(Nx);                   % Constant cell size in x direction
IterN     =tTotal/dt;                % Iteration number
IterNb    =tin/dt;                   % Iteration number for heat flux exposure time
ms        =3*Nx+1;

% Arrays and matrices %

Tn        =zeros(Nx+1,1);            % New temperature values at nodes
Ts        =zeros(1,IterN);           % Temperature values at Cell (1)
ii        =zeros(ms,1);              % Row number of aT sparse matrix
jj        =zeros(ms,1);              % Column number of aT sparse matrix
cc        =zeros(ms,1);              % Values of aT sparse matrix
aT        =zeros(Nx+1,1);            % Coefficients of new heat flux values
aTold1    =zeros(Nx+1,1);            % Coefficients of previous heat flux values
aTold2    =zeros(Nx+1,1);            % Coefficients of one before previous heat flux values
rhsa      =zeros(Nx+1,1);            % Right hand side vector of the energy equation
Told      =zeros(Nx+1,1);            % Previous values at nodes

```

```

Told2 =zeros(Nx+1,1);      % One before previous temperature values at nodes

% Optical properties %

% For 808 nm laser
Rd      =0.05;      % Diffuse reflectance
mu_a    =78;      % Absorption coefficient [m^-1]
mu_sr   =2104;     % Reduced scattering coefficient [m^-1]

delta   =1/sqrt(3*mu_a*(mu_a+mu_sr));    % Effective optical penetration depth [m]

% Coefficients of diffusion theory equation

C1=3.09+5.44*Rd-2.12*exp(-21.5*Rd);
D1=1-(1-(1/sqrt(3)))*exp(-20.1*Rd);
C2=2.09-1.47*Rd-2.12*exp(-21.5*Rd);
D2=1.63*exp(3.40*Rd);

% For 1940 nm laser
Rs      =0.0475;    % Specular reflectance
mu_a_a  =5643;     % Absorption coefficient [m^-1]

% Boundary Conditions %

qin_A   =0;        % Laser intensity for 1940 nm laser [W/m^2]
qin_S   =14000;    % Laser intensity for 808 nm laser [W/m^2]

%%%%%%%%%%%%%%%%%%%%%%%%%%%%%%%%%%%%%%%%%%%%%%%%%%%%%%%%%%%%%%%%%%%%%%%%
%%%%%%%%%%%%%%%%%%%%%%%%%%%%%%%%%%%%%%%%%%%%%%%%%%%%%%%%%%%%%%%%%%%%%%%% Initial values and boundary conditions %%%%%%%%%
%%%%%%%%%%%%%%%%%%%%%%%%%%%%%%%%%%%%%%%%%%%%%%%%%%%%%%%%%%%%%%%%%%%%%%%%

h        =10;      % Heat convection [W/mK]
T_Inf    =22.35;   % Room temperature [C]
qm       =368.1;   % Constant metabolic heat generation [W/m^3]
Tb       =33.2;   % Constant blood temperature [K]

```

```

Tn(1:Nx+1,1)      =33.2;      % Temperature values at nodes
Told(1:Nx+1,1)    =33.2;      % Previous Temperature values at nodes
Told2(1:Nx+1,1)   =33.2;      % One before previous temperature values at nodes
qold1(1:Nx+1,1)   =0;        % Previous Heat Flux values at nodes
qold2(1:Nx+1,1)   =0;        % One before previous heat flux values at nodes
qin_s_old         =0;        % Previous laser irradiance values [W/m^2]
qin_a_old         =0;        % Previous laser irradiance values [W/m^2]

```

```

rho_t             =1081.6;     % Density of tissue [kg/m^3]
rho_b             =1060;     % Density of blood [kg/m^3]
k_t               =0.4108;    % Thermal Conductivity for tissue [W/m*k]
k_b               =0.5066;    % Thermal Conductivity for blood [W/m*k]
c_t               =3238.5;    % Heat Capacity of tissue [J/kg*K]
c_b               =3770;     % Heat Capacity of blood [J/kg*K]
w                 =0.0012;    % Blood perfusion rate [m^3/m^3*s]

```

```

% Thermal Diffusivity %

```

```

alpha             =k_t/(rho_t*c_t);

```

```

%%%%%%%%%%%%%%%%%%%%%%%%%%%%%%%%%%%%%%%%%%%%%%%%%%%%%%%%%%%%%%%%%%%%%%%%
%%%%%%%%%%%%%%%%%%%%%%%%%%%%%%%%%%%%%%%%%%%%%%%%%%%%%%%%%%%%%%%%%%%%%%%% End of problem definition %%%%%%%%%
%%%%%%%%%%%%%%%%%%%%%%%%%%%%%%%%%%%%%%%%%%%%%%%%%%%%%%%%%%%%%%%%%%%%%%%%

```

```

%%%%%%%%%%%%%%%%%%%%%%%%%%%%%%%%%%%%%%%%%%%%%%%%%%%%%%%%%%%%%%%%%%%%%%%%
%%%%%%%%%%%%%%%%%%%%%%%%%%%%%%%%%%%%%%%%%%%%%%%%%%%%%%%%%%%%%%%%%%%%%%%% Solution Process %%%%%%%%%
%%%%%%%%%%%%%%%%%%%%%%%%%%%%%%%%%%%%%%%%%%%%%%%%%%%%%%%%%%%%%%%%%%%%%%%%

```

```

for Iter=1:IterN;

```

```

    ww=0;

```

```

    tol=10;

```

```

    if (Iter<=IterNb);

```

```

        qin_s      =qin_S;      % Source term

```

```

        qin_a      =qin_A;      % Source term
    end

```

```

else

    qin_s    =0;        % Source term
    qin_a    =0;        % Source term

end

k    =0;                % Counter for sparse matrix

%%%%%%%%%%%%%%%%%%%%%%%%%%%%%%%%%%%%%%%%%%%%%%%%%%%%%%%%%%%%%%%%%%%%%%%%
% Energy equation
%%%%%%%%%%%%%%%%%%%%%%%%%%%%%%%%%%%%%%%%%%%%%%%%%%%%%%%%%%%%%%%%%%%%%%%%

% Cell (1)
i    =1;                % Indices

cP    =i;                %Cell number of cell (i,j),i.e cell P
cE    =cP+1;            %Cell number of East neighbor

aTold1(cP)    =-0.5*((w*rho_b*c_b*dx*dt)/(2*rho_t*c_t))-0.5*((alpha*h*dt)/k_t)+(dx/2);
% Previous P coeff.

aT(cE)        =-0.5*((alpha*dt)/dx); % E coeff.

% E coeff. for sparse form
k    =k+1;
ii(k)    =cP;
jj(k)    =cE;
cc(k)    =aT(cE);

% Distance from the boundary layer %
xb    =(i-1)*dx;

% Part of heat source for 808 nm laser
qrs    =((mu_a*dt*(dx/2)*qin_s)/(rho_t*c_t))*(C1*exp((-D1*xb)/delta)

```

```

        - C2*exp((-D2*xb)/delta));
% Part of heat source for 1940 nm laser
qra    =(1-Rs)*((mu_a_a*dt*(dx/2)*qin_a)/(rho_t*c_t))*exp(-mu_a_a*xb);

Sq     =qrs+qra;                % Heat Source for laser irradiance
Sm     =(qm*(dx/2)*dt)/(rho_t*c_t); % Heat Source due to metabolic heat generation

S      =Sq+Sm;                  % Heat Source.

% P coeff. for sparse form
k      =k+1;
ii(k)  =cP;
jj(k)  =cP;
cc(k)  =0.5*((w*rho_b*c_b*dx*dt)/(2*rho_t*c_t))+0.5*((alpha*h*dt)/k_t)+(dx/2)-aT(cE);

% Parts of RHS value
a1     =aTold1(cP)*Told(cP)+S;
a2     =0.5*((alpha*dt)/dx)*(Told(cE)-Told(cP));
a3     =((w*rho_b*c_b*dx*dt)/(2*rho_t*c_t))*Tb;
a4     =((alpha*h*dt)/k_t)*T_Inf;

% RHS value
rhsa(cP) = a1+a2+a3+a4;

% Cell (2) to (Nx)

for i=2:Nx

cP     =i;                %Cell number of cell (i,j),i.e cell P
cE     =cP+1;            %Cell number of East neighbor
cW     =cP-1;            %Cell number of West neighbor

aTold1(cP) =dx-0.5*((w*rho_b*c_b*dx*dt)/(rho_t*c_t));    % Previous P coeff.

aT(cE)    =-0.5*((alpha*dt)/dx);    % E coeff.

```

```
aT(cW)      =-0.5*((alpha*dt)/dx); % W coeff.
```

```
% E coeff. for sparse form
```

```
k          =k+1;
```

```
ii(k)      =cP;
```

```
jj(k)      =cE;
```

```
cc(k)      =aT(cE);
```

```
% W coeff. for sparse form
```

```
k          =k+1;
```

```
ii(k)      =cP;
```

```
jj(k)      =cW;
```

```
cc(k)      =aT(cW);
```

```
% Distance from the boundary layer %
```

```
xb         =(i-1)*dx;
```

```
% Part of heat source for 808 nm laser
```

```
qrs        =((mu_a*dt*dx*qin_s)/(rho_t*c_t))*(C1*exp((-D1*xb)/delta)  
            - C2*exp((-D2*xb)/delta));
```

```
% Part of heat source for 1940 nm laser
```

```
qra        =(1-Rs)*((mu_a_a*dt*dx*qin_a)/(rho_t*c_t))*exp(-mu_a_a*xb);
```

```
Sq         =qrs+qra; % Heat Source for laser irradiance
```

```
Sm         =(qm*dx*dt)/(rho_t*c_t); % Heat Source due to metabolic heat generation.
```

```
S          =Sq+Sm; % Heat Source.
```

```
% P coeff. for sparse form
```

```
k          =k+1;
```

```
ii(k)      =cP;
```

```
jj(k)      =cP;
```

```
cc(k)      =dx-aT(cE)-aT(cW)+0.5*((w*rho_b*c_b*dx*dt)/(rho_t*c_t));
```



```

% Parts of RHS value
a1      =aTold1(cP)*Told(cP)+S;
a2      =0.5*((alpha*dt)/dx)*(Told(cE)-Told(cP))+0.5*((alpha*dt)/dx)*(Told(cW)-Told(cP));
a3      =((w*rho_b*c_b*dx*dt)/(rho_t*c_t))*Tb;

% RHS value
rhsa(cP) = a1+a2+a3;

end

% Cell (Nx+1)

i      =Nx+1;

cP     =i;          %Cell number of cell (i,j),i.e cell P
cW     =cP-1;      %Cell number of West neighbor

aTold1(cP) = (dx/2)-0.5*((w*rho_b*c_b*dx*dt)/(2*rho_t*c_t)); % Previous P coeff.

aT(cW)    =-0.5*((alpha*dt)/dx); % W coeff.

% W coeff. for sparse form
k      =k+1;
ii(k)   =cP;
jj(k)   =cW;
cc(k)   =aT(cW);

% Distance from the boundary layer %
xb     =(i-1)*dx;

% Part of heat source for 808 nm laser
qrs    =((mu_a*dt*(dx/2)*qin_s)/(rho_t*c_t))*(C1*exp((-D1*xb)/delta)
        - C2*exp((-D2*xb)/delta));

```

```

% Part of heat source for 1940 nm laser
qra      =(1-Rs)*((mu_a_a*dt*(dx/2)*qin_a)/(rho_t*c_t))*exp(-mu_a_a*xb);

Sq       =qrs+qra;           % Heat Source for laser irradiance
Sm       =(qm*(dx/2)*dt)/(rho_t*c_t); % Heat Source due to metabolic heat generation.

S        =Sq+Sm;           % Heat Source.

% P coeff. for sparse form
k        =k+1;
ii(k)    =cP;
jj(k)    =cP;
cc(k)    =(dx/2)-aT(cW)+0.5*((w*rho_b*c_b*dx*dt)/(2*rho_t*c_t));

% Parts of RHS value
a1       =aTold1(cP)*Told(cP)+S;
a2       =0.5*((alpha*dt)/dx)*(Told(cW)-Told(cP));
a4       =((w*rho_b*c_b*dx*dt)/(2*rho_t*c_t))*Tb;

% RHS value
rhsa(cP) = a1+a2+a3+a4;

% Creating Sparse matrix %

aTnew=sparse(ii,jj,cc,Nx+1,Nx+1);

% New heat flux values after the time step

Tn=aTnew\rhsa;

% Stored values
qin_s_old =qin_s;           % Stored laser irradiance value
qin_a_old =qin_a;           % Stored laser irradiance value
Told2     =Told;            % Stored one before previous temperature values
Told      =Tn;              % Stored previous temperature values

```

```
Ts(1,Iter)=Tn(1);           % Temperature values at cell (1)
```

```
end
```

```
toc;
```

APPENDIX F

MATLAB Code for DPL Model

```

clear all;

clc;

close all;

%%%%%%%%%%%%%%%%%%%%%%%%%%%%%%%%%%%%%%%%%%%%%%%%%%%%%%%%%%%%%%%%%%%%%%%%
%%%%%%%%%%%%%%%%%%%%%%%%%%%%%%%%%%%%%%%%%%%%%%%%%%%%%%%%%%%%%%%%%%%%%%%% Problem Definition %%%%%%%%%%%%%%%%%%%%%%%%%%%%%%%%%%%%%%%%%%%%%%%%%%%%%%%%%%%%%%%%%%%%%%%%%
%%%%%%%%%%%%%%%%%%%%%%%%%%%%%%%%%%%%%%%%%%%%%%%%%%%%%%%%%%%%%%%%%%%%%%%%

tic;                                % Used for measuring run time
tTotal      =90;                    % Total time [s]
tin         =10;                    % Exposure time [s]
dt          =0.01;                  % Constant time step [s]
Nx          =120;                   % Number of cells in x direction
L           =0.05;                  % Length [m]
dx          =L/(Nx);                % Constant cell size in x direction
IterN       =tTotal/dt;              % Iteration number
IterNb      =tin/dt;                % Iteration number for heat flux exposure time
tav_T       =0.05;                  % Phase lag for temperature for different models [s]
tav_q       =16;                    % Phase lag for heat flux for different models [s]
ms          =3*Nx+1;

% Arrays and matrices %

Tn          =zeros(Nx+1,1);          % New temperature values at nodes
Ts          =zeros(1,IterN);         % Temperature values at Cell (1)
ii          =zeros(ms,1);            % Row number of aT sparse matrix
jj          =zeros(ms,1);            % Column number of aT sparse matrix
cc          =zeros(ms,1);            % Values of aT sparse matrix
aT          =zeros(Nx+1,1);          % Coefficients of new heat flux values
aTold1     =zeros(Nx+1,1);           % Coefficients of previous heat flux values

```

```

aTold2 =zeros(Nx+1,1);      % Coefficients of one before previous heat flux values
rhsa   =zeros(Nx+1,1);      % Right hand side vector of the energy equation
Told   =zeros(Nx+1,1);      % Previous values at nodes
Told2  =zeros(Nx+1,1);      % One before previous temperature values at nodes

```

```

% Optical properties %

```

```

% For 808 nm laser

```

```

Rd      =0.05;              % Diffuse reflectance
mu_a    =78;                % Absorption coefficient [m^-1]
mu_sr   =2104;              % Reduced scattering coefficient [m^-1]

```

```

delta =1/sqrt(3*mu_a*(mu_a+mu_sr)); % Effective optical penetration depth [m]

```

```

% Coefficients of diffusion theory equation

```

```

C1=3.09+5.44*Rd-2.12*exp(-21.5*Rd);
D1=1-(1-(1/sqrt(3)))*exp(-20.1*Rd);
C2=2.09-1.47*Rd-2.12*exp(-21.5*Rd);
D2=1.63*exp(3.40*Rd);

```

```

% For 1940 nm laser

```

```

Rs      =0.0475;           % Specular reflectance
mu_a_a  =5643;             % Absorption coefficient [m^-1]

```

```

% Boundary Conditions %

```

```

qin_A   =0;                % Laser intensity for 1940 nm laser [W/m^2]
qin_S   =14000;            % Laser intensity for 808 nm laser [W/m^2]

```

```

%%%%%%%%%%%%%%%%%%%%%%%%%%%%%%%%%%%%%%%%%%%%%%%%%%%%%%%%%%%%%%%%%%%%%%%%
%%%%%%%%%%%%%%%%%%%%%%%%%%%%%%%%%%%%%%%%%%%%%%%%%%%%%%%%%%%%%%%%%%%%%%%% Initial values and boundary conditions %%%%%%%%%
%%%%%%%%%%%%%%%%%%%%%%%%%%%%%%%%%%%%%%%%%%%%%%%%%%%%%%%%%%%%%%%%%%%%%%%%

```

```

h      =10;                 % Heat convection [W/mK]

```

```

T_Inf      =22.35;          % Room temperature [C]
qm         =368.1;         % Constant metabolic heat generation [W/m^3]
Tb         =33.2;         % Constant blood temperature [K]

Tn(1:Nx+1,1)    =33.2;      % Temperature values at nodes
Told(1:Nx+1,1)  =33.2;      % Previous Temperature values at nodes
Told2(1:Nx+1,1) =33.2;      % One before previous temperature values at nodes
qold1(1:Nx+1,1) =0;        % Previous Heat Flux values at nodes
qold2(1:Nx+1,1) =0;        % One before previous heat flux values at nodes
qin_s_old      =0;        % Previous laser irradiance values [W/m^2]
qin_a_old      =0;        % Previous laser irradiance values [W/m^2]

rho_t       =1081.6;       % Density of tissue [kg/m^3]
rho_b       =1060;        % Density of blood [kg/m^3]
k_t         =0.4108;      % Thermal Conductivity for tissue [W/m*k]
k_b         =0.5066;      % Thermal Conductivity for blood [W/m*k]
c_t         =3238.5;      % Heat Capacity of tissue [J/kg*K]
c_b         =3770;        % Heat Capacity of blood [J/kg*K]
w           =0.0012;      % Blood perfusion rate [m^3/m^3*s]

```

```

% Thermal Diffusivity %

```

```

alpha      =k_t/(rho_t*c_t);

```

```

%%%%%%%%%%%%%%%%%%%%%%%%%%%%%%%%%%%%%%%%%%%%%%%%%%%%%%%%%%%%%%%%%%%%%%%%
%%%%%%%%%%%%%%%%%%%%%%%%%%%%%%%%%%%%%%%%%%%%%%%%%%%%%%%%%%%%%%%%%%%%%%%% End of problem definition %%%%%%%%%
%%%%%%%%%%%%%%%%%%%%%%%%%%%%%%%%%%%%%%%%%%%%%%%%%%%%%%%%%%%%%%%%%%%%%%%%

```

```

%%%%%%%%%%%%%%%%%%%%%%%%%%%%%%%%%%%%%%%%%%%%%%%%%%%%%%%%%%%%%%%%%%%%%%%%
%%%%%%%%%%%%%%%%%%%%%%%%%%%%%%%%%%%%%%%%%%%%%%%%%%%%%%%%%%%%%%%%%%%%%%%% Solution Process %%%%%%%%%
%%%%%%%%%%%%%%%%%%%%%%%%%%%%%%%%%%%%%%%%%%%%%%%%%%%%%%%%%%%%%%%%%%%%%%%%

```

```

for lter=1:lterN;

```

```

if (lter<=lterNb);

```

```

    qin_s    =qin_S;          % Source term

```

```

    qin_a    =qin_A;                % Source term
else
    qin_s    =0;                    % Source term
    qin_a    =0;                    % Source term
end

k          =0;                    % Counter for sparse matrix

%%%%%%%%%%%%%%%%%%%%%%%%%%%%%%%%%%%%%%%%%%%%%%%%%%%%%%%%%%%%%%%%%%%%%%%%
% Energy equation
%%%%%%%%%%%%%%%%%%%%%%%%%%%%%%%%%%%%%%%%%%%%%%%%%%%%%%%%%%%%%%%%%%%%%%%%

% Cell (1)
i          =1;                    % Indices

cP         =i;                    %Cell number of cell (i,j),i.e cell P
cE         =cP+1;                %Cell number of East neighbor

% One before previous P coeff.
aTold2(cP) =0.5*((alpha*tav_T*h)/k_t)-((tav_q*(dx/2))/dt);

% Part of previous P coeff.
a1         =-0.5*((w*rho_b*c_b*dx*dt)/(2*rho_t*c_t))-0.5*((alpha*h*dt)/k_t);

% Previous P coeff.
aTold1(cP) =a1+(tav_q*dx)/dt+(1+(w*rho_b*c_b*tav_q)/(rho_t*c_t))*(dx/2);

aT(cE)     =-0.5*((alpha*dt)/dx+(tav_T*alpha)/dx);    % E coeff.

% E coeff. for sparse form
k          =k+1;
ii(k)     =cP;
jj(k)     =cE;
cc(k)     =aT(cE);

```

```

% Distance from the boundary layer %
xb      =(i-1)*dx;

% Part of heat source for 808 nm laser
qrs1    =((mu_a*dt*(dx/2)*qin_s)/(rho_t*c_t))*(C1*exp((-D1*xb)/delta)
        - C2*exp((-D2*xb)/delta));

% Part of heat source for 808 nm laser
qrs2    =(((tav_q*mu_a*(dx/2))/(rho_t*c_t))*(C1*exp((-D1*xb)/delta)
        -C2*exp((-D2*xb)/delta))*(qin_s-qin_s_old);

% Part of heat source for 1940 nm laser
qra1    =(1-Rs)*((mu_a_a*dt*(dx/2)*qin_a)/(rho_t*c_t))*exp(-mu_a_a*xb);

% Part of heat source for 1940 nm laser
qra2    =tav_q*(1-Rs)*((mu_a_a*(dx/2))/(rho_t*c_t))*exp(-mu_a_a*xb)*(qin_a-qin_a_old);

Sq      =qrs1+qrs2+qra1+qra2;      % Heat Source for laser irradiance
Sm      =(qm*(dx/2)*dt)/(rho_t*c_t); % Heat Source due to metabolic heat generation

S       =Sq+Sm;                    % Heat Source.

% P coeff. for sparse form
k       =k+1;
ii(k)   =cP;
jj(k)   =cP;
a1      =0.5*((w*rho_b*c_b*dx*dt)/(2*rho_t*c_t))+0.5*((alpha*h*dt)/k_t)
        +0.5*((alpha*tav_T*h)/k_t);
cc(k)   =a1+(tav_q*(dx/2))/dt+(1+(w*rho_b*c_b*tav_q)/(rho_t*c_t))*(dx/2)-aT(cE);

% Parts of RHS value
a1      =aTold1(cP)*Told(cP)+aTold2(cP)*Told2(cP)+S;
a2      =0.5*((alpha*dt)/dx)*(Told(cE)-Told(cP));

```



```

a3      =(-0.5)*((alpha*tav_T)/dx)*(Told2(cE)-Told2(cP));
a4      =((w*rho_b*c_b*dx*dt)/(2*rho_t*c_t))*Tb;
a5      =((alpha*h*dt)/k_t)*T_Inf;

% RHS value
rhsa(cP) = a1+a2+a3+a4+a5;

% Cell (2) to (Nx)

for i=2:Nx

cP      =i;           %Cell number of cell (i,j),i.e cell P
cE      =cP+1;       %Cell number of East neighbor
cW      =cP-1;       %Cell number of West neighbor

aTold2(cP) =-((tav_q*dx)/dt);           % One before previous P coeff.

aTold1(cP) = (2*tav_q*dx)/dt+(1+(w*rho_b*c_b*tav_q)/(rho_t*c_t))*dx-
0.5*((w*rho_b*c_b*dx*dt)/(rho_t*c_t)); % Previous P coeff.

aT(cE)     =-0.5*((alpha*dt)/dx+(tav_T*alpha)/dx); % E coeff.
aT(cW)     =-0.5*((alpha*dt)/dx+(tav_T*alpha)/dx); % W coeff.

% E coeff. for sparse form
k         =k+1;
ii(k)     =cP;
jj(k)     =cE;
cc(k)     =aT(cE);

% W coeff. for sparse form
k         =k+1;
ii(k)     =cP;
jj(k)     =cW;
cc(k)     =aT(cW);

```

% Distance from the boundary layer %

xb = (i-1)*dx;

% Part of heat source for 808 nm laser

qrs1 = ((mu_a*dt*dx*qin_s)/(rho_t*c_t))*(C1*exp((-D1*xb)/delta)-C2*exp((-D2*xb)/delta));

% Part of heat source for 808 nm laser

qrs2 = (((tav_q*mu_a*dx)/(rho_t*c_t))*(C1*exp((-D1*xb)/delta)-C2*exp((-D2*xb)/delta)))*(qin_s-qin_s_old);

% Part of heat source for 1940 nm laser

qra1 = (1-Rs)*((mu_a_a*dt*dx*qin_a)/(rho_t*c_t))*exp(-mu_a_a*xb);

% Part of heat source for 1940 nm laser

qra2 = tav_q*(1-Rs)*((mu_a_a*dx)/(rho_t*c_t))*exp(-mu_a_a*xb)*(qin_a-qin_a_old);

Sq = qrs1+qrs2+qra1+qra2; % Heat Source for laser irradiance

Sm = (qm*dx*dt)/(rho_t*c_t); % Heat Source due to metabolic heat generation.

S = Sq+Sm; % Heat Source.

% P coeff. for sparse form

k = k+1;

ii(k) = cP;

jj(k) = cP;

a1 = 0.5*((w*rho_b*c_b*dx*dt)/(rho_t*c_t));

cc(k) = a1+(tav_q*dx)/dt+(1+(w*rho_b*c_b*tav_q)/(rho_t*c_t))*dx-aT(cE)-aT(cW);

% Parts of RHS value

a1 = aTold1(cP)*Told(cP)+aTold2(cP)*Told2(cP)+S;

a2 = 0.5*((alpha*dt)/dx)*(Told(cE)-Told(cP))+0.5*((alpha*dt)/dx)*(Told(cW)-Told(cP));

a3 = (-0.5)*((alpha*tav_T)/dx)*(Told2(cE)-Told2(cP))+(-

0.5)*((alpha*tav_T)/dx)*(Told2(cW)-Told2(cP));

a4 = ((w*rho_b*c_b*dx*dt)/(rho_t*c_t))*Tb;

```

% RHS value
rhsa(cP) = a1+a2+a3+a4;

end

% Cell (Nx+1)

i      =Nx+1;

cP     =i;           %Cell number of cell (i,j),i.e cell P
cW     =cP-1;       %Cell number of West neighbor

aTold2(cP) =-((tav_q*(dx/2))/dt);           % One before previous P coeff.

aTold1(cP) = (tav_q*dx)/dt+(1+(w*rho_b*c_b*tav_q)/(rho_t*c_t))*(dx/2)
              -0.5*((w*rho_b*c_b*dx*dt)/(2*rho_t*c_t));           % Previous P coeff.

aT(cW)     =-0.5*((alpha*dt)/dx+(tav_T*alpha)/dx);           % W coeff.

% W coeff. for sparse form
k         =k+1;
ii(k)     =cP;
jj(k)     =cW;
cc(k)     =aT(cW);

% Distance from the boundary layer %
xb        =(i-1)*dx;

% Part of heat source for 808 nm laser
qrs1      =((mu_a*dt*(dx/2)*qin_s)/(rho_t*c_t))*(C1*exp((-D1*xb)/delta)
              -C2*exp((-D2*xb)/delta));

```

```

% Part of heat source for 808 nm laser
qrs2    =(((tav_q*mu_a*(dx/2))/(rho_t*c_t))*(C1*exp((-D1*xb)/delta)
        -C2*exp((-D2*xb)/delta)))*(qin_s-qin_s_old);

% Part of heat source for 1940 nm laser
qra1    =(1-Rs)*((mu_a_a*dt*(dx/2)*qin_a)/(rho_t*c_t))*exp(-mu_a_a*xb);

% Part of heat source for 1940 nm laser
qra2    =tav_q*(1-Rs)*((mu_a_a*(dx/2))/(rho_t*c_t))*exp(-mu_a_a*xb)*(qin_a-qin_a_old);

Sq      =qrs1+qrs2+qra1+qra2;      % Heat Source for laser irradiance
Sm      =(qm*(dx/2)*dt)/(rho_t*c_t); % Heat Source due to metabolic heat generation.

S       =Sq+Sm;      % Heat Source.

% P coeff. for sparse form
k       =k+1;
ii(k)   =cP;
jj(k)   =cP;
a1      =0.5*((w*rho_b*c_b*dx*dt)/(2*rho_t*c_t));
cc(k)   =a1+(tav_q*(dx/2))/dt+(1+(w*rho_b*c_b*tav_q)/(rho_t*c_t))*(dx/2)-aT(cW);

% Parts of RHS value
a1      =aTold1(cP)*Told(cP)+aTold2(cP)*Told2(cP)+S;
a2      =0.5*((alpha*dt)/dx)*(Told(cW)-Told(cP));
a3      =(-0.5)*((alpha*tav_T)/dx)*(Told2(cW)-Told2(cP));
a4      =((w*rho_b*c_b*dx*dt)/(2*rho_t*c_t))*Tb;

% RHS value
rhsa(cP) = a1+a2+a3+a4;

% Creating Sparse matrix %
aTnew=sparse(ii,jj,cc,Nx+1,Nx+1);

% New heat flux values after the time step

```

```

Tn=aTnew\rhsa;

% Stored values
qin_s_old    =qin_s;      % Stored laser irradiance value
qin_a_old    =qin_a;      % Stored laser irradiance value
Told2        =Told;       % Stored one before previous temperature values
Told         =Tn;         % Stored previous temperature values

Ts(1,Iter)   =Tn(1);      % Temperature values at cell (1)

end

toc;

```

APPENDIX G

MATLAB Code for Tzou's Study

```
clear all;
clc;
close hidden;

tic;
syms k
z_t=0.001; % Phase lag for temperature for different models [s]
z_q=0.05; % Phase lag for heat flux for different models [s]
T_d=0; % Time derivative of temperature at t=0

Beta=0.05;

A=@(y) (z_q.*T_d)/(1+z_q.*y);

B=@(y) sqrt((y.*(1+z_q.*y))/(1+z_t.*y));

T_=@(x,y) (1./y).*(A(y)+(1-A(y)).*(cosh((1-x).*B(y))./cosh(B(y))));

T=@(x) (exp(4.7)/Beta).*((T_(x,94))./2+real(symsum(T_(x,94+((1i.*k.*pi)/Beta)).*(-1).^k, k, 1, Inf)));

x=0:0.001:1;
Tp=double(T(x));

toc;
```



HACETTEPE UNIVERSITY
GRADUATE SCHOOL OF SCIENCE AND ENGINEERING
THESIS/DISSERTATION ORIGINALITY REPORT

HACETTEPE UNIVERSITY
GRADUATE SCHOOL OF SCIENCE AND ENGINEERING
TO THE DEPARTMENT OF MECHANICAL ENGINEERING

Date: 18/09/2019

Thesis Title / Topic: **Investigation of Thermal Effects On Tissues During Laser Applications**

According to the originality report obtained by my thesis advisor by using the *Turnitin* plagiarism detection software and by applying the filtering options stated below on 18/09/2019 for the total of 53 pages including the a) Title Page, b) Introduction, c) Main Chapters, d) Conclusion sections of my thesis entitled as above, the similarity index of my thesis is 9%.

Filtering options applied:

1. Bibliography/Works Cited excluded
2. Quotes included
3. Match size up to 5 words excluded

I declare that I have carefully read Hacettepe University Graduate School of Science and Engineering Guidelines for Obtaining and Using Thesis Originality Reports; that according to the maximum similarity index values specified in the Guidelines, my thesis does not include any form of plagiarism; that in any future detection of possible infringement of the regulations I accept all legal responsibility; and that all the information I have provided is correct to the best of my knowledge.

I respectfully submit this for approval.

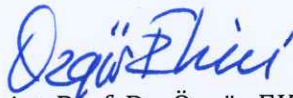
18/9/2019


Date and Signature

Name Surname: Umut KAYA
Student No: N15224637
Department: Mechanical Engineering
Program: Mechanical Engineering
Status: Masters Ph.D. Integrated Ph.D.

ADVISOR APPROVAL

“ APPROVED.



Assist. Prof. Dr. Özgür EKİCİ

(Title, Name Surname, Signature)

CURRICULUM VITAE

Credentials

Name, Surname : Umut KAYA
Place of Birth : Amasya, Turkey
Marital Status : Single
E-mail : umuddkaya@gmail.com
Address : Kuzykent Mh.. Elmas Sk. No: 4/1/10 Merkez/ KASTAMONU

Education

B.Sc. : Middle East Technical University, Department of Mechanical Engineering
(2014)
M.Sc. : Hacettepe University, Department of Mechanical Engineering

Foreign Languages

English

Work Experience

SAFER Engineering, Mechanical Engineer (HVAC), February 2015- February 2016
Kastamonu University, Research Assistant, February 2016-

Areas of Experience

Renewable Energy Systems, Heat Transfer, Fluid Mechanics

Projects and Budgets

-

Publications

-

Oral and Poster Presentations

-